The Mohr-Coulomb Fracture Failure Curve $\tau_{nt}(\sigma_n)$ and Associated Topics.

Is this curve really correctly applied in design viewing brittle isotropic and brittle transversely-isotropic UD materials under uni-axial and multi-axial stress states?

Novel simulation-driven product development shifts the role of physical testing to virtual testing, to simulation. This requires High Fidelity concerning the material models used. *Usual assumption for the models is an ideally homogeneous material*.
In this context the basic research objective of this non-funded investigation was to prove that the Mohr-stresses based Mohr-Coulomb failure curve can be generated from the usually structural stresses-based one and an accurate cohesive strength can be predicted. This task was mathematically very challenging and caused several further questions. These questions are treated in the Annexes.

Prof. Dr.-Ing. habil. Ralf Cuntze VDI, engineer and hobby material modeler
Ingenieurbüro für Leichtbau, Markt Indersdorf, Ralf_Cuntze@t-online.de, 0049 8136 7754
After retirement from industry linked to Composites United e. V. , board member of CU Construction.
Founded, headed the CU working groups "Engineering", "Composite fatigue" (in mechanical engineering) and "Bemessung und Nachweis", "Automatisierte Fertigung im Bauwesen inklusiv serielles Bauen" (in civil engineering)

1. Task

The Mohr Envelope curve or Mohr-Coulomb fracture failure curve is of interest when brittle dense materials are used in the design (*'dense', only very little porous in material mapping sense. See also Annex 2*) with $R^c/R^t > \approx 3$. Such a failure curve begins at the uni-axial compressive strength point ($-R^c$, 0) and usually the end of use is at the so-called cohesive strength point (R^τ, $\sigma_n = 0$). The cohesive strength value is essential for rock mechanics design.
Due to the brittle behavior, the curve is initially dominated by shear fracture SF and at the end by normal fracture NF. Two modes have to be considered and these will commonly generate a fracture 'plane' changing from about 50° to 90°. In consequence: A shear fracture strength condition alone can principally not be alone to determine by extrapolation a value for R^τ.
In this context a pretty difficult mathematical task had to be solved: *The transformation of the failure curve usually formulated in structural stresses into a curve formulated in Mohr stresses.*
This means for the example UD-material, that the $\sigma_3(\sigma_2)$-curve is to transform into the corresponding Mohr-Coulomb fracture failure curve $\tau_{nt}(\sigma_n)$. Further, the angle $\Theta_{fp}°$ of the altering failure plane is to compute. For another example, a concrete material, two further topics came up: Which is the effect of the altering meridian on $\Theta_{fp}°$ on the way from the compressive strength point on the compressive meridian to the tensile meridian on which the tensile strength is located? "How does the fracture angle alter when a concrete cube or cylinder is multi-axially compressed"? Stimulated by discussions during the performance of this investigation other questions arose. These questions, necessary for understanding and performing design verification as the basic objective behind this work, have been hopefully sufficiently well responded in the Annexes.

1.1 General

Structural load-carrying capacity is mainly determined on material level by the stress situation in the critical material location. There is a crack-driven and a crack-free fracture. Whereas crack-driven fracture is treated by Damage Tolerance Tools (technical cracks are present) the onset-of-fracture which means onset of developing cracks is treated by Strength Failure Conditions SFCs.

In the development of structural components the application of *3D-validated* stress-based strength failure conditions (nowadays most often termed 'criteria') is one essential pre-condition for achieving the required design fidelity for the structural engineer as user. This includes Yield Failure Conditions (ductile behavior) and it further includes conditions to verify that fracture does not occur, i.e. for Onset-of-Fracture considering brittle and ductile behavior.
Basically, the <u>focus</u> here is: <u>Brittle behavior and monotonic short time loading</u>.

A necessarily physically-based failure function *F* to generate a SFC is the basis for the determination of a material stressing effort *Eff* and a load-defined reserve factor *RF* required for design verification. The applicability of such a SFC ends when the driving mode stress σ^t or τ becomes zero or the associate *Eff* becomes negative. $|F|$ is often termed failure index and also used in design. This is only permitted for the fracture state when $F = 1$ and $Eff = 1 = 100\%$.

Different SFCs are dedicated to the various technical strength failure types or failure modes, respectively: Normal Fracture NF, Shear Fracture SF and also Shear Yielding SY, Normal Yielding NY [*Cun20b*]. These failure modes are associated to so-called Limit Failure States.
For porous materials additional SFCs are necessary, see [*Cun14*] for foams and the Annex for slightly brittle isotropic materials in Design Dimensioning (Auslegung, Bemessung) and Design Verification (Nachweis).

Mind: *Today's FEA gives 3D FE stress results as output. The evaluation of these 3D stress states therefore requires 3D conditions that predict the onset-of-failure. Unfortunately, due to a lack of 3D test results, the known standard 'global' SFCs - even for isotropic materials – they are usually not sufficiently well 3D-validated.*

Strength verification of non-cracked structural components is demonstrated through SFCs: by

"*If no relevant limit failure state is met* considering *all dimensioning load cases".*

In the case of a general 3D stress state several failure types may be activated, whereby each strength failure mode contributes to failure. The mode-commonly obtained failure is reached when the joint so-called material stressing effort (in German very appropriately denoted by the technical term Werkstoff-Anstrengung) $Eff = f(Eff^{modes}) = 100\%$.

In tension and compression, a deformation-rich material experiences sliding failure under the influence of the failure-driving shear stress. In a deformation-poor brittle case, the material is plastically non-deformable and breaks under tension perpendicular to the normal stress as soon as the normal driving mode stress σ^t reaches the separation strength R^t or tensile strength, respectively. Compression of brittle materials causes shear failure, because the shear stress τ is decisive. This includes as well sliding failure of ductile materials in the tensile and the compressive range as friction-sliding fracture failure of brittle materials in the compressive range. The mathematically challenging topic here is the derivation of the fracture plane angles $\Theta_{fp}°$ which are of high interest for the understanding of the physics behind the desired transformation.

A Mohr-Coulomb fracture curve captures the domain between its uni-axial limit points compressive strength and tensile strength. Its friction-related part ends at the cohesive point. That practically means it captures the transition zone between the two interacting modes SF and NF. The two required SFCs to determine Onset-of-Fracture in this transition zone will be generated on basis of Cuntze's successful Failure-Mode-Concept FMC.

It should be noted: The author could not find any investigation in literature where the SFC transformation from structural stresses into Mohr stresses has been performed.

1.2 Designations

For a better understanding, because many disciplines are met, some designations are presented:

Cohesive strength: maximum tensile stress σ^t ($\equiv$ separation strength R^t) of bonding between surfaces or of tensile stressed particles building a material. However, in rock and soil mechanics cohesive strength is 'differently' defined as the inherent shear strength $R^\tau = \tau_{nt}$ of a plane, where the normal compressive Mohr stress $\sigma_n^c = 0$ on the about $\Theta_{fp}° \approx 70°$ bias shear fracture plane and whereby the cohesive strength value R^τ is extrapolated from compression point-associated quantities. This seems to be not accurate because R^τ is an brittle-dependent entity of the transition zone between shear fracture mode SF and Normal Fracture mode NF. →*Difference* between the technical disciplines

Condition versus criterion: $F = 1$ versus $F < = > 1$

Confining pressure: lithostatic pressure in geo-mechanics, the pressure forced on a layer of soil or rock by the heaviness of the overlying substance. Corresponds to a hydrostatic pressure p_{hyd}

Confining stress: usually stress σ_z caused by p_{hyd} at level z

Damage (Beschädigung): physical harm, which captures in English as well micro-damage (Schädigung) as macro-damage (Schaden)

Eff: material stressing effort $Eff = f(Eff^{modes})$ representing as interaction equation - *captures the damaging portions of all activated modes* - the mathematical equation of the surface of the fracture (failure) body (*Eff* is a compromise agreed to by the English organizers of the WWFE)

Equivalent stress σ_{eq}: (a) equivalent to the stress state, as performed in σ_{eq}^{Mises}, and (b) comparable to the value of the strength *R* which dominates one single failure mode or failure type

Failure: state of inability of an item to perform a required function in its limit state. A situation when a structural part does not fulfil its functional requirements such as the failure modes Onset-of-Yielding, brittle fracture (NF, SF, Crushing Fracture CrF), Fiber-Failure FF, Inter-Fiber-Failure IFF (matrix failure), leakage, deformation limit (tube widening), delamination size limit, frequency bound, or heat flow etc. A failure is a project-defined 'defect'. For each failure mode a Limit State with *F* = Limit State Function or Failure Function is to formulate. A specific mark for failure exemplarily is: A second loading, under a distinct failure mode (here SF), cannot be sustained anymore, like a slightly porous UltraHighPerformanceConcrete UHPC compression test specimen after a crushing test under p_{hyd} = 1000 MPa where the first loading of the crumbles might have been still further increased, densification enables it)

Failure criterion: $F >= < 1$, Failure Condition: $F = 1 = 100\% \leftarrow Eff$

Failure mode: Failure mode is a commonly used generic term for the types of failures, is a name for a potential way a system may fail (in design verification usually a project- associated failure)

Failure surface and failure body: the surface of the failure body is the shape defined by $F = 1$

Failure type (isotropic): NF, SF, CrF, Normal Yielding NY, Shear Yielding SY

Flaw versus micro-crack: a micro-crack is a sharp flaw (Ungänze), grade of singularity is decisive

Fracture: separation of a whole into parts

Fracture 'plane' angle Θ_{fp°: average value of the scattering fracture plane that is seldom a plane. A tensile stress causes an angle perpendicular to the stress direction, of 90°. This definition matches with the 90°-wound UD tensile-compression-torsion test specimen

Fracture (failure) body: Surface of the tips of all fracture (failure stress) vectors. Fracture is the failure of brittle materials

Friction: slope of the Mohr-Coulomb failure curve (Mohr failure envelope) defined after the ratio of the derivation shear stress $d\tau_{nt}$ to normal stress $d\sigma_n$ at failure in the so-called touch point. The ratio $d\tau_{nt} / d\sigma_n$ is termed internal friction value μ

Inelastic versus plastic: *inelastic* → micro-damage, brittle, fracture mod***es***, friction occurs and is indicated by the paraboloid-shaped SFCs (an inelastic potential shall be not termed yield potential); *plastic* → metal plasticity, ductile, yield mod***e***, frictionless sliding indicated by the cylinder shape of 'Mises', yield potential

Material: 'homogenized' (macro-)model of the envisaged complex solid or heterogeneous material combination which principally may be a metal, a lamina or further a laminate stack analyzed with effective properties. Homogenizing (smearing) simplifies modelling

Material behavior: *brittle* behavior can be characterized with the complete loss of tensile strength capacity at first fracture, R^t. Quasi-brittle behavior shows - after reaching R^t - a slight strain hardening followed by a gradual decay of tensile strength capacity during a strain softening domain. Thereby *Eff* remains 100%. *Ductile* behavior is accompanied by a gradual increase of tensile stress (strain hardening), and after reaching R^t a strain softening domain follows

Material Stressing Effort (*Werkstoffanstrengung, nicht Werkstoffausnutzung*): definition as $Eff^{mode} = \sigma_{eq} / R$; max*Eff* =100% is reached at $F = 1 = 100\%$. Just for 100% $F = Eff$

Mathematical stresses: structural stresses used as mathematical stresses means $\sigma_I > \sigma_{II} > \sigma_{III}$

Meridian: axial cross-section of the failure body. Tensile meridian mathematically defined as $\sigma_I > \sigma_{II} = \sigma_{III}$, compressive meridian defined as $\sigma_I = \sigma_{II} > \sigma_{III}$. These meridians are those meridians where tests are usually performed along. The shear meridian is the neutral meridian where $\sigma_{II} = -\sigma_{III} \rightarrow$ shear

'Modal' versus 'Global' SFCs: Modal means that only a test data set of one failure mode domain is mapped whereas global (examples Drucker-Prager isotropic, Tsai UD) means that mapping is performed over several mode domains. The bottle-neck of a global SFC respectively 'Single Failure Surface Description ' is, that any change in one of the 'forcibly married' modes requires a new global mapping which also changes the failure curve in the physically not met mode

Multi-fold stress state: example isotropic material: $\sigma_I = \sigma_{II}$, $\sigma_I = \sigma_{II} = \sigma_{III} \rightarrow \sigma_{hyd}$; 3-fold)

Proportional loading: often assumed loading procedure applied to stresses here. How the material stressing effort *Eff* is derived from the failure function *F*. In the case of a non-homogeneous function *F* the associated values are only equal for the failure state $F = 1 \equiv Eff = 100\%$

Reserve factor: ratio of a 'resistance value' and a so-called 'action value'. $RF > 1$ permits a further increase of loading. This is terminated by $Eff = 100\%$ 'material stressing effort' (Werkstoffanstrengung) in the last critical Hot Spot, when no more stress redistribution in the structural component is possible

Splitting (longitudinal): failure mechanism, resulting from compression loading that creates cracks parallel to the compression load axis generated by perpendicular tensile stresses acting at internal flaw tips which are usually combined with so-called wing cracks

Strain approach: approach, if limiting strains are used in design. Not advantageous in case of brittle materials where on top residual stresses have to be considered

Strength: in engineering linked to a uni-axial fracture stress. (1) Characteristic strength: in mechanical engineering the typical average strength, in civil engineering a reduced (5% fractile) average strength value! (2) Design strength: a statistically reduced average strength

Strength denotations: R is strength, in general, and also the statistically-reduced value. $\bar{R}$ denotes the average strength which is used when mapping a course of test data points. In construction, still most often: letter $R \rightarrow f$.

Strength Failure Condition (SFC): mathematical formulation of the strength failure surface, that takes the form $F = 1$. Tool, to assess a 'multi-axial failure stress state' in a critical material location of the structural component. The usually macro-mechanical SFC should consider, that failure usually occurs at a lower than macro-mechanic level, micromechanically, such as the matrix in a the macro-mechanically described SFC of the often composite material (*Fig.7-2*)

Stress (not stress component!): component of the stress tensor defined as the force divided by the area of cross-section. R = general strength and also the statistically reduced 'strength design allowable. $\bar{R}$ (bar over the *R)* means *average* strength and is to apply when mapping, like here

(model) Validation: result of a successful qualification of a model (i.e. material model)

(design) Verification: fulfillment of a set of design requirement data

Yield strength: distinct stress linked to yielding. As it is difficult to determine a precise onset-of-yield point, in general, one should discriminate from practical engineering reasons the proportional (tensile) limit R_p ($\equiv f_y$) and $R_{p0.2}$ ($\equiv R_{0.2}^t$), where the offset yield point is taken as the stress at which 0.2% plastic deformation remains (*in English literature $R_{p0.2}$ is termed proof stress)*

120°-symmetry of the isotropic failure body: wording according to the equality of the 3 principal stresses each 'perturbation' of the rotational failure body exists 3 times

C: fracture angle measure C = 1/3 with $\Theta_{fp}° = 35°$ (very ductile); C = 0, $\mu = 0$ with $\Theta_{fp}° = 45°$ (bound of F^{SF}); C = - 1 with $\Theta_{fp}° = 90°$ (very brittle)

FRP, FRC: fiber-reinforced plastic (polymer), fiber-reinforced concrete

d: non-circularity parameter of the hoop cross-section of the failure body which is here a fracture failure body or also termed π-plane shape parameter

ρ or ϕ: slope of Mohr-Coulomb curve (Mohr envelope)

Θ_{fp}°: angle of the fracture 'plane'

μ: friction value, practically $0 < \mu < 0.3$.

2 Material Symmetry-dedicated Basics of Cuntze's Failure-Mode-Concept FMC

2.1 Material symmetry facts used for generating SFCs

Helpful information is coming from demands of the material symmetry: A basic number of material quantities can be derived from the corresponding tensors. This leads to a minimum of 'generic' numbers, which is crucial for theoretical modeling and for the test effort.

In this context can be concluded from and for material behavior:

1 If a material element can be homogenized to an ideal crystal (= frictionless), then material symmetry requires for the isotropic material:
- 2 e*lastic 'constants', 2 strengths, 2 'basic' invariants* I_1, J_2 *, 2 strength failure modes* for *yielding* (NY, SY) and 2 for *fracture* (NF, SF) and *2 fracture toughness values (presumed it is an ideal homogeneous material [Cun17,19a]*
  → for isotropic materials may be recognized a 'generic number' of 2. For instance, one needs just 2 invariants for formulate SFCs. This is valid as long as a one-fold acting failure mode is to describe by the distinct SFC and not a multi-fold one
- 1 *physical parameter (such as coefficient of thermal expansion CTE, coefficient of moisture expansion CME, etc.)*

For transversely-isotropic UD-materials UD- materials the witnessed respective *generic numbers* are *5* and *2 for physical parameters*

2 A real solid material model is represented by a description of the ideal crystal (frictionless) + a description of its friction behavior. → Mohr-Coulomb requires for the real crystal another *physical parameter, namely the inherent material friction value μ: 1 for isotropic and 2 for UD materials*

3 Fracture morphology gives finally evidence
Each strength corresponds to a distinct *strength failure mode* and to a distinct *strength fracture type,* to Normal Fracture (NF) or Shear Fracture (SF)

4 Densely packed frictional material experiences dilatation when sheared.

2.2 Isotropic Invariants, needed for generating stress-based SFCs (strength criteria)

Following the contents of the previous sub-chapters for the derivation of invariant-based SFCs just two invariants are necessary to describe a failure mode, namely I_1, J_2 . Following Beltrami these are physically interpretable.

J_3 is required when the same 'strength fracture mode' multiply occurs, which practically means for brittle isotropic materials that a 120° rotational symmetry of the fracture body is to face. The author was able to successfully use these material symmetry specifics in strength mechanics, applying his failure mode concept for homogenized isotropic and UD materials in many data sets.

In this context different effects are to discuss:

Mixed Strength (fracture) Failure: Several different failure modes may be activated by the acting stress state. The interaction of both the activated fracture mode types Normal Fracture NF with Shear Fracture SF under compression increases the danger to fail! Hence, the associated fracture test data are so-called joint-probabilistic results of 2 acting modes (if isotropic).

Multi-fold (fracture) Failure Mode: The acting stress state with maximally equal orthogonal stresses activates the same mode multi-fold. Hence, the associated fracture test data are so-called joint-probabilistic results of a multi-fold acting mode!

Usually, SFCs consider just one single failure mode (mechanism) and do not capture the bi-axial effect of $\sigma_I = \sigma_{II}$ or hydrostatic tensile or compressive failure stress states. This must be considered by an additional term in the SFC!

The case, <u>*2-fold*</u> or $\sigma_{II} = \sigma_I$, is the reason for the 120°-symmetry of isotropic brittle behaving materials in the domains $I_1 > 0$ and $I_1 < 0$. This causes inward and outward dents of the (here fracture) failure body and is elegantly solved by applying the invariant J_3 in the π-plane also termed hoop or deviatoric plane). The dents may be seen and modelled as pertubations along the meridian axis of the failure body. Whether such an additional pertubation is necessary could not be cleared by the author's effortful numerical investigations for the available multi-axially compressed concrete data set. In compression, a multi-fold fracture mode decreases the danger to fail depicted by $R^{cc} > R^c$ (*redundancy effect*), $I_1 < 0$, dense . In compression $R^t > R^{tt}$ is valid.

The case <u>*3-fold*</u> *with* $\sigma_{II} = \sigma_I = \sigma_{III}$, termed hydrostatic stressing, leads to a closing tensile cap state and to a closing bottom under a compressive stress state in the case of porous materials if failure occurs under this stress state.

<u>*Lesson Learned LL*</u>*:*

(1) In the case of a multi-fold acting mode, the respective SFC formula must get an additional term: This is best performed for isotropic materials by a third invariant, namely J_3, and could be performed for UD materials (if $\sigma_2^t = \sigma_3^t$), by an additional Eff term

(2) In design verification, nowadays, a SFC has to map 3D stress states. It can be validated, principally by 3D test data sets only. If just 2D test data is available, then a 3D-SFC can be 'just 2D-validated'. This means that the necessary 3D mapping quality is not fully proven and just a '2D-reduced' 3D SFC is applied

(3) A test series along a tensile meridian (it delivers R^t, R^{cc}) alone or along a compressive meridian (delivers R^c, R^{tt}) alone is not sufficient. On both the meridians tests should be performed, because all essential strength points must be considered when mapping. Bi-axial failure stress states (R^{tt} , R^{cc}) are required which generate a two-fold failure mode. Then the significant inherent 120°-symmetry of brittle isotropic materials can be mapped.

(4) Assessment of critical isotropic stress states: The formulations of invariant-based isotropic strength failure conditions (criteria) SFC just need 2 invariants. Due to the fact that a stress state may activate a multi-fold fracture failure type NF or SF the original rotationally symmetric fracture body becomes 120°-symmetric. This is tackled by employing the invariant J_3

(5) Bi-axial compression may further activate a critical tensile strain, which must be checked.

*2.3 Basic features of the **Failure-Mode-Concept FMC** (formulated in 1995)*

- *Each failure mode represents 1 independent failure mechanism, and thereby represents 1 piece of the complete (global) failure surface*
- *Each failure mechanism is governed by 1 basic strength (this is witnessed)*
- *Each failure mode can be represented by 1 failure condition SFC.* [*Cun04,12,15a*]

Therefore, equivalent stresses can be computed for each mode. This is of advantage when deriving S-N curves and Haigh diagrams in fatigue with minimum test effort

- Consequently, the FMC-approach *requires an interaction* of all (isotropic 2) *modes*!

$$Eff = \sqrt[m]{(Eff^{\text{mode 1}})^m + (Eff^{\text{mode 2}})^m + ...} = 1 = 100\%, \; if \quad \text{Onset-of-Failure}$$

From engineering reasons, Cuntze takes the same interaction exponent *m* for each transition domain between failure mode domains. This interaction of adjacent failure modes is modelled by a 'series failure system". That permits to formulate the total material stressing effort from all activated failure modes as the 'accumulation' of *Effs* ≡ sum of all the failure danger proportions.

Eff = 1 represents the mathematical description of the surface of a failure body!

The value of the interaction exponent m depends on the ratio R^c / R^t. For brittle materials with about R^c / R^t > 3 the value is about m = 2.6 from mapping experience in the transition zone of the two modes. A smaller m is ‘design verification conservative’.

3 Generation of the FMC-based Strength Fracture Condition ('criteria') SFCs

3.1 Isotropic Invariants and their physical meaning

At first *Fig.3-1* shall present all types of stresses used in the invariants and later in this document.

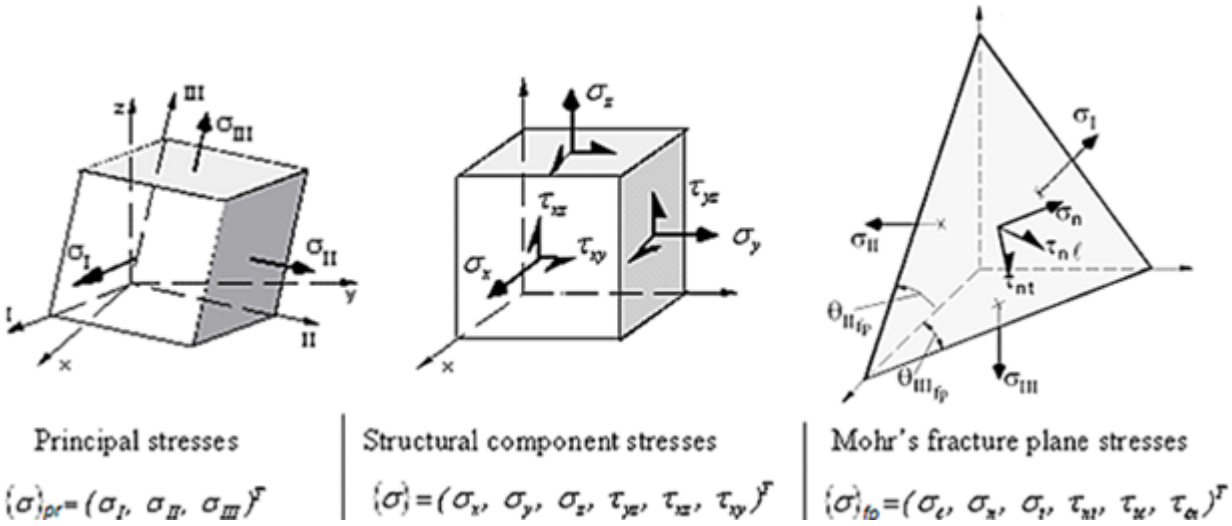

Fig.3-1,isotropic: Principal stresses (left) on the material cube's surfaces and Mohr stresses acting at the associated fracture plane; (right) Mohr stresses in the cylindrical coordinate system.

The collected knowledge about the materials leads in the FMC to perform them regarding:

1. *Rigorous postulation of a number of failure modes = number of strengths!*
2. *Application of a failure mode-wise concept for the generation of SFCs.*
3. *Direct use of the friction value μ in the SFC.*

Material symmetry demands gave reason that the FMC just strictly describes single independent failure modes by its failure mode–wise concept. This will make the derivation of equivalent stresses possible despite of the fact whether the material is isotropic, transversely-isotropic or orthotropic.

In parallel to the material symmetry demands and the strict failure-mode thinking, further driving ideas were using invariants and considering their physical content. These invariants are formulated in 3D structural component stresses, principal stresses and Mohr stresses and are depicted for isotropic materials in *Table 3-1*.

In order to only use experimentally derivable material quantities, the author directly introduced in his 3D-SFCs for the compression domain, internal friction μ as a formula parameter. Friction is a well-known physical property in engineering. One does not yet find a direct use of μ in the textbooks! Why using Mohr's friction angle φ if $\mu\ (\varphi)$ exists? How to derive μ will be shown later.

> *The Hypothesis of Beltrami states:*
> *"At onset-of-failure (Beltrami said yielding) the strain energy density W in a solid material element consists of two portions; one describes the strain energy due to a change in volume (= dilatation or dilation in US) and the other the strain energy due to a change in shape (distortion)".*

These two portions can be related to invariants: Dilatational energy to I_1^2 considering a volume change of the material element and distortional energy to $J_2 \equiv$ ('Mises') for a shear distortion under volume consistency, forming a shape change of the material element. If friction is activated under compression then the frictional energy is to consider by applying I_1.

Creating SFCs, Beltrami's statement guarantees an advantageous use of the 'physics-based' invariants I_1 and J_2 for very different materials such as Normal Concrete, Ultra-High-Performance-Concrete, PMMA and Sandstone.

Rounding-off, by employing an interaction equation in mode interaction domains of adjacent mode failure curves (2D) or of partial failure surfaces is leading again to a *pseudo*-global failure curve or surface. In other words, a 'single surface failure description' is achieved such as with Tsai/Wu [Tsa71], however, without the well-known shortcomings.

In *Fig.3-2* the dedication of invariants is exemplarily applied.

shape change friction volume change

$$F^{SF} = c_1^{SF} \cdot \frac{3J_2 \cdot \Theta^{SF}}{(\bar{R}^c)^2} + c_2^{SF}(\mu) \cdot \frac{I_1}{\bar{R}^c} + c_3^{SF} \cdot (\frac{I_1}{\bar{R}^c})^2 = 1$$

'Mises Cylinder' formula

(Above *general* strength failure condition SFC is normalized by the compressive strength $\bar{R}^c$

Two-fold failure danger can be modelled by using the well known invariant J_3.

The non-circularity function Θ^{SF} includes d^{SF} as non-circularity parameter.

It represents the 120°-rotational symmetry of isotropic materials, caused by the equivalency of the 3 principal stresses and directions (see the fracture bodies,following).

$$\Theta^{SF}(J_3, J_2) = \sqrt[3]{1 + d^{SF} \cdot \sin(3\vartheta)} = \sqrt[3]{1 + d^{SF} \cdot 1.5 \cdot \sqrt{3} \cdot J_3 \cdot J_2^{-1.5}}$$

Compressive Meridian: $\Theta^{SF} = \sqrt[3]{1 - d^{SF}}$, Tensile Meridian: $\Theta^{SF} = \sqrt[3]{1 + d^{SF}}$,

Neutral Meridian: $\Theta^{SF} = 1$, see *Fig*.3 - 3.

Fig.3-2: Schematic example for the use of invariants for isotropic, slightly porous materials, $I_1 < 0$

LL:

(1) Three energy terms – represented by two invariants, only - are required to establish 'isotropic SFCs'. Hence, the FMC approach is not without any energy basis as some other 'stress-based criteria.'

(2) Material symmetry seems to have told the author: In the case of isotropic materials, for the quantities a generic (basic) number of 2 is inherent. This is valid for modes, invariants, yield strengths, fracture strengths, fracture mechanical SIFs [Cun20] and more quantities. And this also affects the test effort considering 'What is the minimum test effort to be necessarily measured?

(3) *The 120°-rotational symmetry could be mapped by employing J3 (only reason for a further invariant).*

Table3-1: Invariant formulations using structural component stresses, principal stresses and Mohr stresses

Structural stresses:

$$I_1 = \sigma_x + \sigma_y + \sigma_z \ , \quad I_2 = \sigma_x \cdot \sigma_y + \sigma_y \cdot \sigma_z + \sigma_x \cdot \sigma_z - \tau_{xy}^2 - \tau_{yz}^2 - \tau_{xz}^2$$

$$I_3 = \sigma_x \cdot \sigma_y \cdot \sigma_z + 2\tau_{xy} \cdot \tau_{yz} \cdot \tau_{xz} - \sigma_x \cdot \tau_{yz}^2 - \sigma_z \cdot \tau_{xy}^2 - \sigma_y \cdot \tau_{xz}^2$$

$$6J_2 = (\sigma_y - \sigma_z)^2 + (\sigma_z - \sigma_x)^2 + (\sigma_x - \sigma_y)^2 + 6 \cdot (\tau_{xy}^2 + \tau_{yz}^2 + \tau_{xz}^2)$$

$$27J_3 = 2I_1^3 - 9I_1 \cdot I_2 + 27I_3$$

$$2D: \ I_1 = \sigma_x + \sigma_y$$

$$6J_2 = (\sigma_y)^2 + (-\sigma_x)^2 + (\sigma_x - \sigma_y)^2 + 6 \cdot \tau_{xy}^2$$

Principal stresses:

$$I_1 = \sigma_I + \sigma_{II} + \sigma_{III} = \ f(\sigma)$$

$$6J_2 = (\sigma_I - \sigma_{II})^2 + (\sigma_{II} - \sigma_{III})^2 + (\sigma_{III} - \sigma_I)^2 = \ f(\tau)$$ ('Mises' invariant)

$$27J_3 = \ (2\sigma_I - \sigma_{II} - \sigma_{III}) \cdot (2\sigma_{II} - \sigma_I - \sigma_{III}) \cdot (2\sigma_{III} - \sigma_I - \sigma_{II})$$

$$3 \cdot \sigma_{oct} = \sigma_I + \sigma_{II} + \sigma_{III} = \ \sigma_\ell + \sigma_n + \sigma_t;$$

$$9 \cdot \tau_{oct}{}^2 = 6J_2 = 4 \cdot (\tau_{III}{}^2 + \tau_I{}^2 + \tau_{II}{}^2)$$

$\tau_{II} = \max \tau(mathematically)$, $\sigma_I, \sigma_{II}, \sigma_{III}$ are principal stresses,

$\sigma_I > \sigma_{II} > \sigma_{III}$ are mathematical stresses (the sign > means more positive)

$$2D: \ I_1 = \sigma_{II} + \sigma_{III}$$

$$6J_2 = \ 2 \cdot (\sigma_{II}{}^2 + \sigma_{II} \cdot \sigma_{III} + \sigma_{III}{}^2)$$

$$27J_3 = \ (-\sigma_{II} - \sigma_{III}) \cdot (2\sigma_{II} - \sigma_{III}) \cdot (2\sigma_{III} - \sigma_{II}).$$

Mohr stresses: fracture angle measure C

$$I_1 = \sigma_n + \sigma_\lambda + \sigma_t \ , \quad I_2 = \sigma_n \cdot \sigma_t + \sigma_t \cdot \sigma_\lambda + \sigma_n \cdot \sigma_\lambda - \tau_{nt}^2 - \tau_{t\lambda}^2 - \tau_{n\lambda}^2$$

$$I_3 = \sigma_n \cdot \sigma_t \cdot \sigma_\lambda + 2\tau_{nt} \cdot \tau_{t\lambda} \cdot \tau_{n\lambda} - \sigma_n \cdot \tau_{t\lambda}^2 - \sigma_\lambda \cdot \tau_{nt}^2 - \sigma_t \cdot \tau_{n\lambda}^2$$

$$6J_2 = (\sigma_n - \sigma_t)^2 + (\sigma_t - \sigma_\lambda)^2 + (\sigma_\lambda - \sigma_n)^2 + 6 \cdot (\tau_{nt}^2 + \tau_{t\lambda}^2 + \tau_{n\lambda}^2)$$

$$27J_3 = 2I_1^3 - 9I_1 \cdot I_2 + 27I_3$$

$$2D: \quad I_1 = \sigma_n \ + \sigma_t, \quad I_2 = -\tau_{nt}^2 + \sigma_n \cdot \sigma_t, \quad I_3 = 0$$

$$6J_2 = (\sigma_n - \sigma_t)^2 + (\sigma_t)^2 + (-\sigma_n)^2 + 6 \cdot \tau_{nt}^2$$

$$27J_3 = 2(\sigma_n + \sigma_t)^3 - 9 \cdot (\sigma_n + \sigma_t) \cdot (\sigma_n \cdot \sigma_t - \tau_{nt}^2).$$

According to Mohr's theory the stress σ_t is not effective. It can be eliminated in the 2D case using addition theorems, thus linking structural stresses to Mohr stresses

$$\sigma_n - \sigma_t = C \cdot (\sigma_x - \sigma_y), \quad \sigma_t = \sigma_n - C \cdot (\sigma_x - \sigma_y), \quad C = \cos(2 \cdot \Theta_{fp}{}^\circ \cdot \pi / 180^\circ)$$

Interpreting structural stresses as mathematical stresses would mean $\sigma_x \equiv \sigma_{III}, \sigma_y \equiv \sigma_{II}$.

3.2 Visualization of a Failure Body consisting of the Mode Domains SF and NF

As still mentioned $F = 1$ or $Eff = 100\%$ mathematically defines the surface of the fracture failure body. Such a body is rendered here using the Haigh-Westergaard-Lode coordinates with $I_1 / \sqrt{3}$ as y-coordinate and $\sqrt{2 \cdot J_2}$ as x-coordinate.

In *Fig.3-3* the upper left part figure confirms, that above coordinate choice physically makes sense.

The part figure, left down, depicts the stress states belonging to a tensile meridian and to a compressive meridian. Thes are those axial cross–sections of the failure body (right) along most of

the two above compression tests are run.
On the fracture failure body figure the 3 main meridians are outlined. For the tensile meridian the Lode angle ϑ = +30° is valid and for the compressive meridian -30°. 3D-stress states are added linked to the indicated fracture body points.
The shear meridian was chosen here as neutral meridian with a Lode angle ϑ = 0.
Finally, for three essential design quantities the formulas are presented at the right side down.

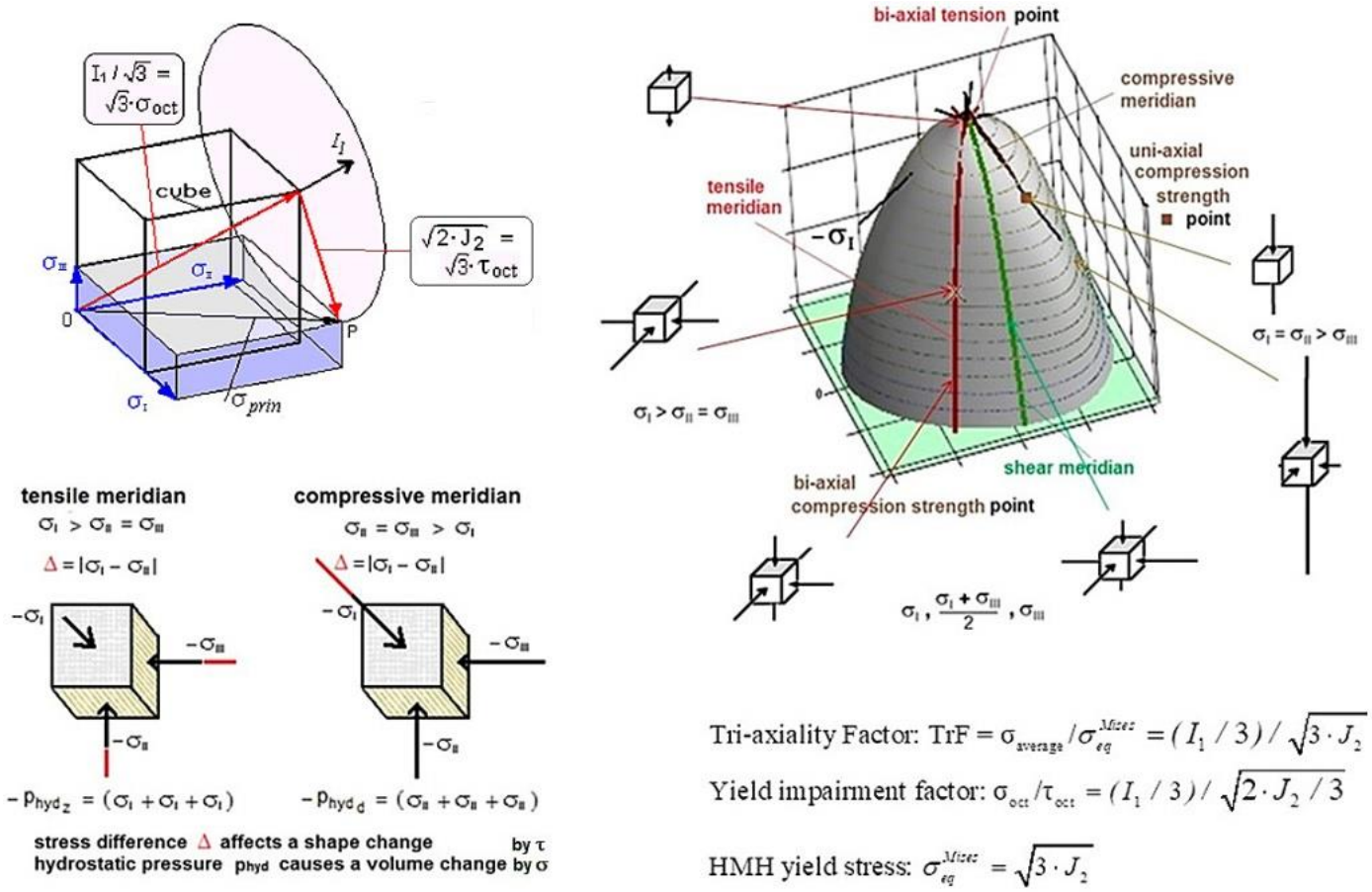

Fig.3-3: Visualization of the main meridians using Haigh-Westergaard Lode-coordinates $I_1/\sqrt{3}$, $\sqrt{2\cdot J_2}$ and various multi-axial stress states. Squares ■ ■ indicate strength values (strengths are defined as uni-axial failure stresses) and crosses mark bi-axial points (bi-axial failure stresses)

3.3 Onset-of-Fracture Failure Body of Isotropic brittle, dense materials

In order to introduce fracture planes the *Fig.3-4* depicts two pictures there-of.
The FMC-derived SFCs, applied in tensile and in compression domain (is topic here), are presented in *Table 3-2*. For each mode, the SFC model parameters must be determined in each associated 'pure' failure mode domain.

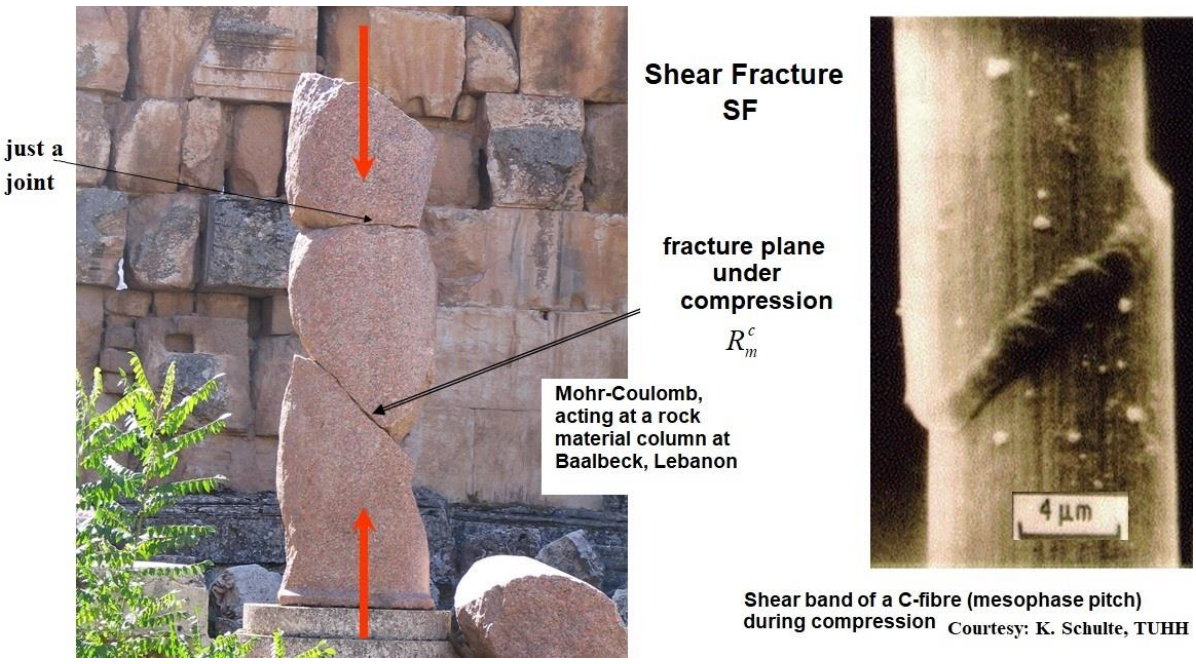

Fig.3-4: Shear fracture of a rock column and a pitch carbon-fiber

Table 3- 2: SFC formulations for NF and SF, 120°-rotational symmetry

Normal Fracture for $I_1 > 0$ **Shear Fracture** for $I_1 < 0$ (topic)

$$F^{NF} = c^{NF} \cdot \Theta^{NF} \cdot \frac{\sqrt{4J_2 \cdot \Theta^{NF} - I_1^2/3} + I_1}{2 \cdot \bar{R}^t} = 1 \quad \leftrightarrow \quad F^{SF} = c^{SF}_{1\Theta} \cdot \frac{3J_2 \cdot \Theta^{SF}}{\bar{R}^{c2}} + c^{SF}_{2\Theta} \cdot \frac{I_1}{\bar{R}^c} = 1$$

$$Eff^{NF} = c^{NF} \cdot \frac{\sqrt{4J_2 \cdot \Theta^{NF} - I_1^2/3} + I_1}{2 \cdot \bar{R}^t} = \frac{\sigma^{NF}_{eq}}{\bar{R}^t} \quad \leftrightarrow \quad Eff^{SF} = \frac{c^{SF}_{2\Theta} \cdot I_1 + \sqrt{(c^{SF}_{2\Theta} \cdot I_1)^2 + 12 \cdot c^{SF}_{1\Theta} \cdot 3J_2 \cdot \Theta^{SF}}}{2 \cdot \bar{R}^c} = \frac{\sigma^{SF}_{eq}}{\bar{R}^c}$$

Two-fold failure danger can be modelled by using the invariant J_3 and d is non-circularity parameter

$$\Theta^{NF} = \sqrt[3]{1 + d^{NF} \cdot \sin(3\vartheta)} = \sqrt[3]{1 + d^{NF} \cdot 1.5 \cdot \sqrt{3} \cdot J_3 \cdot J_2^{-1.5}} \quad \leftrightarrow \quad \Theta^{SF} = \sqrt[3]{1 + d^{SF} \cdot \sin(3\vartheta)} = \sqrt[3]{1 + d^{SF} \cdot 1.5 \cdot \sqrt{3} \cdot J_3 \cdot J_2^{-1.5}}$$

Lode angle ϑ, here set as $\sin(3 \cdot \vartheta)$ with 'neutral' shear meridian angle $0° \rightarrow \Theta = 1$;

tensile meridian angle $30° \rightarrow \Theta^{NF} = \sqrt[3]{1 + d^{SF} \cdot (+1)}$; compressive meridian angle $-30° \rightarrow \Theta^{SF} = \sqrt[3]{1 + d^{SF} \cdot (-1)}$.

If a yield body is rotationally symmetric, then $\Theta = 1$ like for the neutral or shear meridian, respectively .

A two-fold acting mode makes the rotationally symmetric fracture body 120°-symmetric and is captured by $\Theta(J_3)$

Equation of the fracture body: $Eff = [(Eff^{NF})^m + (Eff^{SF})^m]^{m^{-1}} = 1 = 100\%$ total effort.

$$Eff = \sqrt[m]{\left(c^{NF} \cdot \frac{\sqrt{4J_2 \cdot \Theta^{NF} - I_1^2/3} + I_1}{2 \cdot \bar{R}^t}\right)^m + \left(\frac{c^{SF}_{2\Theta} \cdot I_1 + \sqrt{(c^{SF}_{2\Theta} \cdot I_1)^2 + 12 \cdot c^{SF}_{1\Theta} \cdot 3J_2 \cdot \Theta^{SF}}}{2 \cdot \bar{R}^c}\right)^m} = 1.$$

Curve parameter relationships obtained by inserting the compressive strength point $(0, \bar{R}^c, 0)$:

* Rotationally symmetric: $c^{SF}_{1\Theta} = 1 + c^{SF}_{2\Theta}$, $d^{SF} = 0$.

$c^{SF}_2, c^{SF}_{2\Theta} \approx (1 + 3 \cdot \mu)/(1 - 3 \cdot \mu)$ from $\theta^c_{fp}°$ *with* $45° (\mu = 0$, is bound of F^{SF}!), $50° (\mu = 0.174)$.

* 120°-rotationally symmetric: $c^{SF}_{1\Theta} = 1 + c^{SF}_{2\Theta} \cdot \sqrt[3]{1 + d^{SF} \cdot (-1)}$, $\mu = \cos(2 \cdot \theta^c_{fp}° \cdot \pi / 180)$. with

c^{NF}, Θ^{NF} *from the two points* $(\bar{R}^t, 0, 0)$ and $(\bar{R}^{tt}, \bar{R}^{tt}, 0)$ or by a minimum error fit, if data is available,

c^{SF}, Θ^{SF} from the two points $(-\bar{R}^c, 0, 0)$ -see above- and $(-\bar{R}^{cc}, -\bar{R}^{cc}, 0)$ or by minimum error fit of the course of test data.

Notes:

(1) The chosen NF-function enables to map a straight line of test data in the principle stress plane

(2) If the failure body is fully rotational symmetric then c^{NF} (Θ^{NF} = 1 or d^{NF} = 0) = 1. Above NF can manage inward and outward dents by c^{NF} (Θ^{NF}) < 1 which renders the 120°-rotational symmetry

(3) The friction effect decreases with increasing porosity. Ideal dense materials possess no porosity. A fully porous material may be defined by $R^{cc} \cong R^{c}$. This case must be modelled like foam material [*Cun16a*]

(4) The multiaxial strength capacity of a material is visualized by its failure body. The technical strength or 1D- failure stress is defined by standards. The evaluated technical strength cannot be increased. Its value is defined, fixed. The failure body is the location of all 1D, 2D and 3D-failure stress states. These are all points on the failure surface.

(5) When mapping, then R must be $\overline{R}$, because the average value is required.

(6) Only *Eff* for 100% is equal to the SFC, F =1.

(7) If any plane is a plane of maximum danger, being possible to become a fracture plane, then that plane with the most unfavorable flaw situation becomes the fracture plane.

4 Stress States and Transformation of F^{SF} into Mohr Stresses

4.1 General Relationships

Fig.4-1 informs about the stress terms and angle terms used in the envisaged uni-axial stress state $\sigma^c = F_{fr} / Area$. These are φ ($\equiv \rho$) for the slope and c ($\equiv R^{\tau}$) for the cohesive strength.

Further, the fracture plane angle Θ_{fp} is displayed on the test specimen together with its complementary angle α.

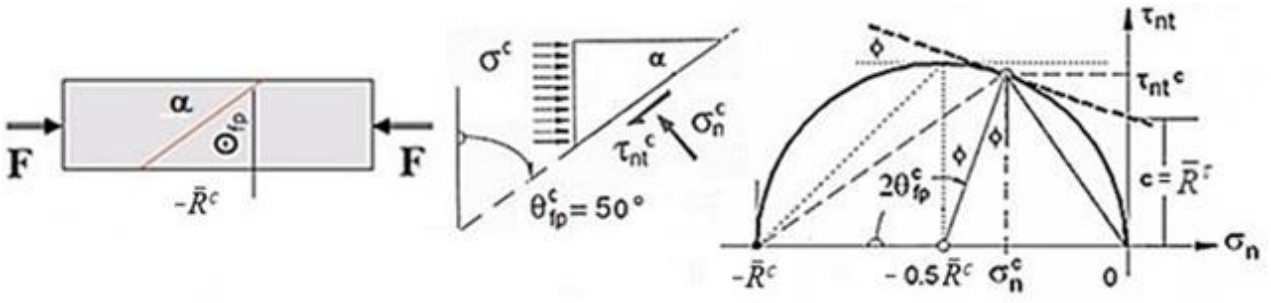

Fig.4-1: Shear fracture plane angles in touch point and 'linear' Mohr-Coulomb friction curve (uni-axial)

Mohr fracture stresses act on the fracture plane. Mohr's failure envelope is generally a curved line which most often is approximated by a straight line consisting of two parts, cohesive strength $\bar{R}_\tau \equiv$ c and frictional part, often written as $\tau_{nt} = c - \sigma_n \cdot \tan(\phi)$ (in civil engineering: $c + |\sigma_n| \cdot \tan(\phi)$).

When dealing with fracture plane angles and the Mohr-Coulomb theory some further basic notions should be visualized. In Fig.4-2 an arbitrary spatial fracture plane is shown for an isotropic and a transversely-isotropic material (a fiber-reinforced polymer or a fiber-reinforced concrete matrix).

For practical purposes, it is sufficient to reduce the mathematical variety of possible fracture planes problem by defining a distinct plane. Tests are performed on basis of mathematical stresses where σ_{III} is the most negative stress

- Uni-axial stress states: $\{\sigma\} = (0,\ \sigma_{II},\ 0)^T$
- Bi-axial stress states: $\{\sigma\} = (0,\ \sigma_{II},\ \sigma_{III})^T$
- Hydrostatic pressure-linked stress states along Tensile Meridian and Compressive Meridian are $\{\sigma\} = (\sigma_I,\ \sigma_{II},\ \sigma_{III})^T$ for the cube test specimen and $\{\sigma\} = (\sigma_\varphi,\ \sigma_r,\ \sigma_{ax})^T$ for the cylindrical test specimen. In mathematical stresses the stress situation under p_{hyd} in the tests reads:

Tensile Meridian: $(\sigma_{ax}^t - \boldsymbol{p}_{hyd}, -\boldsymbol{p}_{hyd}, -\boldsymbol{p}_{hyd}) = (\sigma_I, \sigma_{II}, \sigma_{III}) \rightarrow \sigma_I > \sigma_{II} = \sigma_{III}$

Compressive Meridian: $(-\boldsymbol{p}_{hyd}, -\boldsymbol{p}_{hyd}, \sigma_{ax}^c - \boldsymbol{p}_{hyd}) = (\sigma_I, \sigma_{II}, \sigma_{III}) \rightarrow \sigma_I = \sigma_{II} > \sigma_{III}$.

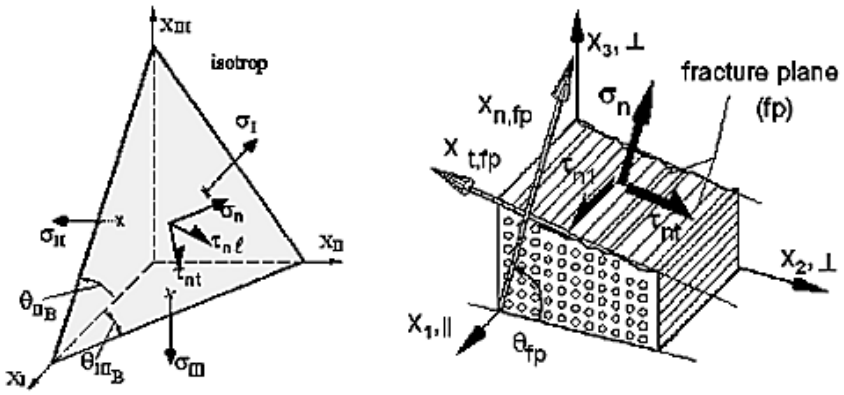

Fig.4-2: Mohr stresses of isotropic and transversely-isotropic UD materials

Model validation has as pre-requisite: Realistic test data sets are available for mapping. The required fidelity further demands to look at test rig with associated test specimen. In compression tests, i.e. massive casted concrete test specimens are used (load transfer: grain-to-grain), see *Fig.4-3* left. However, for other material just' thin' flat test specimens are only possible to obtain, *Fig.4-3* right. This causes different problems to be solved:

- Massive test specimens (*Fig.5-2*, too): Lateral strain constraining by a rigid compression plate causes a barreling of the test specimen which generates a transversal tensile failure stress. This is approximately by-passed by using a transversely 'weak' brush-like compression
- Flat test specimens: A change of the fracture plane from a crack of-the-plane, as shown below, must be prevented. This simply means that a shear stress $\tau = \sigma_{ax} - \sigma_x > \sigma_{ax} - \sigma_z$ acts. The out-of-plane cracking in a 2D-stress situation and in a 3D situation is prevented if the test specimen is deformation-controlled by rigid side walls in thickness direction.

Fig.4-3 also presents the mathematical stresses used when applying Mohr-Coulomb theory. The different principal structural stresses and principal Mohr stresses are rendered in the right picture.

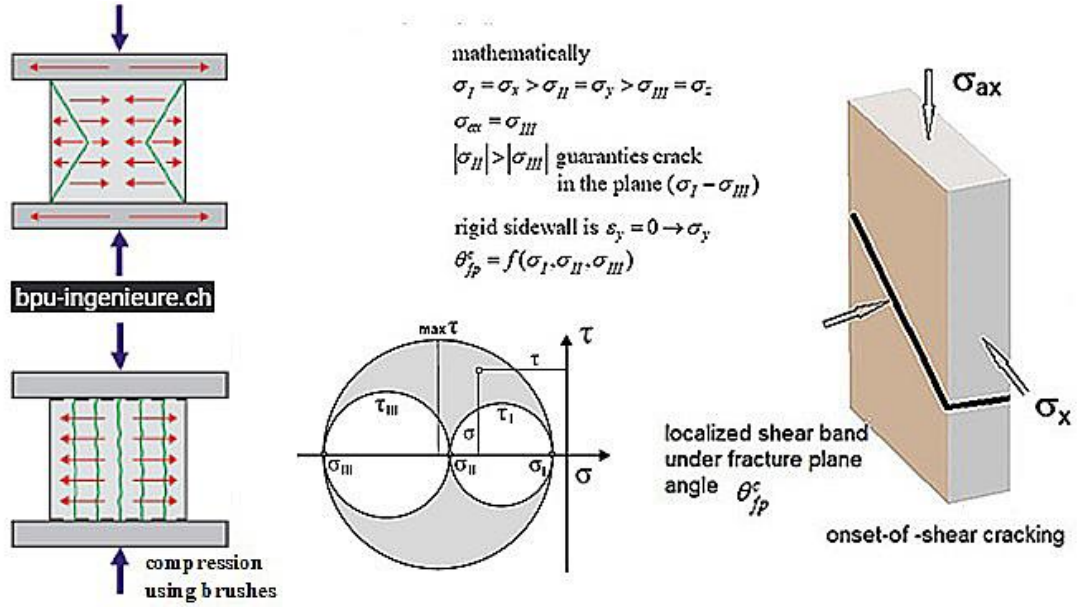

Fig.4-3: Idea for a test set-up to measure the fracture plane angle Θ_{fp}° with acting principal stresses (90° represents the horizontal crack plane)

Before the transformation of the SFCs from the structural stresses into Mohr stresses-based ones the relations shall be depicted in *Table 4-1*.

Table 4-1: Transformation of Cartesian principal stresses into Mohr stresses, addition theorem relations

* Cartesian coordinate system, isotropic

$$\{\sigma\}=\begin{Bmatrix}\sigma_\ell\\ \sigma_n\\ \sigma_t\\ \tau_{nt}\\ \tau_{t\lambda}\\ \tau_{t\lambda}\end{Bmatrix}=\begin{bmatrix}1&0&0&0&0&0\\ 0&c^2&s^2&2sc&0&0\\ 0&s^2&c^2&-2sc&0&0\\ 0&-sc&sc&(c^2-s^2)&0&0\\ 0&0&0&0&c&-s\\ 0&0&0&0&s&c\end{bmatrix}=\begin{Bmatrix}\sigma_I\\ \sigma_{II}\\ \sigma_{III}\\ 0\\ 0\\ 0\end{Bmatrix},\quad \varphi=\varphi^\circ\cdot\frac{\pi}{180^\circ}$$

Transformed structural stresses and addition theorems used: $\tau=0$

$$s=\sin(\varphi),\quad c=\cos(\varphi),\quad s^2+c^2=1,\quad S^2+C^2=1,\quad C=c^2-s^2=2c^2-1,$$

$$\sigma_n=c^2\sigma_{II}+s^2\sigma_{III}=0.5\cdot[(C+1)\cdot\sigma_{II}+(1-C)\cdot\sigma_{III}],\quad \sigma_t=s^2\sigma_{II}+c^2\sigma_{III}$$

$$\tau_{nt}=-s\cdot c\cdot\sigma_{II}+s\cdot c\cdot\sigma_{III},\ S=2sc,\ c^2=(C+1)\cdot 0.5,\ s^2=(1-C)\cdot 0.5\ .$$

$$\sigma_n-\sigma_t=C\cdot(\sigma_{II}-\sigma_{III}),\quad \tau_{nt}=-s\cdot c\cdot(\sigma_{II}-\sigma_{III})=-0.5\cdot S\cdot(\sigma_{II}-\sigma_{III})$$

$$\sigma_n-\sigma_t=c^2\cdot(\sigma_{II}-\sigma_{III})-s^2\cdot(\sigma_{II}-\sigma_{III})=C\cdot(\sigma_{II}-\sigma_{III}),\quad C=\cos(2\varphi)$$

$$\sigma_n+\sigma_t=\sigma_{II}+\sigma_{III}\ ,\quad \tau_{nt}=-0.5\cdot S\cdot(\sigma_{II}-\sigma_{III}).\ S=\sqrt{1-C^2}$$

The derivation yields the slope in the touch point ($\sigma_{III}=0$), index ^{c} :

$$d\sigma_n/d\Theta_{fp}=d(c^2\cdot\sigma_{II}+s^2\cdot\sigma_{III})/d\Theta_{fp}=-2\cdot s\cdot c\cdot\sigma_{II}=-S^c\cdot\sigma_{II}$$

$$d\tau_{nt}/d\Theta_{fp}=\ d(-s\cdot c\cdot\sigma_{II}+s\cdot c\cdot\sigma_{III})/d\Theta_{fp}=(-c^2+s^2)\cdot\sigma_{II}=-C^c\cdot\sigma_{II}$$

$$\Rightarrow\quad \frac{d\tau_{nt}}{d\sigma_n}=-\frac{C^c}{S^c}=\operatorname{cotan}(2\Theta_{fp}).\ C^c=\cos(2\cdot\Theta_{fp}{}^\circ\cdot\pi/180^\circ)$$

* Cylinder coordinate system (for cube and cylinder tests pecimens)

$$\{\sigma\}=\begin{Bmatrix}\sigma_\ell\\ \sigma_n\\ \sigma_t\\ \tau_{nt}\\ \tau_{t\lambda}\\ \tau_{t\lambda}\end{Bmatrix}=\begin{bmatrix}1&0&0&0&0&0\\ 0&c^2&s^2&2sc&0&0\\ 0&s^2&c^2&-2sc&0&0\\ 0&-sc&sc&(c^2-s^2)&0&0\\ 0&0&0&0&c&-s\\ 0&0&0&0&s&c\end{bmatrix}=\begin{Bmatrix}\sigma_\varphi\\ \sigma_r\\ \sigma_{ax}\\ 0\\ 0\\ 0\end{Bmatrix}$$

* Cartesian coordinate system, transversely-isotropic UD Material (1 is fiber direction)

$$\{\sigma\}=\begin{Bmatrix}\sigma_\ell\\ \sigma_n\\ \sigma_t\\ \tau_{nt}\\ \tau_{t1}\\ \tau_{t1}\end{Bmatrix}=\begin{bmatrix}1&0&0&0&0&0\\ 0&c^2&s^2&2sc&0&0\\ 0&s^2&c^2&-2sc&0&0\\ 0&-sc&sc&(c^2-s^2)&0&0\\ 0&0&0&0&c&-s\\ 0&0&0&0&s&c\end{bmatrix}=\begin{Bmatrix}\sigma_1\\ \sigma_2\\ \sigma_3\\ 0\\ 0\\ 0\end{Bmatrix},$$

$$\sigma_n-\sigma_t=c^2\cdot(\sigma_2-\sigma_3)-s^2\cdot(\sigma_2-\sigma_3)=C\cdot(\sigma_2-\sigma_3)$$

$$\sigma_n+\sigma_t=\sigma_2+\sigma_3\ ,\quad \tau_{nt}=-0.5\cdot S\cdot(\sigma_2-\sigma_3).\ S=\sqrt{1-C^2}$$

Table 4-2: Derivation of the Mohr stresses-transformed FMC-based strength failure conditions

$$F^{SF} = c_{1\Theta}{}^{SF} \cdot \frac{3J_2 \cdot \Theta^{SF}}{\bar{R}^{c2}} + c_2{}^{SF} \cdot \frac{I_1}{\bar{R}^c} = 1 \quad \text{or} \quad Eff^{SF} = \frac{c_{2\Theta}^{SF} \cdot I_1 + \sqrt{(c_{2\Theta}^{SF} \cdot I_1)^2 + 12 \cdot c_{1\Theta}^{SF} \cdot 3J_2 \cdot \Theta^{SF}}}{2 \cdot \bar{R}^c}$$

Inserting compressive strength $\bar{R}^c$ delivers $1 + c_{2\Theta}{}^{SF} = c_{1\Theta}{}^{SF} \cdot \Theta^{SF}$ with the non-circularity function $\Theta^{SF} = \sqrt[3]{1 + d^{SF} \cdot \sin(3\vartheta)} = \sqrt[3]{1 + d^{SF} \cdot 1.5 \cdot \sqrt{3} \cdot J_3 \cdot J_2^{-1.5}}$

which reads $\Theta = 1$ if $\bar{R}^{cc} = \bar{R}^c \Leftrightarrow$ rotationally-symmetric

$$\frac{c_{1\Theta}{}^{SF}}{2\bar{R}^{c2}} \cdot [(\sigma_n - \sigma_t)^2 + (\sigma_t - \sigma_\lambda)^2 + (\sigma_\lambda - \sigma_n)^2 + 6 \cdot (\tau_{nt}{}^2 + \tau_{n1}{}^2 + \tau_{t1}{}^2)] + c_{2\Theta}{}^{SF} \cdot \frac{\sigma_n + \sigma_\lambda + \sigma_t}{\bar{R}^c} = 1$$

Derivation of the slope equation in Mohr stresses, $\sigma_\lambda,\ \tau_{t\lambda},\ \tau_{n\lambda} = 0$

$$\frac{dF^{SF}}{d\sigma_n} = \frac{c_{1\Theta}{}^{SF}}{2\bar{R}^{c2}} \cdot [4\sigma_n - 2\sigma_t - 2\sigma_\lambda] + \frac{c_{2\Theta}{}^{SF}}{\bar{R}^c}; \qquad \frac{dF^{SF}}{d\tau_{nt}} = 12\frac{c_{1\Theta}{}^{SF} \cdot \tau_{nt}}{2 \cdot \bar{R}^{c2}}$$

$$\frac{d\tau_{nt}}{d\sigma_n} = -\frac{dF}{d\sigma_n} / \frac{dF}{d\tau_{nt}} \text{ (implicit diff.)} = -\left[\frac{c_{1\Theta}{}^{SF}}{\bar{R}^{c2}} \cdot [2\sigma_n - \sigma_t - \sigma_\lambda] + \frac{c_{2\Theta}{}^{SF}}{\bar{R}^c}\right] / \left[6\frac{c_{1\Theta}{}^{SF} \cdot \tau_{nt}}{\bar{R}^{c2}}\right]$$

Transformed structural stresses and addition theorems used: $\sigma\lambda = 0$ set

$$S^2 + C^2 = 1,\ C = c^2 - s^2 = 2c^2 - 1,\ S = 2sc,\ c^2 = (C+1) \cdot 0.5,\ s^2 = (1-C) \cdot 0.5$$

$$\sigma_n - \sigma_t = C \cdot (\sigma_{II} - \sigma_{III}),\ \tau_{nt} = -s \cdot c \cdot (\sigma_{II} - \sigma_{III}) = -0.5 \cdot S \cdot (\sigma_{II} - \sigma_{III})$$

Transformation relations for equalizing the angle in the touch point , $\sigma_{II} - \sigma_{III} = \eta$

$$\frac{d\tau_{nt}}{d\sigma_n} = -\left[\frac{c_{2\Theta}{}^{SF} \cdot \eta + c_{1\Theta}{}^{SF} \cdot (2 \cdot c^2 - s^2) \cdot \eta}{6 \cdot c_{1\Theta}{}^{SF} \cdot (-s \cdot c \cdot \eta)}\right] = -\left[\frac{c_{2\Theta}{}^{SF} - c_{1\Theta}{}^{SF}\left(2\frac{C+1}{2} - \frac{1-C}{2}\right)}{6 \cdot c_{1\Theta}{}^{SF} \cdot (-0.5 \cdot S)}\right].$$

Equal slope of curves in touch point: η is multi-axial and cut out

$$\frac{d\tau_{nt}}{d\sigma_n} = \frac{C}{S} = -\left[\frac{c_{2\Theta}{}^{SF} - c_{1\Theta}{}^{SF}\left(C + 1 - \frac{1-C}{2}\right)}{6 \cdot c_{1\Theta}{}^{SF} \cdot (-0.5 \cdot S)}\right] \quad \text{with} \quad C \Rightarrow C^c = \frac{c_{2\Theta}{}^{SF} - c_{1\Theta}{}^{SF}}{-3 \cdot c_{1\Theta}{}^{SF}}$$

Determination of $c_{2\Theta}{}^{SF}$ after inserting $1 + c_{2\Theta}{}^{SF} = c_{1\Theta}{}^{SF}$ for neutral meridian $\Theta^{SF} = 1$:

$$C^c = \frac{c_{2\Theta}{}^{SF} - (1 + c_{2\Theta}{}^{SF})}{-3 \cdot (1 + c_{2\Theta}{}^{SF})} = \frac{-1}{-3 \cdot (1 + c_{2\Theta}{}^{SF})} \Rightarrow \quad c_{2\Theta}{}^{SF} = \frac{-3 \cdot C^c + 1}{3 \cdot C^c + 1}$$

Mohr, linear fracture condition: $\tau_{nt} = \mathrm{R}^\tau - \mu \cdot \sigma_n$ *or* $F = \frac{\tau_{nt}}{\mathrm{R}^\tau - \mu \cdot \sigma_n} = 1$

$$\frac{d\tau_{nt}}{d\sigma_n} = -\frac{dF}{d\sigma_n} / \frac{dF}{d\tau_{nt}} = -\frac{\tau_{nt} \cdot \mu}{(\mathrm{R}^\tau - \mu \cdot \sigma_n)^2} / \frac{1}{\mathrm{R}^\tau - \mu \cdot \sigma_n} = -\frac{\tau_{nt} \cdot \mu}{(\mathrm{R}^\tau - \mu \cdot \sigma_n)} = -\mu \equiv \frac{C^c}{S^c}$$

Now, it is possible to sort out the relations between all friction-linked parameters

$$\mu = -\tan\rho = \frac{d\tau_{nt}}{d\sigma_n} = \frac{-C^c}{S^c}, \text{ small friction angles} \cong -C^c,\ \tan\phi \equiv \tan\rho$$

$$c_{2\Theta}{}^{SF} = \frac{3\mu + 1}{-3\mu + 1} \quad \text{and} \quad \text{if an angle is measured, then } C^c = \cos\left(\frac{2 \cdot \Theta_{fp}{}^\circ}{180^\circ} \cdot \pi\right).$$

From *Fig*.4-1 relationships can be derived and from them follows for $\Theta_{fp}^c{}^\circ = 50^\circ$

brittle $\Theta_{fp}^c{}^\circ = 50^\circ \rightarrow C^c = -0.174,\ c_{2\Theta}{}^{SF} = c_2{}^{SF} = 3.7\ ,\ \mu = 0.18,$

F^{SF}bound $\Theta_{fp}^c{}^\circ = 45^\circ \rightarrow C^c = 0;\ \mu = 0,\ \rho = -\mathrm{atan}(\mu) = 0.$

4.2 'Rotationally-symmetric Fracture Body' Model versus '120°-rotationally-symmetric Model

It exist above two fracture body models, where the transformation is to perform into a Mohr stresses-based formulation. *Table 4-2* lists all necessary relations to enable this transformation and to finally determine $\Theta_{fp}°$ and μ. For the simpler *Rotationally-symmetric Model* nothing changes, except that c_1^{SF} replaces $c_{1\Theta}^{SF} \cdot \Theta^{SF}$. The fracture representing parametersare the same, $c_2^{SF} = c_{2\Theta}^{SF}$!

Of special interest may be the dependence of μ from the fracture plane angle Θ_{fp}, in *Fig.4-4*.

$$\mu(\Theta fpc°) := \frac{-\cos\left(2 \cdot \Theta fpc° \cdot \frac{\pi}{180}\right)}{\sqrt{1 - \cos\left(2 \cdot \Theta fpc° \cdot \frac{\pi}{180}\right)^2}}$$

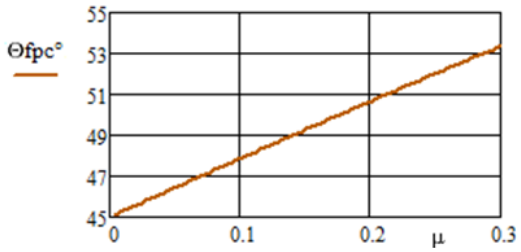

Fig.4-4: Dependence $\Theta_{fp}^{c}(\mu)$

4.3 Pure F^{SF}-based Mohr-Coulomb Fracture Failure Curve and Cohesive Strength Prediction

A Mohr-Coulomb curve is fully linked to the second quadrant of the principal structural stress plane $\sigma_y(\sigma_x)$ or $\sigma_{II}(\sigma_{III})$, respectively. *Fig.4-5* demonstrates that for this special brittle material at σ_{III} = > - 30 MPa the F^{NF} begins to dominate the fracture danger portions of F^{NF} and F^{SF} in the modes' interacting transition zone or, respectively, NF tops SF. The sketch at the right highlights the stress state in the associated test specimen.

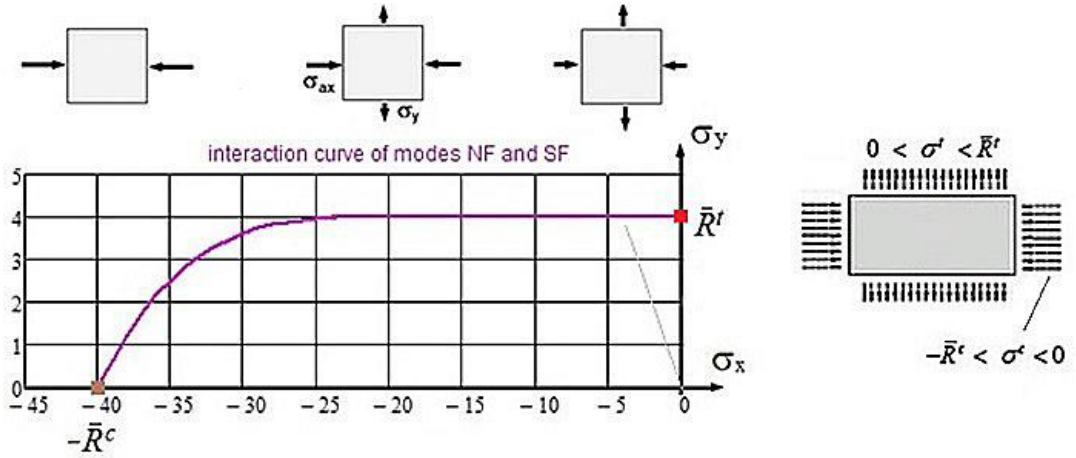

Fig.4-5: Schematic visualization of principal structural stress states belonging to the Mohr-Coulomb curve

Physical experience: The fracture plane angle at the compressive strength point (uni-axial, mode SF) is about 50° for brittle materials like Normal Concrete, grey cast iron and is approximately 70° at the cohesive strength point $(\bar{R}^{\tau},\ \sigma_n = 0) \equiv (\sigma_{II} = -\bar{R}^{\tau} \cdot s / c,\ \sigma_{III} = \bar{R}^{\tau} \cdot c / s)$, *Table 4-1*,

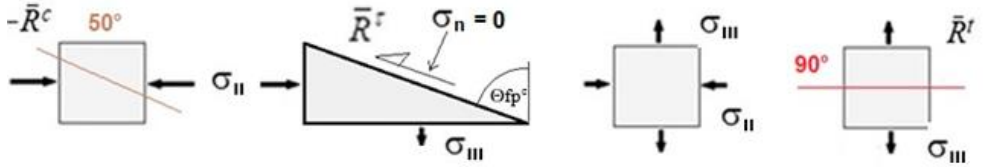

Span : $(\tau_{nt}^{\ c}, \sigma_n^{\ c}) \rightarrow (\bar{R}^{\tau},\ 0) \rightarrow (\tau_{nt}, \sigma_n) \rightarrow (0,\ \sigma_n = \bar{R}^t) \Leftrightarrow (\sigma_{II} = -\bar{R}^c, 0) \rightarrow (\sigma_{II},\ \sigma_{III}) \rightarrow (0,\ \sigma_{III} = \bar{R}^t)$.

In *Table 4-3* the traditional way of predicting the $\tau_{nt}(\sigma_n)$and of cohesive strength $\bar{R}^{\tau}$ is presented:

Table 4-3 : Derivation of Mohr shear curve $\tau_{nt}(\sigma_n)$ and cohesive strengths from different models

Rotationally symmetric	SFCs	120°-Rotationally symmetric
$F^{SF} = c_1^{SF} \cdot \frac{3J_2 \cdot 1}{\bar{R}^{c2}} + c_2^{SF} \cdot \frac{I_1}{\bar{R}^c} = 1$	$\Leftrightarrow$	$F^{SF} = c_{1\Theta}^{SF} \cdot \frac{3J_2 \cdot \Theta^{SF}}{\bar{R}^{c2}} + c_{2\Theta}^{SF} \cdot \frac{I_1}{\bar{R}^c} = 1$
$Eff^{SF} = \frac{c_1^{SF} \cdot I_1 + \sqrt{(c_2^{SF} \cdot I_1)^2 + 12 \cdot c_1^{SF} \cdot 3J_2}}{2 \cdot \bar{R}^c}$	$\Leftrightarrow$	$Eff^{SF} = \frac{c_{1\Theta}^{SF} \cdot I_1 + \sqrt{(c_{2\Theta}^{SF} \cdot I_1)^2 + 12 \cdot c_{1\Theta}^{SF} \cdot 3J_2 \cdot (\Theta^{SF})}}{2 \cdot \bar{R}^c}$

$\Theta^{NF} = \sqrt[3]{1 + d^{SF} \cdot (+1)} \equiv \Theta^{TM}$, $\Theta^{SF} = \sqrt[3]{1 + d^{SF} \cdot (-1)} \equiv \Theta^{CM}$, $\Theta^{NM} = \sqrt[3]{1 + d^{SF} \cdot (0)} = 1$

$\Leftrightarrow$ Determination of friction-related parameters using

* Information $c_2(C_{fp}^c)$ assumption $c_2^{SF} \approx (1 + 3 \cdot \mu) / (1 - 3 \cdot \mu)$ here friction parameter

$c_1^{SF} = 1 + c_2^{SF}$, $d^{SF} = 0$ $\leftarrow$ inserting $(-\bar{R}^c,\ 0)$ $\rightarrow$ $c_{1\Theta}^{SF} = 1 + c_{2\Theta}^{SF} \cdot \sqrt[3]{1 + d^{SF} \cdot (-1)}$

* Mapping of the course of available test data by a minimum error fit

Simulation process necessary: Numerical tuning to optimally map the course of test data

* Approximated, by using information on $\theta_{fp}^c\,°$ or μ: $C^c = \cos(2 \cdot \theta_{fp}^c\,° \cdot \pi / 180) \cong -\mu$,

point $(-\bar{R}^c,\ 0)$ from compr. meridian test *plus* $(-\bar{R}^{cc}, -\bar{R}^{cc},\ 0)$ trom tensile meridian test.

* The Mohr-Coulomb curve $\tau_{nt}(\sigma_n)$ depends on the non-circularity function Θ^{SF}

* Introducing σ_λ, τ_{nt}, $\tau_{nt} = 0$, $1 + c_{2\Theta}{}^{SF} = c_{1\Theta}{}^{SF} \cdot \Theta^{SF}$.

$$\frac{c_{1\Theta}{}^{SF}\Theta^{SF}}{2\bar{R}^{c2}} \cdot [(\sigma_n - \sigma_t)^2 + (\sigma_t - 0)^2 + (0 - \sigma_n)^2 + 6 \cdot (\tau_{nt}{}^2)] + c_{2\Theta}{}^{SF} \cdot \frac{\sigma_n + 0 + \sigma_t}{\bar{R}^c} = 1.$$

$\Leftrightarrow$ Determination of the $\tau_{nt}(\sigma_n)-$curve using addition theorems and inserting $(-\bar{R}^c,\ 0)$

$(\sigma_{II} - \sigma_{III}) = \eta = -\bar{R}^c$, $\sigma_n - \sigma_t = C \cdot \eta$, $\tau_{nt} = -s \cdot c \cdot \eta = -0.5 \cdot S \cdot \eta$, $\sigma_n - C \cdot \eta = \sigma_t$

$$\frac{c_{1\Theta}^{SF} \cdot \Theta^{SF}}{2\bar{R}^{c2}} \cdot [(C \cdot \eta)^2 + (\sigma_n - C \cdot \eta)^2 + (-\sigma_n)^2 + 6 \cdot (\tau_{nt}{}^2)] + c_{2\Theta}^{SF} \cdot \frac{\sigma_n + \sigma_n - C \cdot \eta}{\bar{R}^c} = 1$$

$$\tau_{nt}(\sigma_n) = \frac{\sqrt{3 \cdot \sqrt{-c_{1\Theta}^{SF} \cdot \Theta^{SF} \cdot (c_{1\Theta}^{SF} \cdot \Theta^{SF} \cdot [C^2 \cdot \bar{R}^{c2} + C \cdot \bar{R}^c \cdot \sigma_n + \sigma_n{}^2] - \bar{R}^{c2} + c_{2\Theta}^{SF} \cdot [C \cdot \bar{R}^{c2} + 2 \cdot \bar{R}^c \cdot \sigma_n])}}{3c_{1\Theta}^{SF} \cdot \Theta^{SF}}$$

$c_{2\Theta}{}^{SF} = (3\mu + 1) / (1 - 3\mu)$, $\mu = -\tan\rho \cong -C^c = -\cos(2 \cdot \Theta_{fp}^c\,° \cdot \pi / 180°)$

Example: $\Theta_{fp}^c\,° = 50° \rightarrow C^c = -0.174$, $\mu = 0.176 \cong -C^c$, $d^{SF} = 0.49$, $\Theta^{SF} = 0.80$

Rotationally-symmetric $c_2{}^{SF} = 3.7$, $c_1{}^{SF} = 1 + c_2{}^{SF} = 4.7$, $C = C^c$

120°-rot.-sym:metric $c_{2\Theta}{}^{SF} = 3.7!$, $c_{1\Theta}{}^{SF} = 1 + c_{2\Theta}{}^{SF} \cdot \Theta^{SF} = 5.88$, C alters with ϑ

$\Leftrightarrow$ Determination of cohesive shear strengths:

Linear Mohr-Coulomb: $\bar{R}^\tau = \tau_{nt}{}^c + \mu \cdot \sigma_n{}^c$, $\mu = -(1 - c_2{}^{SF}) / (-3c_2{}^{SF} + 3)$, $\bar{R}^\tau = 17$ MPa

Rotationally-symmetric: point $(\tau_{nt} = \bar{R}^\tau,\ \sigma_n = 0)$, $\bar{R}^\tau = 13.5$ MPa or N/mm^2

120°-Rotat.-symm.: point $(\tau_{nt} = \bar{R}^\tau,\ \sigma_n = 0)$, $\bar{R}^\tau = 12.5$ MPa, δ = -25.1°, $\Theta_{fp}\,° = 72.2°$

$(\bar{R}^\tau,\ \sigma_n = 0) \equiv (\sigma_{II} = -\bar{R}^\tau \cdot s / c,\ \sigma_{III} = \bar{R}^\tau \cdot c / s) = (\sigma_{II} = -32$ MPa $, \sigma_{III} = 3.33$ MPa$)$

Geometry: $d\tau_{nt} / d\sigma_n = \tan\rho = (0.5 \cdot \bar{R}^c - |\sigma_n{}^c|) / \tau_{nt}{}^c \rightarrow \tau_{nt}{}^c = (0.5 \cdot \bar{R}^c - |\sigma_n{}^c|) / \tan\rho$

$$\tau_{nt}{}^c = \sqrt{|\sigma_n{}^c| \cdot (\bar{R}^c - |\sigma_n{}^c|)} = \left(\frac{(0.5 \cdot \bar{R}^c - |\sigma_n{}^c|)}{\tan\rho}\right)^2, \quad |\sigma_n{}^c| = \frac{(\bar{R}^c + \bar{R}^c \cdot \tan\rho^2) - \bar{R}^c \cdot \tan\rho \cdot \sqrt{1 + \tan\rho^2}}{2 + 2 \cdot \tan\rho^2}$$

Touch point coordinates: $\tau_{nt}{}^c = 19.7$ MPa, $\sigma_n{}^c = -16.5$ MPa.

Input: $\bar{R}^t = 4$ MPa, $\bar{R}^c = 40$ MPa (on CM), $\bar{R}^{cc} = 49$ MPa (on TM), further point on the CM (or TM) is required, CM test curve point, $(I_1 / (\bar{R}^t \cdot \sqrt{3}) = -20,\ \sqrt{2 \cdot J_2} / \bar{R}^t = 14)$, usual normalisation by $\bar{R}^t$.

As numerical example a material has been chosen with the friction entities $\Theta_{fp}^{c}\,° = 50° \rightarrow C^{c} = -0.174,\ \ \mu = 0.176$.

Mohr-Coulomb relation:

In order to be able to derive the friction value μ, the slope of the linear Mohr envelope at the compressive strength associated point, termed touch point, must be provided. $\Theta_{fp}{}^{c}$ is the fracture angle in the touch point which is linked to the compressive strength, indexed ^{c}. Viewing *Fig.4-1* the relation exists $(\rho \equiv \phi)$: $\mu = -\tan\rho \cong -\ C^{c} = -\ \cos(2 \cdot \Theta_{fp}^{c}\,° \cdot \pi / 180°)$.

Table 4-2 summarizes the derivation and all relations.

Table 4-2: Derivation of relations μ, Θ_{fp} applying the Linear Mohr-Coulomb approach

$$F_{Mohr}^{SF} = \frac{\tau_{nt}}{\bar{R}^{\tau} - \mu \cdot \sigma_n} = 1 \qquad \text{- compressive SFC, angle } \Theta_{fp}{}^{c} \text{ unknown}$$

$$\frac{dF_{Mohr}^{SF}}{d\sigma_n} = \frac{\mu \cdot \tau_{nt}}{(\bar{R}^{\tau} - \mu \cdot \sigma_n)^2} \qquad \text{and} \qquad \frac{dF_{Mohr}^{SF}}{d\tau_{nt}} = \frac{1}{R^{\tau} - \mu \cdot \sigma_n}$$

$$\rightarrow \quad \frac{d\tau_{nt}}{d\sigma_n} = \frac{-\mu \cdot \tau_{nt}}{(\bar{R}^{\tau} - \mu \cdot \sigma_n)^2} / \left(\frac{1}{R^{\tau} - \mu \cdot \sigma_n}\right) = \frac{-\mu \cdot \tau_{nt}}{(\bar{R}^{\tau} - \mu \cdot \sigma_n)^1} = \frac{-\mu \cdot (\bar{R}^{\tau} - \mu \cdot \sigma_n)}{(\bar{R}^{\tau} - \mu \cdot \sigma_n)}$$

$$= -\mu \quad \textit{implicite differentiation.}$$

$$F_{Mohr}^{NF} = \sigma_n / \bar{R}^{t} = 1 \qquad \text{- tensile SFC,} \qquad \text{angle } \Theta_{fp}{}^{t} = 90°$$

The following chapters show applications where 2D- and 3D-test data sets could be obtained.
For providing these test data sets the author is very grateful.

Fig.4-6 at first verifies that the Mohr-Coulomb shear curve practically captures the transition zone between the uni-axial border points compressive strength and – if extended – the tensile strength which means it has to capture the interaction between the two modes F^{SF} and F^{NF}.

The upper left sketch in *Fig.4-6* depicts the decomposition of cohesive strength into its normal failure stress components still indicating that the tensile stress will dominate the failure behavior.

The upper right sketch in *Fig.4-6* depicts three stress states generated between the compressive strength and the cohesive strength point. The lower part in *Fig.4-6* presents $\tau_{nt}(\sigma_n)$-curves including the models Linear Mohr-Coulomb, rotationally-symmetric F^{SF} and 120°-rotationally-symmetric F^{SF}.

The differences between the classical rotationally-symmetric model and the 120°-rotationally symmetric model is caused because the 120°-rotationally symmetric model does not stay with the compressive meridian CM which runs through the uni-axial compressive strength point. It reflects that under bi-axial stressing the meridian-marking Lode angle ϑ varies from CM via NM (*ϑ = 0°, due to J_3 = 0 ! This corresponds to the rotationally symmetric model*) at the cohesive strength point into the direction of the tensile meridian TM with ϑ = 90°.

The results obtained by the three shear stress mode-linked approaches Linear Mohr-Coulomb, Rotational Symmetric and the more realistic 120°-Rotationally Symmetric reveal for the cohesive strength that the ‘extrapolated’ value decreases with the better description but nevertheless stays a

little too high.

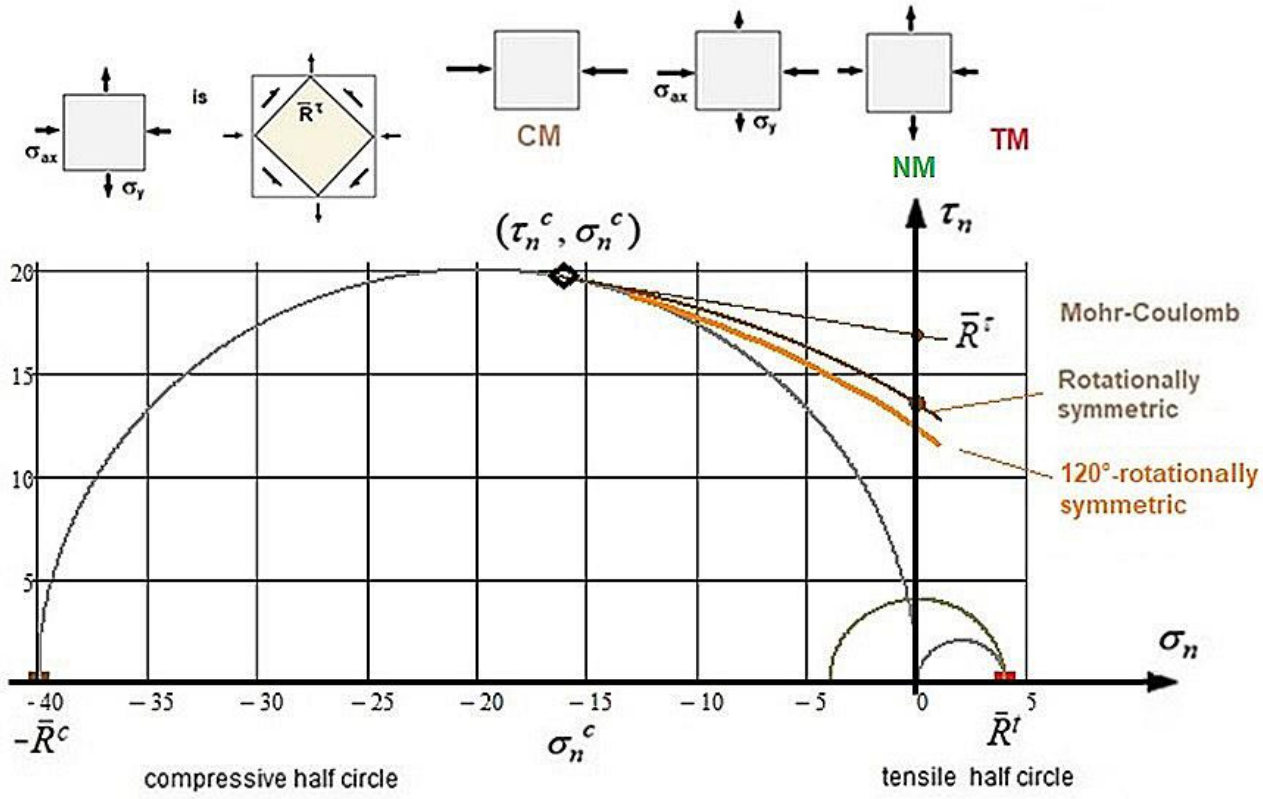

Fig.4-6: (upper left) Decomposition of cohesive strength into its normal failure stress components; (upper right) Stress states along the Mohr-Coulomb failure curve; /lower) Mohr stresses- dedicated failure curves $\tau_{nt}(\sigma_n)$ *and cohesive strengths* $\bar{R}^{\tau}$ *. Example* $\Theta_{fp}{}^{c} = 50°$ *or* $\mu = 0.176$*,*
CM means compressive meridian, TM tensile meridian, NM neutral meridian

4.6 Estimation of a Friction Value μ from Fracture Angle Θ_{fp} or Slope

When evaluating friction tests, in order to derive a friction value μ, the computed value of μ marginally depends upon whether a linear or a parabolic Mohr-Coulomb model is used.

Experience of the author: Which Mohr-Coulomb model is to prefer depends on the formulation of the SFC. Usually a linear friction model is applied and sufficient. This decision is necessary for the determination of the friction parameters which is performed in the touch point ($\tau_{nt}^{c}, \sigma_{n}^{c}$).

There are different procedures to *estimate* a friction value: uni-axially from fracture plane angle Θ_{fp} and bi-axially from a slope:

(1) From fracture plane angles $\Theta_{fp}{}^{c}$ (uni-axially):

Here the angle is defined to be measured from hoop to axial direction.

The estimation is on basis of a uni-axial compressive failure stress measured at onset-of-fracture failure if a reliable fracture plane angle $\Theta_{fp}{}^{c}$ can be monitored. This works, however, a pretty high scatter is faced.

The equation in the evaluation reads $\mu = \cos(2 \cdot \theta_{fp}^{c} \circ \cdot \pi / 180)$, $tan\rho = \mu$.

(2) From slope (bi-axially):

From a determination of the curve parameters computed via two points on the respective mode curve, here the shear fracture F^{SF}. Two curve parameters require two points, analogous to *Fig. 7-10* right.

LL:

(1) A physically realistic investigation, performed in structural stresses and including both the modes, tells us that the fracture angle at the cohesive strength point where $\sigma_n = 0$ must be 90° for really brittle materials like normal concrete..

(2) The friction value μ is a so-called 'physical property. This practically means: A good average value is sufficient for analysis in design dimensioning where always average values should be used.

(3) The rotationally-symmetric model corresponds to the Neutral Meridian Θ^{NM} ($\vartheta = 0°$).

Some Pre-notes on Testing:

- Most of the tri-axial tests are performed on tensile and compressive meridians. These meridians are the opposite lines of an axial cross-section of the fracture failure body, see *Fig.5-1*.
- Looking at the Mohr-Coulomb curve, the angle alters with Θ from ($\vartheta = -30°$) via Θ^{NM} ($\vartheta = 0°$, *it represents the rotationally-symmetric model*) → Θ^{TM} ($\vartheta = +30°$). In other words, an essential change is faced with C from $C^c \approx - 0.2$ at ($\sigma_{II} = - R^c$, 0) along the bi-axial stress states (σ_{II} , σ_{III}).
- Measurement results are 'only' the result of a test agreement defined in a standard, a guideline etc. which serves the comparability of different test investigations and the credibility of the process. The test agreement consists of test facility, test certificate, test specimen and evaluation procedure. This means that we can only speak of 'exact' test results within the frame of the test agreement.
- It must be noted that environment and loading rate affect the results.
- The compressive strength of concrete is determined by a pressure test with specially manufactured test specimens. These are concrete cubes with usually 15 cm edge length (sample cubes) or 30 cm long concrete cylinders with 15 cm diameter (DIN EN 12390-1)
- For the production and storage of test cubes for strength tests, DIN EN 12390-2 applies in addition. The compressed surfaces should be flat and parallel. Otherwise, they must be sanded wet or provided with a thin matching layer.

.

5 The Influence of Hydrostatic Pressure on the Fracture Plane Angle Θ_{fp}

As still mentioned the usual tests are run along the tensile meridian and the compressive meridian. This means, that the fracture angle Θ_{fp} is meridian-dependent or dependent on the Lode angle ϑ, respectively. This situation causes to apply the realistic 120°-rotationally-symmetric model.

The tests are performed by adding an axial load generating σ_{ax} upon a hydrostatic loading p_{hyd}. In *Fig.5-1* the meridian failure curves are depicted and some test points are inserted indicating where the determination of the Mohr quantities τ_{nt} , σ_n , Θ_{fp} has been performed. As coordinates, the Lode-Haigh-Westergaard coordinates are used which equally count in all directions of the 3D stress space.

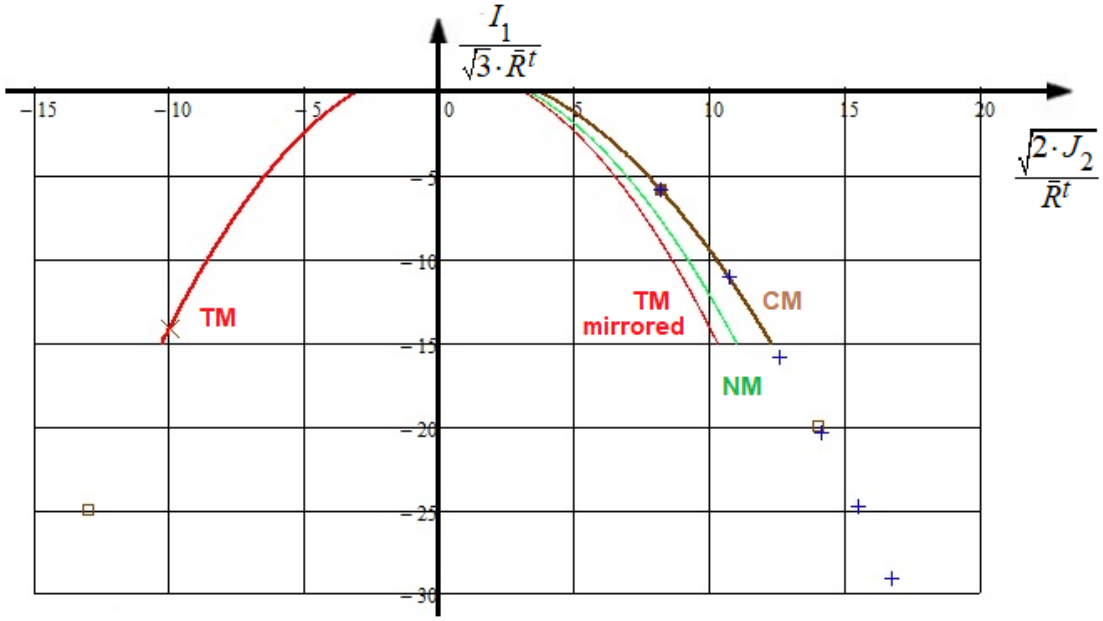

Fig.5-1: Display of all meridians of Normal Concrete. The + are the points where the evaluation of τ_{nt}, σ_n, Θ_{fp} was performed. p = p_{hyd}. (Mathcad unfortunately did not draw below -15 !?)

The basic three meridians are depicted in *Fig.5-1*: Tensile Meridian TM (ϑ = +30°) inside, Neutral Meridian NM (0°) and Compressive Meridian CM (ϑ = -30°), outside. Test points lie on the respective meridian, determined by ϑ, which means on different distances from the axis for a specific $I_1 / \sqrt{3\cdot\bar{R}^t}$. The tensile strength is used for normalization in the case of brittle materials.

Fig.5-2: Test rig and test specimens of concrete

Table 5-1: Derivation of the 3D stress state determined fracture angle Θ_{fp} and Mohr stresses τ_{nt}, σ_n,

SFC: 3D Stress States in structural stresses F^{SF}

$$F^{SF} = c_{1\Theta}{}^{SF} \cdot \frac{3J_2 \cdot \Theta^{SF}}{\bar{R}^{c2}} + c_{2\Theta}{}^{SF} \cdot \frac{I_1}{\bar{R}^{c}} = 1 \text{ inserting stresses } \sigma_{III} = -p = \sigma_I,\ \sigma_{II} = \sigma_{ax} - p,$$

$$\rightarrow \sigma_{ax} = -\ \bar{R}^{c} \cdot \left[c_{2\Theta}{}^{SF} + \sqrt{\bar{R}^{c} \cdot c_{2\Theta}{}^{SF\,2} + c_{1\Theta}{}^{SF} \cdot \Theta^{SF} \cdot (4 \cdot \bar{R}^{c} + 12 c_{1\Theta}{}^{SF} \cdot p)} \,/\, \sqrt{\bar{R}^{c}} \right] / (2 \cdot c_{1\Theta}{}^{SF} \cdot \Theta^{SF})$$

SFC: 3D Stress States in Mohr stresses

$$\frac{c_{1\Theta}{}^{SF}}{2\bar{R}^{c2}} \cdot [(\sigma_n - \sigma_t)^2 + (\sigma_t - \sigma_\lambda)^2 + (\sigma_\lambda - \sigma_n)^2 + 6 \cdot (\tau_{nt}{}^2 + \tau_{n1}{}^2 + \tau_{t1}{}^2)] + c_{2\Theta}{}^{SF} \cdot \frac{\sigma_n + \sigma_\lambda + \sigma_t}{\bar{R}^{c}} = 1$$

* Derivation of the slope equation in Mohr stresses, $\tau_{t\lambda},\ \tau_{n\lambda} = 0$

$$\frac{dF^{SF}}{d\sigma_n} = \frac{c_{1\Theta}{}^{SF}}{2\bar{R}^{c2}} \cdot [4\sigma_n - 2\sigma_t - 2\sigma_\lambda] + \frac{c_{2\Theta}{}^{SF}}{\bar{R}^{c}}; \qquad \frac{dF^{SF}}{d\tau_{nt}} = 12 \cdot \frac{c_{1\Theta}{}^{SF} \cdot \tau_{nt}}{2 \cdot \bar{R}^{c2}}$$

$$\frac{d\tau_{nt}}{d\sigma_n} = -\frac{dF}{d\sigma_n} / \frac{dF}{d\tau_{nt}} = -\ [\frac{c_{1\Theta}{}^{SF} \cdot \Theta^{SF}}{\bar{R}^{c2}} \cdot [2\sigma_n - \sigma_t - \sigma_\lambda] + \frac{c_{2\Theta}{}^{SF}}{\bar{R}^{c}}] / [6 \frac{c_{1\Theta}{}^{SF} \cdot \Theta^{SF} \cdot \tau_{nt}}{\bar{R}^{c2}}]$$

$$\frac{d\tau_{nt}}{d\sigma_n} = \frac{c_{1\Theta}{}^{SF} \Theta^{SF} [2\sigma_n - \sigma_t - \sigma_\lambda] + c_{2\Theta}{}^{SF} \cdot \bar{R}^{c}}{-6 \cdot c_{1\Theta}{}^{SF} \Theta^{SF} \cdot \tau_{nt}} .$$

* Equal slope of curves in touch point: $\sigma_\lambda = \sigma_I,\ \eta = (\sigma_{II} - \sigma_{III})$

$$\frac{d\tau_{nt}}{d\sigma_n} = \frac{C}{S} = \frac{c_{1\Theta}{}^{SF} \Theta^{SF} [2\sigma_n - \sigma_n + C \cdot \eta - \sigma_\lambda] + c_{2\Theta}{}^{SF} \cdot \bar{R}^{c}}{-6 \cdot c_{1\Theta}{}^{SF} \cdot \Theta^{SF} \cdot \tau_{nt}}$$

$$\sigma_n = 0.5 \cdot [(C+1) \cdot \sigma_{II} + (1-C) \cdot \sigma_{III}],\ \sigma_n - \sigma_t = C \cdot \eta,\ \tau_{nt} = -0.5 \cdot S\ \eta,\ \sigma_t = \sigma_n - C\ \eta$$

$$\frac{C}{1} = \frac{c_{1\Theta}{}^{SF} \Theta^{SF} [0.5 \cdot [(C+1) \cdot \sigma_{II} + (1-C) \cdot \sigma_{III} + C \cdot (\sigma_{II} - \sigma_{III}) - \sigma_\lambda] + c_{2\Theta}{}^{SF} \cdot \bar{R}^{c}}{6 \cdot c_{1\Theta}{}^{SF} \Theta^{SF} \cdot [-0.5 \cdot 1 \cdot (\sigma_{II} - \sigma_{III})]}$$

$$C = \frac{2 \cdot c_{2\Theta}{}^{SF} \cdot \bar{R}^{c} + c_{1\Theta}{}^{SF} \cdot \Theta^{SF} \cdot (-2 \cdot \sigma_I + \sigma_{II} + \sigma_{III})}{3 \cdot c_{1\Theta}{}^{SF} \cdot \Theta^{SF} \cdot (\sigma_{II} - \sigma_{III})} \text{ with}$$

$$\Theta^{SF} = \sqrt[3]{1 + d^{SF} \cdot \sin(3\vartheta)} = \sqrt[3]{1 + d^{SF} \cdot 1.5 \cdot \sqrt{3} \cdot J_3 \cdot J_2{}^{-1.5}}$$

* Determination of required quantities:

$$\Theta_{fp} = 0.5 \cdot a\cos(C), \qquad \Theta_{fp}{}^{\circ} = \Theta_{fp} \cdot 180^{\circ} / \pi, \qquad \tau_I = -\ (\sigma_{II} - \sigma_{III}) / 2$$

$$\sigma_n = 0.5 \cdot \{\sigma_{II} \cdot (C+1) + \sigma_{III} \cdot (-C+1)\}, \quad \tau_{nt} = -\ 0.5 \cdot \sqrt{1-C} \cdot (\sigma_{II} - \sigma_{III}).$$

* For the meridians is to insert:

CM: $\Theta^{SF} = \Theta^{CM} = \sqrt[3]{1 - d^{SF}}$; NM: $\Theta^{NM} \cong 1$ (brittle); TM: $\Theta^{NF} = \Theta^{TM} = \sqrt[3]{1 + d^{SF}}$.

$d^{SF} = 0.49 \Rightarrow \Theta^{CM} = 0.80,\ \vartheta = -30°;\ \Theta^{NM} = 1,\ \vartheta = 0°;\ \Theta^{TM} = 1.14,\ \vartheta = 30°,$

$C = \cos(2 \cdot \Theta_{fp}{}^{\circ} \cdot \pi / 180°) \Rightarrow 45° \rightarrow C = 0,\ 50° \rightarrow C = -0.174,\ 90° \rightarrow C = -1.$

In *Fig.5-3* test pressure-dependent axial failure stress on the tensile and on the compressive meridian is presented together with the associated fracture angle curve. In the tri-axial investigation, considering the usual test situation σ_{ax} with p_{hyd}, the courses of the acting axial failure stresses are displayed with and without hydrostatic pressure p_{hyd}, which acts at the same time.

Reminder:

(1) A Linear Mohr-Coulomb model can be employed to obtain a sufficiently good relationship $\boldsymbol{C(\mu)}$.

(2) Establishing the relationship it is assumed that the tangent at the common touch point with the FMC-curve has the same value as that of the linear Mohr envelope curve $\tau_{nt}(\sigma_n)$, see chapter 4.

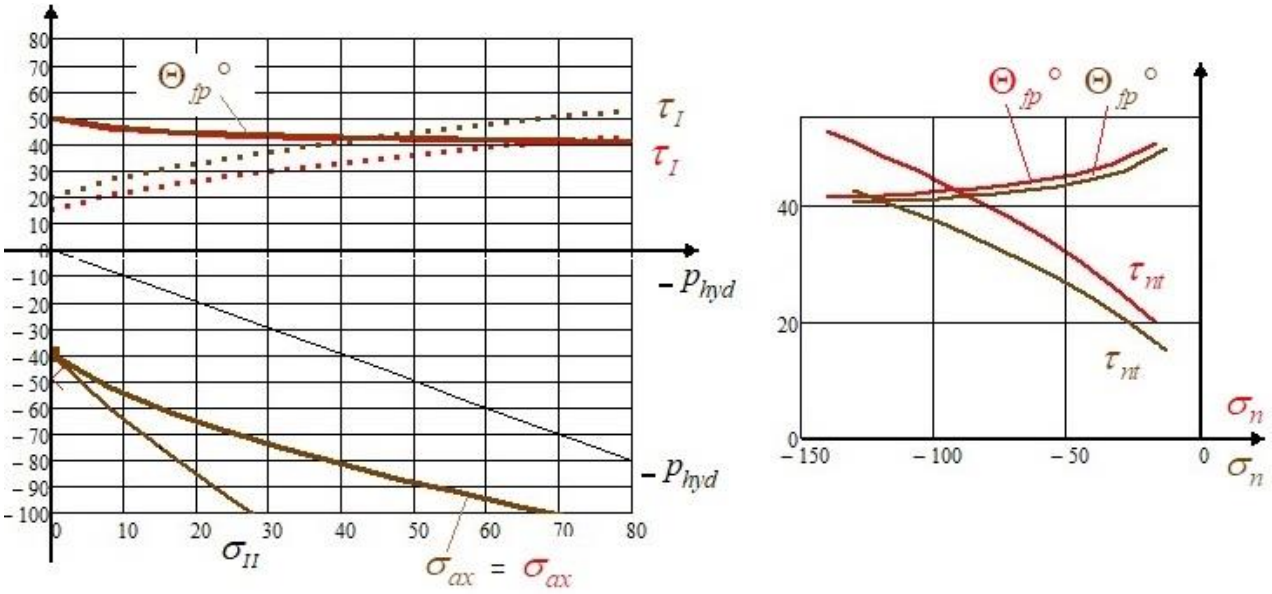

Fig.5-3: For CM and TM, in MPa. (left) Dependency of axial fracture stress from overloaded hydrostatic pressure p_{hyd} together with altering Θ_{fp}. and altering principal shear stress. (right) Alteration of the fracture plane angle as function of $\tau_{nt}(\sigma_n)$. $\sigma_{II} = \sigma_{ax} - p_{hyd}$. Example $\mu = 0.174$

Discussion of *Fig.5-3 presenting CM and TM:*

- The failure plane angle Θ_{fp} reduces with increasing hydrostatic pressure, which means that the behaviour becomes more ductile. This increase of 'ductility', documented by Θ_{fp} from about 50° → 45°, is witnessed even for marble
- The Mohr stresses τ_{nt}, σ_n grow with p_{hyd}. Also the driving principal shear stress $\tau_I = (\sigma_{II} - \sigma_{III}) / 2$ grows with p_{hyd}
- The additional axial stress from the compression force, that finally leads to fracture failure, equals for the loadings CM and TM.

LL:

(1) The M-C curve is an interaction curve. For small compressive Mohr stresses σ_n the curve is ruled by NF and not by SF anymore

(2) The cohesive fracture stress is a stress that is composed of a normal stress component and a compression stress component. Here, the use of the term 'stress component' is to accept !

***(3)** Real isotropic materials have deficiencies to the ideal isotropic material. Hence, fracture will occur according to the actual flaw situation. In the case of crack-like flaws so-called wing-cracks (rock mechanics) occur where the wing crack finally grows into the direction of the compression force [Cun20b]*

***(4)** Additional information for the tensile domain: In literature can be found that $\bar{R}^{tt} > \bar{R}^{t}$. This can be physically not correct, because NF acts twice. The author assumes: The scatter of these tests is very high and the number of these challenging tests was too small.*

6 Fracture Body, Friction Quantities and Mohr-Coulomb Curve of Normal Concrete

Main task of this chapter is the derivation of a more realistic, the mode-interaction considering Mohr-Coulomb Curve $\tau_n(\sigma_n)$. This curve spans from the compressive to the tensile strength point.

6.1 Invariants, Strength Failure Conditions SFCs and Material data set of Concrete

For preparing the solution of this task in the previous chapters still associated sub-tasks have been solved, see *Tables 3-1, 4-1, 4-3*. Nevertheless, at first the full input for the isotropic example Normal Concrete shall be collected in *Table 6-1* in order to pave the way for a shorter performance of the main numerical task in *Table 6-2*.

Table 6-1: Input formulas for main task. TM tensile meridian, CM compressive meridian

* Transfomation of Efforts in Mohr stresses-based ones

$$Eff^{NF} = c^{NF} \cdot \frac{\sqrt{4J_2 \cdot \Theta^{NF} - I_1^2/3} + I_1}{2 \cdot \bar{R}^t}, \qquad \Theta^{NF} \to \Theta^{TM} = \sqrt[3]{1 + d^{NF} \cdot (+1)},$$

in this application can be set: $c^{NF} = \Theta^{NF} = 1,$

$$Eff^{NF} = 1 \cdot \frac{\sqrt{4 \cdot [(\sigma_n - \sigma_t)^2 + \sigma_t^2 + (-\sigma_n)^2 + 6 \cdot \tau_{nt}^2] \cdot 1/6 - (\sigma_n + \sigma_t)/3} + (\sigma_n + \sigma_t)}{2 \cdot \bar{R}^t}.$$

$$Eff^{SF} = \frac{c_{2\Theta}^{SF} \cdot I_1 + \sqrt{(c_{2\Theta}^{SF} \cdot I_1)^2 + 12 \cdot c_{1\Theta}^{SF} \cdot J_2 \cdot \Theta^{SF}}}{2 \cdot \bar{R}^c}, \quad \Theta^{SF} \to \Theta^{CM} = \sqrt[3]{1 + d^{SF} \cdot (-1)},$$

$$Eff^{SF} = \frac{\sqrt{c_{2\Theta}{}^{SF\,2} \cdot (\sigma_n + \sigma_t)^2 + c_{1\Theta}^{SF} \cdot \Theta^{SF} \cdot 2 \cdot [(\sigma_n - \sigma_t)^2 + \sigma_t^2 + (-\sigma_n)^2 + 6 \cdot \tau_{nt}^2]}}{2\bar{R}^c} + c_{2\Theta}{}^{SF} \cdot \frac{\sigma_n + \sigma_t}{2\bar{R}^c}.$$

In contrast to the friction quantities, which are determined in the compressive strength point, where Θ^{SF} is the constant above, Θ now changes with the Lode angle ϑ. This requires J_3 in Mohr stresses) which can be performed when employing the basic form $27 \cdot J_3 = 2 \cdot I_1^3 - 9 \cdot I_1 \cdot I_2 + 27 \cdot I_3 \cdot I_1^2 \cdot 2/27 - I_1$ because the I_1, I_2, I_3 can be displayed in Mohr stresses (Table 3-1). For the present 2D case it reads :

$I_1 = \sigma_n + \sigma_t$, $6J_2 = (\sigma_n - \sigma_t)^2 + \sigma_t^2 + (-\sigma_n)^2 + 6 \cdot \tau_{nt}^2$, $27J_3 = 2(\sigma_n + \sigma_t)^3 - 9 \cdot (\sigma_n + \sigma_t) \cdot (\sigma_n \cdot \sigma_t - \tau_{nt}^2)$

* Addition theorems considering $\eta = \sigma_{II} - \sigma_{III}$, σ_λ, $\tau_{t\lambda}$, $\tau_{n\lambda} = 0$

$$\sigma_n - \sigma_t = c^2 \cdot \eta - s^2 \cdot \eta = C \cdot \eta \ , \ S = \sqrt{1 - C^2}, \ C = c^2 - s^2 = 2c^2 - 1 = 1 - 2s^2,$$

$$\sigma_n + \sigma_t = \sigma_{II} + \sigma_{III} = I_1, \ \tau_{nt} = -0.5 \cdot S \cdot \eta = -0.5 \cdot \sqrt{1 - C^2} \cdot \eta, \ \sigma_t = \sigma_n - C \cdot \eta \ .$$

* Fracture interaction equation ≡ mathematical equation of the fracture body surface

$$Eff = [(Eff^{NF})^m + (Eff^{SF})^m]^{m^{-1}} \Rightarrow \text{numerically simpler } (Eff^{NF})^m + (Eff^{SF})^m = 1 = 100\% \ .$$

6.2 Fracture Failure Body and principal stress plane Cross-section

Fig.6-1 shows the fracture body of the Normal Concrete, see [*Cun15*].
The three basic meridians and the two strength points, compressive strength (dot) and bi-axial compressive strength (cross), are indicated. The material input data set for the computation reads:

$\bar{R}^t = 4$ MPa, $\bar{R}^c = 40$ MPa, $\bar{R}^{tt} = 0.8 \cdot \bar{R}^t$ (assumed), $\bar{R}^{cc} = 51$ MPa, $\bar{R}^{ccc} = 1000$ MPa (set)

120°-rotationally-symmetry parameter: $c_{1\Theta}{}^{SF} \cdot \Theta^{SF} = 1 + c_{2\Theta}{}^{SF}$ with $c_{2\Theta}{}^{SF}$ the friction parameter

$\mu = 0.17$, $\Theta_{fp}{}^{c} = 50°$, $c_{2\Theta}{}^{SF} = 3.70$, $c_{1\Theta}{}^{SF} = 5.88$, $d^{SF} = 0.49$, $\Theta^{SF} = \Theta^{c} = \Theta^{CM} = 0.51$.

For the interaction exponent m =2.6 and $\mu = 0.17$ is set, a *smaller μ value is more conservative.*

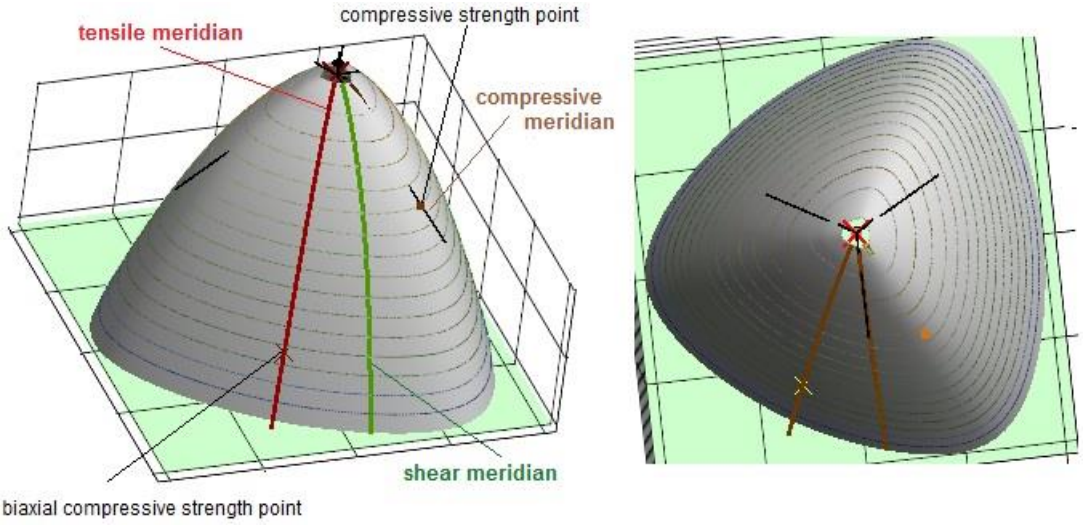

Fig.6-1: Two views of the 120°-rotationally-symmetric fracture body (hoop cross-section) of the Normal Concrete with the basic three meridians and the two strength points [Cun17]

Fig.6-2 displays the course of the measured 2D test data of Normal Concrete, provided by Dr. Silke Scheerer at IfM TU-Dresden (Prof. M. Curbach). It depicts the large scatter of the multi-axial compression tests, which influences the statistically reduced design strength *R* significantly. *Fig 6-2* is a bias cross-section of the Normal Concrete fracture body which is the shape of the principal stress plane. As coordinates the still mentioned Lode-Haigh-Westergaard coordinates are used which equally count in all directions of the 3D stress space.

The measurement of a realistic fracture angle – based on the usually small-scale test level - is practically not possible. The determination of the curve parameters *c* by mapping the course of test data points is the better and practical procedure. Then, the relationship of the curve parameter c to the friction value μ and to the fracture angle Θ_{fp} can be derived. These relations are obtained in the *touch point,* pointed out in *Fig.4-6, Table 4-2*.

The generation of a realistic Mohr-Coulomb curve requires the determination of the slope *along* the full curve, not a single specific value in the touch *point* only. This slope $d\tau_{nt}/d\sigma_n$ is linked to the un-known *fracture plane measure* $C(\Theta_{fp})$. An equation to determine C comes from the differentiation of the Mohr stress-transformed interaction equation because both the two modes are activated. This means, instead of the single SF-formulation the SF-NF-coupling *Eff*-formulation is to apply when moving from the structural stress formulation to a Mohr stress one. *Table 6-2* will show the full procedure, later.

Reminder:

The basic assumption of O. Mohr was: *"The strength of a material is determined by the (Mohr) stresses on the fracture plane".* This means for the here applied linear Mohr-Coulomb (M-C) formulation $\tau_{nt} = \bar{R}^{\tau} - \mu \cdot \sigma_n$. Herein, the value μ is an intrinsic friction property of the material and $\bar{R}^{\tau}$ the so-called cohesion strength. The shear stresses $\tau_{t\lambda}$, $\tau_{n\lambda}$ are zero together with the normal stress σ_λ. The normal stress σ_t must be accounted for in the investigation but will finally have no influence, which has to be proven when following Mohr and this must be shown.

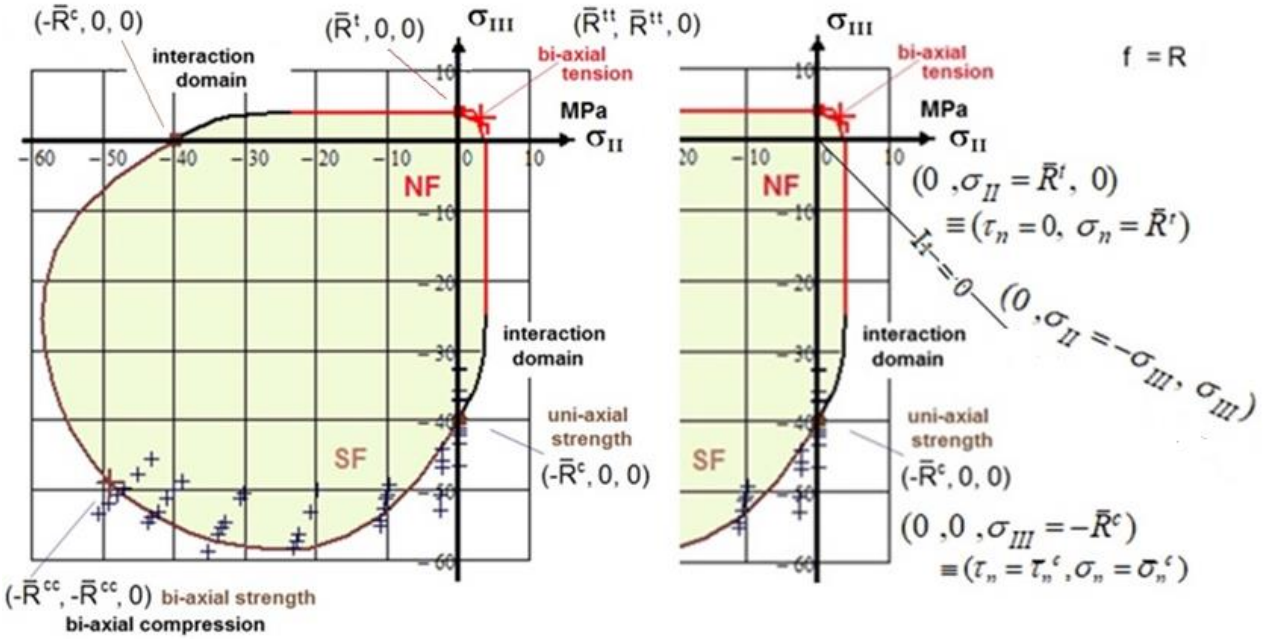

Fig.6-2: Bi-axial failure curve of Normal Concrete, 2D-test data set

Fig.6-3 displays the 2nd quadrant of the bi-axial failure curve formulated in structural stresses and that fully represents the Mohr-Coulomb curve domain. The joint mode situation of the Mohr-Coulomb curve - capturing the transition zone between the pure mode domains NF and SF - requires the application of the interaction equation $(Eff^{NF})^m + (Eff^{SF})^m = 1$. It spans over the regime $0 < \sigma_{III} < \bar{R}^t$ and the Lode angles $(-30° < \delta < +30°)$.

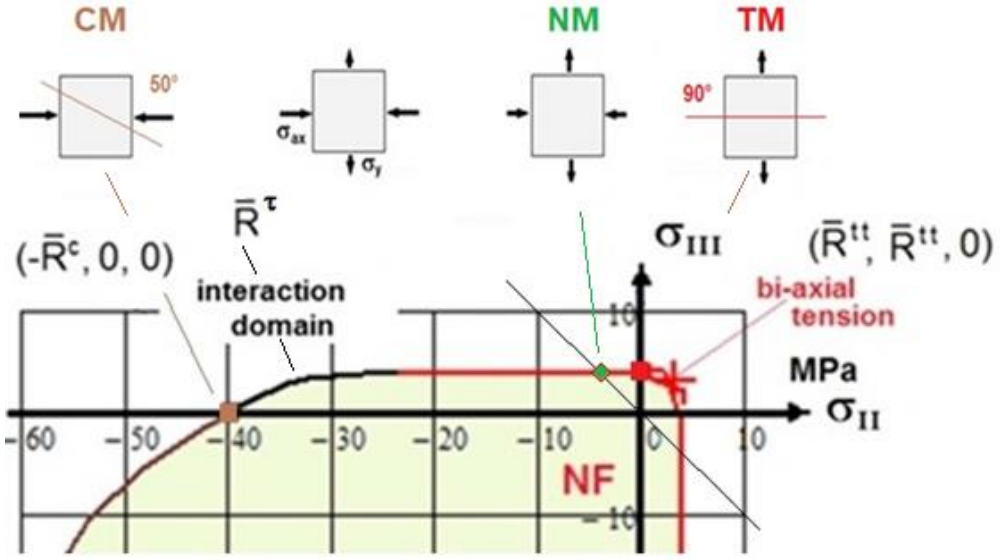

Fig.6-3 Second quadrant and associated stress states, transition zone between the 2 mode domains SF, NF

6.3 Improved Mapping of Failure Stress data with Derivation of a more realistic $\Theta_{fp}°(\vartheta)$

The F^{SF} curve outlines a local shortcoming of the relatively simple FMC-based SF-formulation. In design-verification the Eff^{SF} contribution to *Eff* is not a problem because the interaction is a conservative procedure. However, when searching a local fracture angle $\Theta_{fp}°$ a correction should be material-dependently applied to numerically determine a better value for $\Theta_{fp}°$.

To sort out a procedure it is helpful to know how the pure mode efforts of the activated modes NF and SF share its influence with σ_{II}. *Fig.6-4* shows the courses of the efforts Eff^{NF} (= Eff^{σ}) and Eff^{SF} (= Eff^{τ}) representing the components of the *measured* fracture stress curve.
According to the fact that the compression strength point is located on the compressive meridian and the tensile strength point on the tensile meridian the different Lode angle ϑ is to consider in order to achieve an accurate approach when investigating the Mohr-Coulomb curve. This requires to not just consider the rotationally-symmetric Eff^{SF} but $Eff^{SF\Theta}$, too.

Mathematically-caused, Eff^{SF}-curve and $Eff^{SF\Theta}$–curve become positive in the pale colored curve part and numerically contribute its effort portion to the total effort (again, no problem for designing). This is physically not accurate and could be by-passed by a query in the numerical process not permitting - after a previous decay – the newly increase. Also one could apply a decay function that – physically logically - keeps Eff^{SF} zero, like for the UD material in chapter 7.
The shear material stressing effort $Eff^{\tau} = Eff^{SF}$ must physically become zero at the tensile strength point (0, R^{t}). This specific shortcoming cannot be by-passed by an increased interaction exponent m. This is brought about by a correction function that defines the decay of Eff^{τ} and is practically performed by setting $Eff^{\tau} = 0$ at $\sigma_{II} = 0$. As function was taken an exponential one

$$f_d = 1/(1+\exp(\frac{c_{1d}+\sigma_{II}}{c_{2d}}), \quad \text{with} \quad c_{1d}, c_{2d} \text{ fixed at } (-\bar{R}^{c}, 0.995), (-0.01, +0.01).$$

The corrected Eff^{SF}–curve brings the desired improvement and lowers $\bar{R}^{\tau}$ from 12.5 → 11.

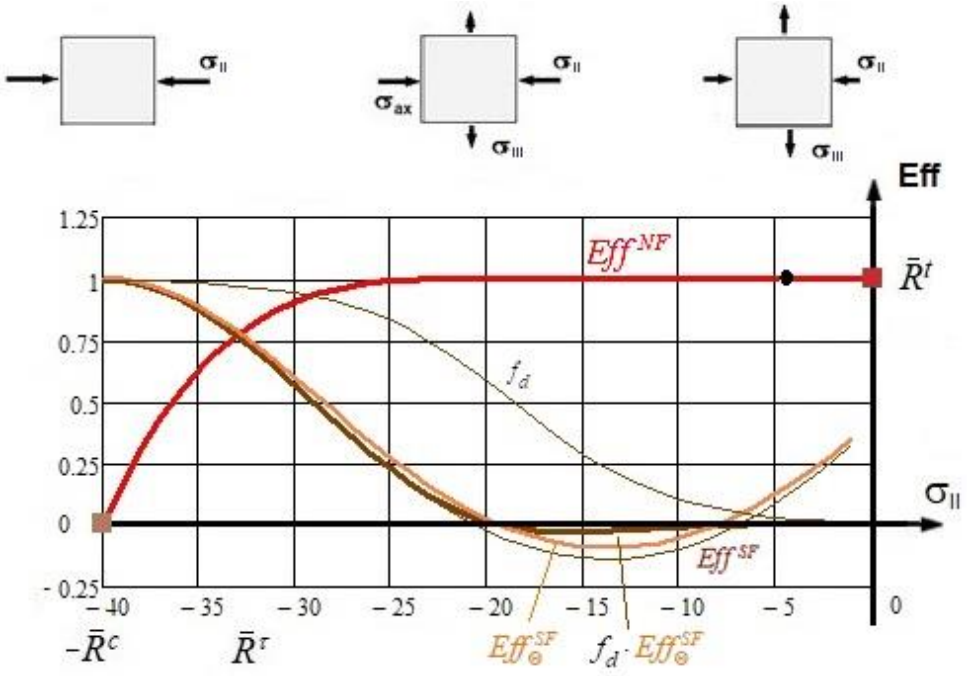

Fig.6-4: Visualisation of the course of the pure mode efforts Eff^{mode} supporting the need to interact them in the case of bi-axial stress states to not exceed Eff = 100 %. c_{1d} = 18.6, c_{2d} = 4.04.
Eff^{NF} , Eff^{SF}, $Eff^{SF\Theta}$, $f_d \cdot Eff^{SF\Theta}$

With the correction above the mandatory locally better $\Theta_{fp}°$ can be computed and then the envisaged transformation performed.

Note, please: Applying - instead of the present Modal SFC - a so-called Global SFC, which globally maps in a single mathematical equation all test data and modes, a similar difficulty would be found too.

6.4 Derivation of a realistic Modes-Interaction Considering Mohr-Coulomb Curve $\tau_n(\sigma_n)$

Table 6-2 summarizes the relations for the derivation of $\tau_{nt}(\sigma_n)$ and $\Theta_{fp}°$ from a given fracture curve $\sigma_{II}(\sigma_{III})$. It is to consider the change of the fracture plane angle $\Theta_{fp}°$ with the Lode angle ϑ from $\Theta_{fp}{}^{c}°$ at $\vartheta = -30°$ on. The biggest challenge is the necessary differentiation of the interaction equation $Eff = 1$ within Mathcad. This further produces a giant formula output, that 'generously' can be cut down by using addition theorems and by inserting the given structural stresses input via its invariants I_1, J_2, J_3. That is the advantage of invariants: *They do not depend on the coordinate system. Hence one can switch within one system being here the Mohr-stresses one!*

Fig.6-5 displays several failure curves and the course of the altering fracture plane angle $\Theta_{fp}°$. Its left part presents the entities in a structural stresses diagram and the right part in a Mohr stresses diagram. This involves the Linear Mohr-Coulomb fracture curve and the real SF-NF interaction curve $\tau_{nt}(\sigma_n)$. The 3 Mohr circles are incorporated.

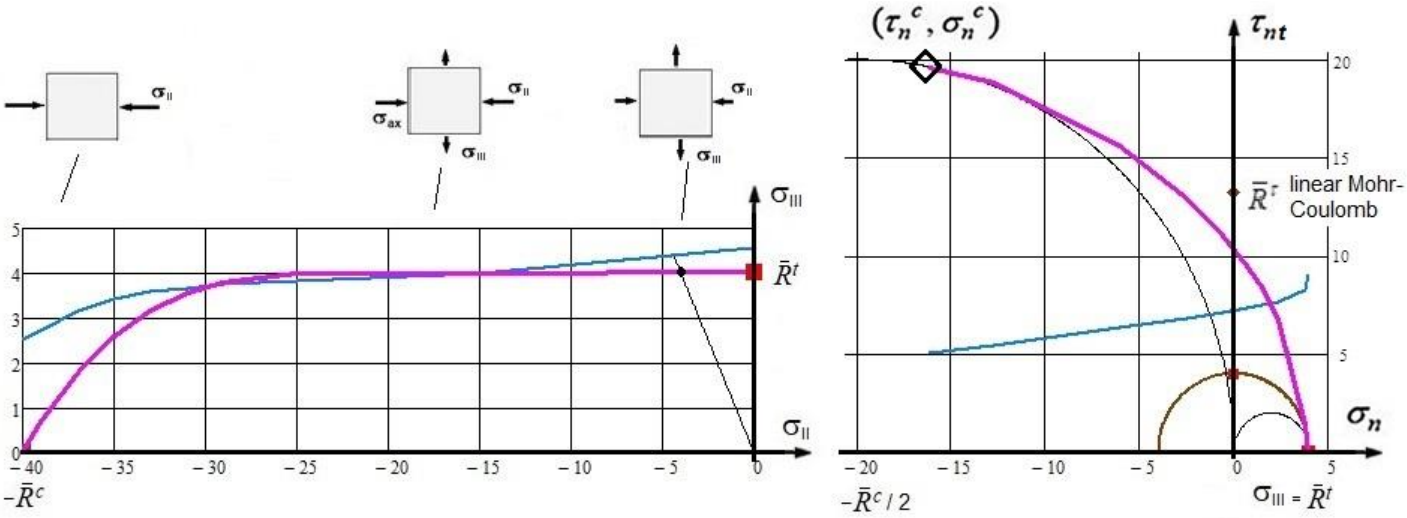

Fig.6-5: Joint display of the magenta failure curve in structural stresses (left) and in Mohr stresses (right) with fracture angle increase $\Theta_{fp}°$, scaled by twenty (left) and ten (right) .

Model: 120°-rotationally-symmetry parameters and improved mapping of measured failure curve by f_d

$c_{1\Theta}{}^{SF} \cdot \Theta^{SF} = 1 + c_{2\Theta}{}^{SF}$ with $c_{2\Theta}{}^{SF}$ the friction parameter, $c_{2\Theta}{}^{SF} = 3.70$, $c_{1\Theta}{}^{SF} = 5.88$, $d^{SF} = 0.49$,

$\bar{R}^t = 4$ MPa, $\bar{R}^c = 40$ MPa, $\Theta^c_{fp}{}^{\circ} = 50.5°$, $C^c = -0.192$, friction value $\mu = 0.195$,

$\bar{R}^{\tau} = 11$ MPa, $\Theta_{fp}{}^{\circ} = 72°$, $\sigma_{II} = -32$ MPa, $\sigma_{III} = 3.3$ MPa, $\delta = -25°$.

$\tau^c_{nt} = 19.6$ MPa, $\sigma^c_n = -16.2$ MPa, $c_{1d} = 18.6$, $c_{2d} = 4.04$, $\Theta^{SF} = \Theta^c = \Theta^{CM} = 0.51$.

The interpretation of the two diagrams in Fig. 6-5 leads to the following results:

- ✓ The interaction equation *Eff* - representing the surface of the fracture body - in structural stresses can be transferred into Mohr stresses
- ✓ The alteration of the fracture plane angle $\Theta_{fp}°$ can be computed
- ✓ Complete failure danger is composed of portions Eff^{NF} and Eff^{SF}, following the idea of the FMC that NF and SF commonly add its *Eff* portions. This leads to the conclusion that the $\Theta_{fp}°$ is approximately 70° at the cohesive strength point
- ✓ The SF approach could not offer a full accuracy of the fracture plane angle $\Theta_{fp}°$ and the Mohr-Coulomb curve to be predicted. Eff^{SF} had to be physically adjusted by a decay function f_d.

Table 6-2: Transformation of a 2D structural stresses-based failure curve into a Mohr-Coulomb one

* Task: Known $\sigma_{II}, \sigma_{III}; \bar{R}^t, \bar{R}^c$. To determine: σ_n, τ_{nt}, $\Theta_{fp}°(C)$, $C = \cos(2 \cdot \Theta_{fp}° \cdot \pi / 180°))$

σ_λ, $\tau_{t\lambda}$, $\tau_{n\lambda} = 0$. $\eta = \sigma_{II} - \sigma_{III}$, $\sigma_{II} + \sigma_{III} = \sigma_n + \sigma_t = I_1$, $\sigma_n - \sigma_t = C \cdot \eta$,

$\sigma_t = \sigma_n - C \cdot \eta$, $\sigma_n = 0.5 \cdot [(C+1) \cdot \sigma_{II} + (-C+1) \cdot \sigma_{III}]$, $\tau_{nt} = -0.5 \cdot \sqrt{1-C^2} \cdot \eta$.

* Interaction equation because 2 modes are activated: $(Eff^{NF})^m + (Eff^{SF})^m = 100\%$

$$Eff^{NF} = \frac{\sqrt{4 \cdot [(\sigma_n - \sigma_t)^2 + \sigma_t^2 + \sigma_n^2 + 6 \cdot \tau_{nt}^2] / 6 - (\sigma_n + \sigma_t)^2 / 3} + (\sigma_n + \sigma_t)}{2 \cdot \bar{R}^t},$$

$$\frac{Eff^{SF}}{f_d} = \frac{c_{2\Theta}^{SF} \cdot (\sigma_n + \sigma_t)}{2 \cdot \bar{R}^c} + \frac{\sqrt{(c_{2\Theta}^{SF} \cdot (\sigma_n + \sigma_t))^2 + 2 \cdot c_{1\Theta}^{SF} \cdot \Theta^{SF} [(\sigma_n - \sigma_t)^2 + \sigma_t^2 + \sigma_n^2 + 6 \cdot \tau_{nt}^2]}}{2 \cdot \bar{R}^c}$$

* Solution of the task: equalizing the slopes at each stress state $\sigma_{II}(\sigma_{III})$

Slope 1: from differentiation of structural stresses-linked Mohr stresses delivers

$$\frac{d\tau_{nt}}{d\sigma_n} = \frac{(s^2 - c^2) \cdot \eta}{-2 \cdot s \cdot c \cdot \eta} = \frac{C}{S} = \frac{C}{\sqrt{1-C^2}}$$, valid uni-axially and bi-axially

Slope 2: from differentiation of the interaction equation, abbreviation $\eta_m = 2\sigma_n - C \cdot \eta$

$$Eff^{NF} = \left\{ \sqrt{4 \cdot [(C \cdot \eta)^2 + (\sigma_n - C \cdot \eta)^2 + \sigma_n^2 + 6 \cdot \tau_{nt}^2] / 6 - \eta_m^2 / 3} + \eta_m \right\} / 2 \cdot \bar{R}^t, \quad \Theta^{NF} = 1$$

$$Eff^{SF} = \left\{ c_{1\Theta}^{SF} \cdot \eta_m + \sqrt{(c_{2\Theta}^{SF2} \cdot \eta_m^2 + 2 \cdot c_{1\Theta}^{SF} \cdot \Theta^{SF} \cdot [(C \cdot \eta)^2 + (\sigma_n - C \cdot \eta)^2 + \sigma_n^2 + 6 \cdot \tau_{nt}^2]} \right\} / 2 \cdot \bar{R}^c$$

$F = (Eff^{NF})^m + (Eff^{SF})^m$ with $dF / d\sigma_n$ and $dF / d\tau_{nt}$

Equating the 2 equations and replacing Mohr stresses by structural stresses

$$\frac{C}{\sqrt{1-C^2}} = -\frac{dF / d\sigma_n}{dF / d\tau_{nt}}$$ a huge formula for the determination of the fracture angle measure C

$$\Theta^{SF}(\vartheta) = \sqrt[3]{1 + d^{SF} \cdot \sin(3\vartheta)} = \sqrt[3]{1 + d^{SF} \cdot 1.5 \cdot \sqrt{3} \cdot J_3 \cdot J_2^{-1.5}}$$ inserting

$6J_2 = 2 \cdot (\sigma_{II}^2 - \sigma_{II} \cdot \sigma_{III} + \sigma_{III}^2)$, $27J_3 = (-\sigma_{II} - \sigma_{III}) \cdot (2\sigma_{II} - \sigma_{III}) \cdot (2\sigma_{III} - \sigma_{II})$

Implicite solution when determining C for the bi-axial stress states $(\sigma_{II}, \sigma_{III})$

$\sigma_n = (C+1) \cdot 0.5 \cdot \sigma_{II} + (1-C) \cdot 0.5 \cdot \sigma_{III}$, $\tau_{nt} = -0.5 \cdot \sqrt{1-C^2} \cdot (\sigma_{II} - \sigma_{III})$

$a = (12J_2 - I_1^2) / 3$, $b = \left((c_{2\Theta}^{SF} \cdot I_1 + \sqrt{d}) / 2\bar{R}^c \right)^{m-1}$,

$c = 4I_1 \cdot (c_{2\Theta}^{SF2} + c_{1\Theta}^{SF} \cdot \Theta^{SF})$, $d = c_{2\Theta}^{SF2} \cdot I_1^2 + 2c_{1\Theta}^{SF} \cdot \Theta^{SF} \cdot 6J_2$.

Vorgabe C:= - 0.1 and inserting points $(\sigma_{II}, \sigma_{III})$

$$\frac{C}{\sqrt{1-C^2}} = -\frac{0.5 \cdot \sqrt{a} \cdot [(\bar{R}^t \cdot b \cdot c) / 4] + \bar{R}^c \cdot \sqrt{d} \cdot \left(\frac{2\sigma_n + \sqrt{a} - C \cdot \eta}{2\bar{R}^t}\right)^{m-1} + \bar{R}^t \cdot c_{2\Theta}^{SF} \cdot b \cdot \sqrt{d}}{\tau_{nt} \cdot [\bar{R}^c \cdot \sqrt{d} \cdot \left(\frac{2\sigma_n + \sqrt{a} - C \cdot \eta}{2\bar{R}^t}\right)^{m-1} + 3\sqrt{a} \cdot \bar{R}^t \cdot c_{1\Theta}^{SF} \cdot \Theta^{SF} \cdot b]}$$

Search(C) $\rightarrow$ equation for the fracture angle measure $C(\Theta_{fp}°)$ and for σ_n, τ_{nt}

$C = C(\sigma_{II}, \sigma_{III}) = \cos(2 \cdot \Theta_{fp})$, $\Theta_{fp} = 0.5 \cdot \arccos C$, $\Theta_{fp}° = \Theta_{fp} \cdot 180° / \pi$,

$\sigma_n = (C+1) \cdot 0.5 \cdot \sigma_{II} + (1-C) \cdot 0.5 \cdot \sigma_{III}$, $\tau_{nt} = -0.5 \cdot \sqrt{1-C^2} \cdot (\sigma_{II} - \sigma_{III})$.

7 Fracture Body, Angle $\Theta_{fp}{}^{c}$ and altering Θ_{fp} of Fiber-Reinforced Matrices FRP, FRC

Extensively linked to Mohr-Coulomb is friction in the σ_2-σ_3–plane. This so-called quasi-isotropic plane is design-relevant for the load-carrying rods and loops in wind energy rotor blades, helicopter blades and at the fiber-strand turning locations of hangers of 'network arch bridges' (Stuttgart Stadtbahn bridge 2020, CFRP hanger) and for bridges from Baltico fabricated with a strand winding technology. The following part is applicable for fiber-reinforced polymer matrix and for fiber-reinforced concrete matrix elements.

7.1 Invariants, strength fracture conditions SFCs and fracture body

As with the isotropic materials at first the derivation of the UD-SFCs shall be shortly presented. Therefore invariants and associated stresses used for the transversely-isotropic UD material are collected in *Fig.7-1*.

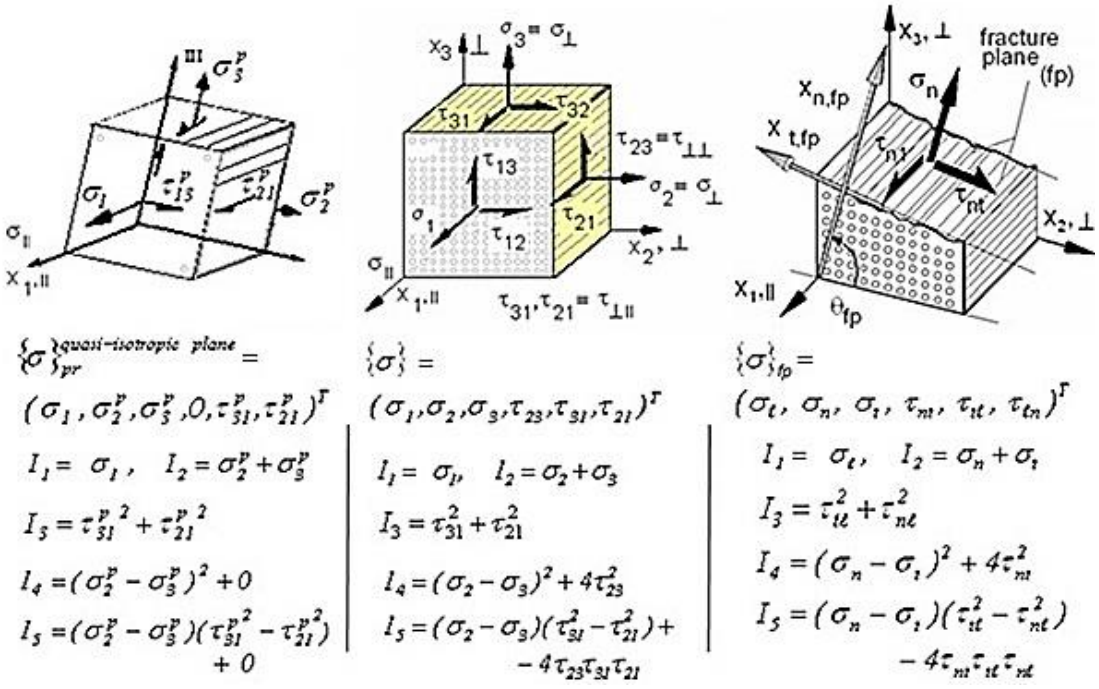

Fig.7-1: UD-Invariants and associated stresses (indices $\ell \equiv 1$, $p \equiv pr$)

Applying again the author's invariant-based Failure Mode Concept (FMC) 5 SFCs are to be derived in total. Replacing the UD-invariants by the stresses they are composed of and after simplifications with practical numerical modifications to by-pass probable 3D-solution problems the set of UD-SFCs for fiber-reinforced material, embedded in a matrix (plastic or mortar), is given in *Fig.7-2*.

The interaction of the separate five modes, 2 FFs (*Fiber-Failure*) + 3 IFFs (*Inter-Fiber-Failure*), is performed as with the isotropic material, by applying the interaction equation

$$Eff^m = (Eff^{\|\tau})^m + (Eff^{\|\sigma})^m + (Eff^{\perp\sigma})^m + (Eff^{\perp\tau})^m + (Eff^{\perp\|})^m = 1\,.$$

LL:

(1) Due to mapping experience in the transition zones the interaction exponent is 2.5 < m < 3. This is as for isotropic materials. For reasons of simplicity the same value is applied for all transition zones. The smaller the value is the more the design verification is conservative!

(2) The Poisson effect is to consider in the macro-mechanical SFCs because bi-axial compression strains the filament without any external σ_1. In Fig.7-2 this fiber constituent failure is considered in FF1.

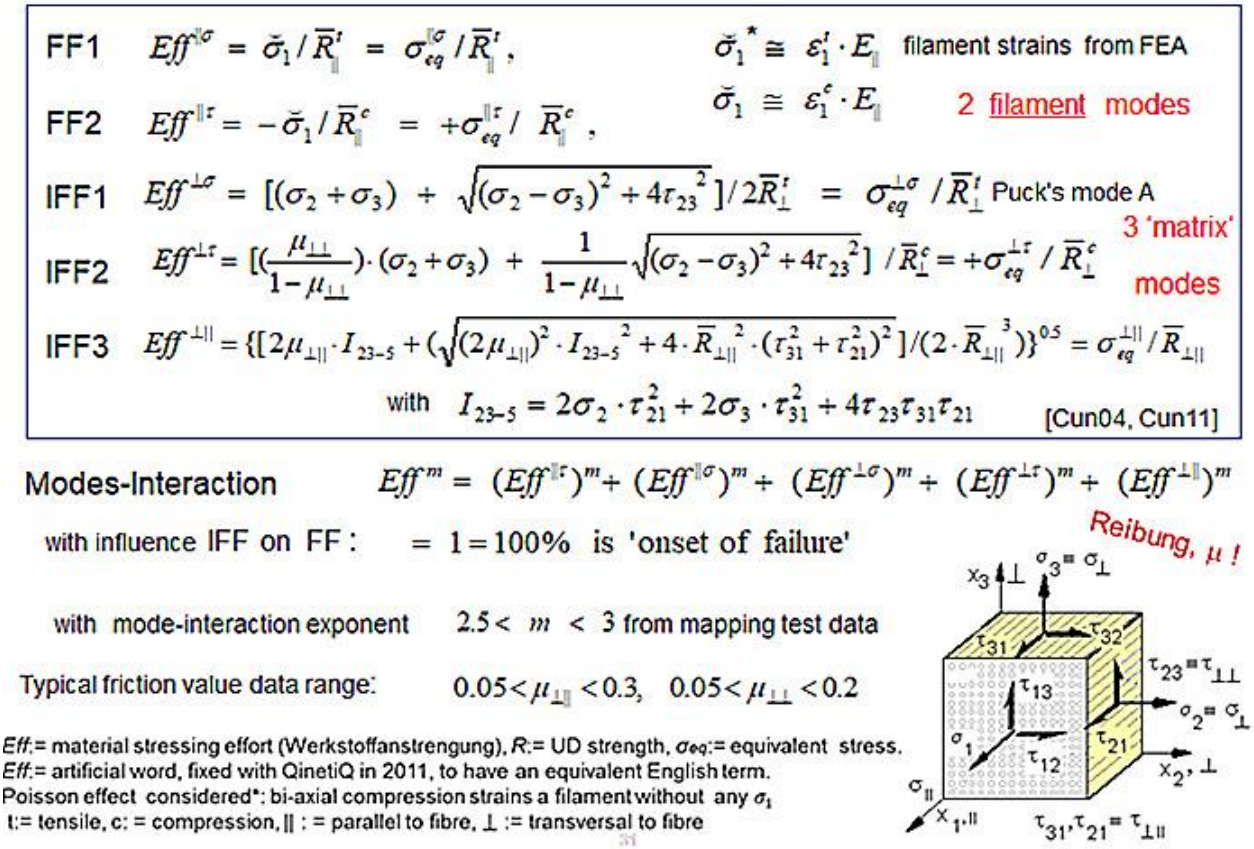

Fig.7-2: UD-SFCs for 'Onset of fracture failure', mode interaction, and value ranges [Cun04,12]

<u>Fig.7-3</u> *presents a visualization of the associated fracture body surface. The composite denotations follow the guideline VDI 2014, sheet 3 [VDI 06].*

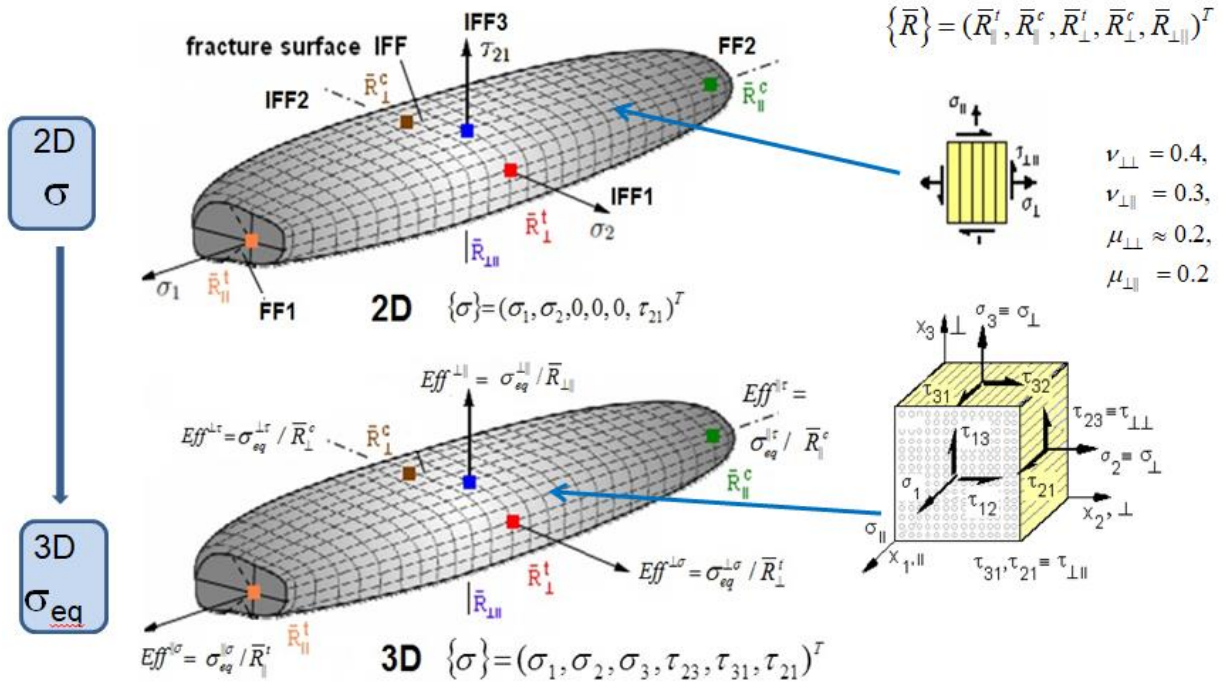

Fig.7-3: Fracture body of the UD material (lamina, lamella, sheet, tape) for 2D and 3D stress states

The figure above further depicts an essential outcome, found by the author after many years:

Taking equivalent stresses instead of lamina stresses one can apply the 2D fracture failure body in the 3D case, too!

NOTES:

(1) There are numerous SFCs describing fracture failure of the uni-directionally fiber-reinforced material family. In the World-Wide-Failure-Exercises-I and –II, practically running from 1992 to 2012. R. Cuntze and A. Puck could place their theories at the top. Cuntze participated successfully with his 'Invariant-based, mode-distinguishing FMC theory' and Puck with his 'Mohr-Coulomb-based Action Plane Theory'

(2) The invariant-based formulation for IFF2 is a pretty simple approach. It is mathematically homogeneous which means that *F = Eff*. An approach is always a compromise

(3) Here, it is - *like for the isotropic concrete material*- a compromise 'on the safe reserve factor side', however, the approach is not accurate enough, if a fracture angle is to determine in cases of not highly brittle materials such as with values below $R_\perp^{c'}/ R_\perp^{t'} < 5$. This is valid for the present UD material.

7.2 Main fracture curves or cross-sections of fracture body in structural stresses

The main cross-section of the fracture body is depicted in *Fig.7-4* with the bare mode mappings (left) together with a demonstration of the goodness of the interaction equation in the transition zone (right).

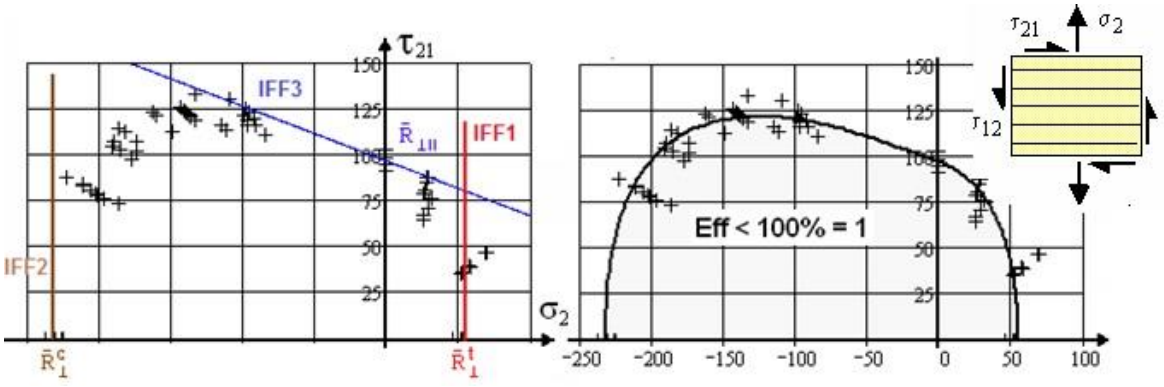

Fig.7-4: Interaction, demonstrated in the IFF cross section, CFRP failure curve. 2D stress state within the lamina, m=2.7

In this paper, the first (positive) quadrant is not of interest. Focus here is the Mohr-Coulomb-associated quasi-isotropic plane $\sigma_2(\sigma_3)$, displayed in *Fig.7-5*. Applying the shear fracture SFC IFF2 (*brown*) and computing the interaction curve (*magenta*) IFF1-IFF2 the failure curves in three quadrants are obtained. The curves are symmetric to the diagonal. For further information in *Fig.7.5* a sketch of the classical tension/compression-torsion UD test specimen is included. Also a 3D fracture failure body $\tau_{21}(\sigma_2,\sigma_3)$ is shown below. One can assume that the interaction curve does not optimally map the usual course of test data (like for isotropic mapping) or – respectively - the mapping quality of IFF2 is not fully sufficient if the alteration of the fracture angle Θ_{fp} in the transition zone is to determine.

This transition zone between a normal fracture mode domain NF and a shear fracture mode domain SF is ruled by interaction and corresponds to the bi-axially stressed Mohr-coulomb curve. This requires both the *Eff-modes* for the insertion into the interaction equation.

As before with isotropic materials: The Mohr Envelope is a bi-axial fracture stress curve and the 2nd quadrant of $\sigma_3(\sigma_2)$ is identical to the so-called Mohr envelope or Mohr-Coulomb curve $\tau_{nt}(\sigma_n)$, respectively. The interaction curve (magenta) can be dedicated to the basic Mohr-Coulomb curve

namely from the compression strength point till the tensile strength point, see *Fig.7-6* and compare *Fig.4-5*.

Like in the isotropic case the bi-axial stress ruled Mohr-Coulomb curve is dominated by two modes, IFF2 (SF) and IFF1 (NF). Therefore, attention must be paid again to the interaction of both these modes in the transition zone in order to finally obtain an accurate fracture angle Θ_{fp}, being the precondition to determine the two Mohr stresses τ_{nt}, σ_n with high fidelity.

Span: $(\tau_{nt}^{\ c}, \sigma_n^{\ c}) \rightarrow (\bar{R}_{\perp\perp}^{\ \tau},\ 0) \rightarrow (0,\ \sigma_n = \bar{R}_{\perp}^{\ t})$ or $(\sigma_2 = -\bar{R}_{\perp}^{\ c},\ 0) \rightarrow (\sigma_2,\ \sigma_3 = -\sigma_2) \rightarrow (0,\ \sigma_3 = \bar{R}_{\perp}^{\ t})$.

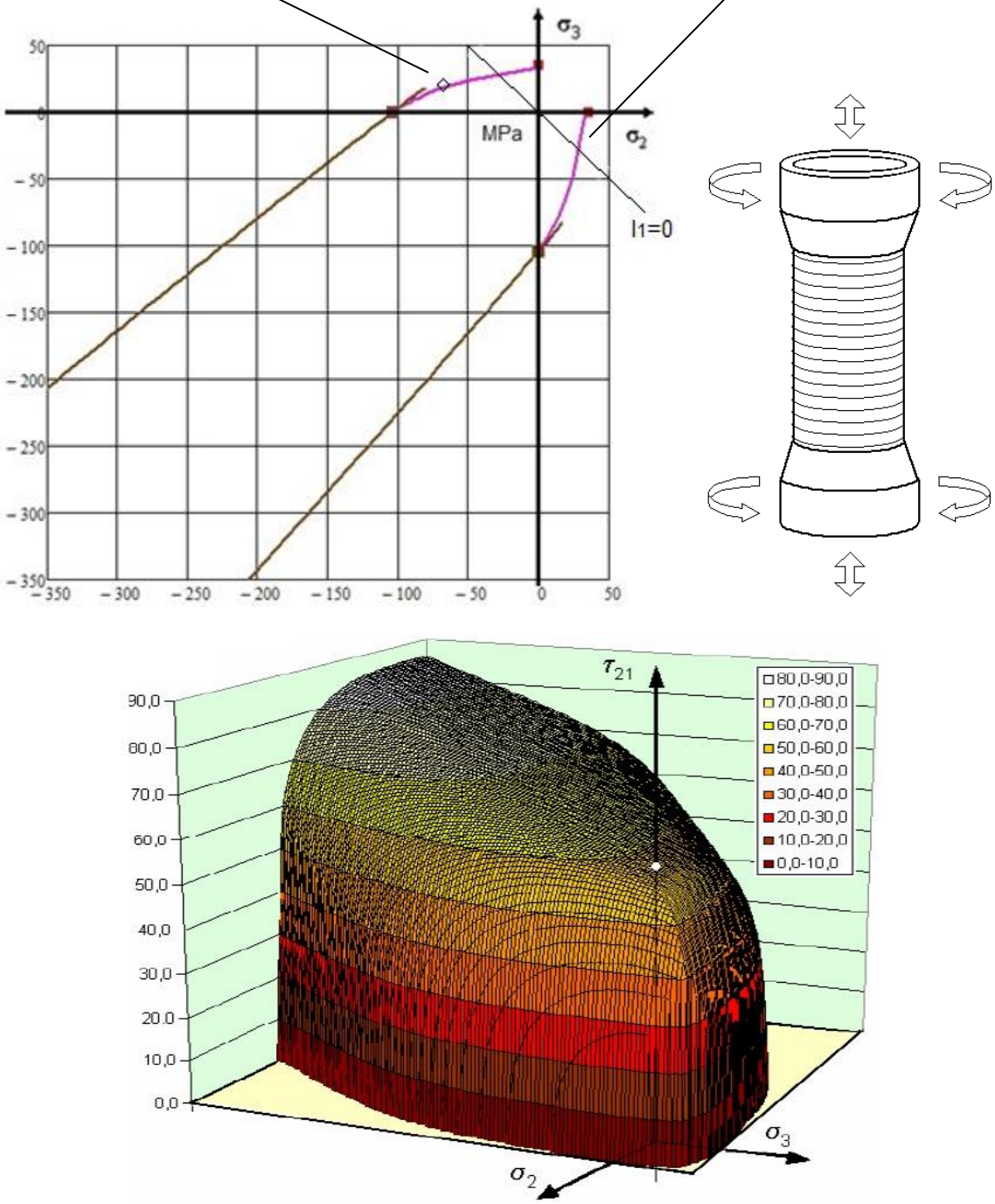

*Fig. 7-5: The UD fracture stress curves in the quasi-isotropic plane.(right) Scheme of the 90°-wound tension/compression-torsion test specimen, (down) 3D fracture body [Cuntze-Sukarie **1997**]*

In *Fig.7-6* the failure curve in the second quadrant of *Fig.7-5* is enlarged. For additional information $\tau_{23}(\sigma_2)$ is included.

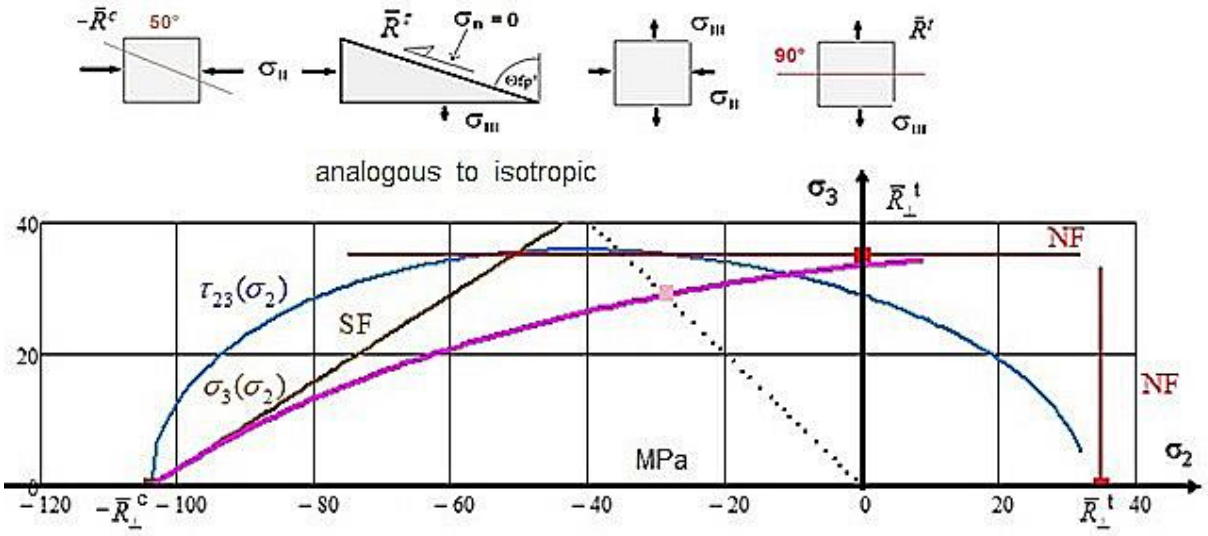

Fig. 7-6, zoom of Fig.7-5 upper, 2nd quadrant: (above) Alteration of fracture angles $\Theta_{fp}°$ allocated to the associated failure stress state $\sigma_2(\sigma_3)$, faced in the transition zone.

$\bar{R}_{\perp}^{c} = 104MPa,\ \bar{R}_{\perp}^{t} = 35\ \text{MPa},\ C_{fp}^{c} = -0.174,\ \Theta_{fp}° = 51°,\ a_{\perp\perp} = 0.26,\ \mu_{\perp\perp} = 0.18 \cong -C_{fp}^{c}$

As with the isotropic material the magenta curve cannot accurately map the course of test data. It shows that with the relatively simple IFF2-FMC approach the shear effort $Eff^{\perp\tau}$ cannot become zero. This numerical behavior is a shortcoming of the IFF2 approach in the transition zone between the two modes SF and NF. An accurate alteration of the fracture angle $\Theta_{fp}°$ and of the associated Mohr stresses τ_{nt}, σ_n is not to achieve with the mathematical course of IFF2 or $Eff^{\perp\tau}$, respectively. In this context it is essential how the pure mode efforts of the activated modes IFF1 and IFF2 ($Eff^{\perp\tau}$) share its influence along the σ_2-axis, *Fig.7-7*.

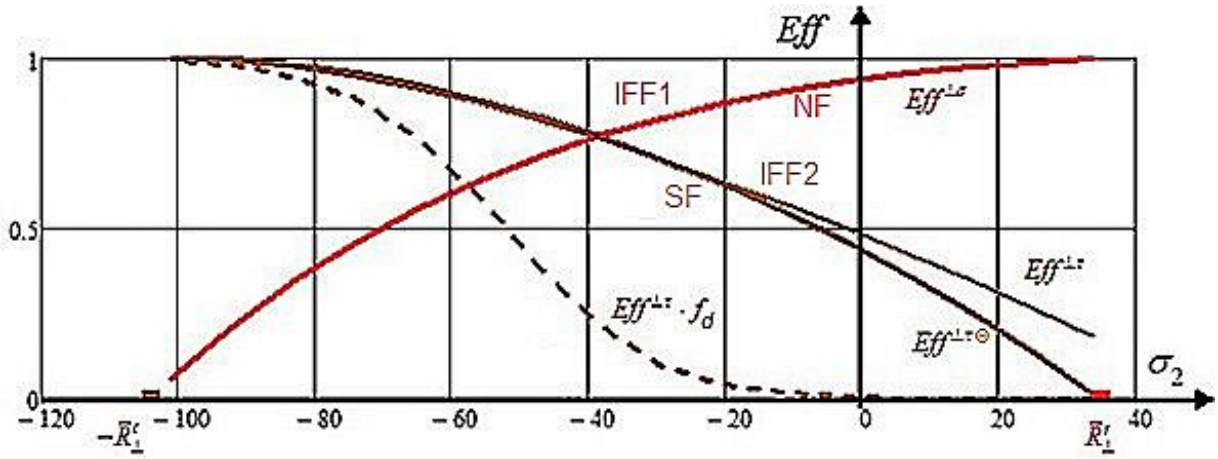

Fig.7-7: Course of the two efforts Eff^{NF}, Eff^{SF} components of the fracture stress curve
$c_1 = 48.3$, $c_2 = 10.5$

$Eff^{\perp\tau}$ firstly become zero at $\sigma_2 = \sigma_3 = R^{tt}$, most often termed bi-axial tensile 'strength'. This zero point is physically too 'late'. Again, this is not problematic for design verification but for an

accurate transformation of the test curve formulated in structural stresses into a Mohr stress formulation. SF must become physically zero when reaching the pure NF domain. This is brought about by a correction function f_d that defines the decay of $Eff^{\perp\tau}$ and is practically performed by setting $Eff^{\perp\tau} = 0$ at $\sigma_2 = 0$. As function for the decay the previously applied exponential one is taken again

$$f_d = 1/(1+\exp(\frac{c_{1d}+\sigma_2}{c_{2d}}), \quad \text{with} \quad c_{1d}, c_{2d} \text{ fixed at } (-\bar{R}_{\perp}^{c}, 0.995), (-0.01, +0.01).$$

7.3 Relations of friction parameter $a_{\perp\perp}$ to fracture angle Θ_{fp}^{c} and to friction value $\mu_{\perp\perp}$

Again, the measurement of a realistic fracture angle – based on the usually small-scale test level - is practically not possible. The determination of the curve parameters $a_{\perp\perp}$ and $b_{\perp\perp}$ by mapping the course of test data points is the practical procedure. Then, the relationship of the curve parameter to the friction value and to the fracture angle can be derived according to <u>*Table 7-1*</u>.

Analogous to the isotropic case the required IFF2-relationships are to derive:
The basic assumption, lying behind all action-plane SFCs (e.g. UD Puck/Hashin) is the *brittle-fracture hypothesis* which goes back to O. Mohr's "*The strength of a material is determined by the Mohr stresses on the fracture plane".* This means for the here again applied Linear Mohr-Coulomb (M-C) formulation $\tau_{nt} = \bar{R}_{\perp\perp}^{\tau} - \mu_{\perp\perp} \cdot \sigma_n$. The friction value μ is an intrinsic property of the UD material and $\bar{R}_{\perp\perp}^{\tau}$ the so-called cohesion strength which corresponds to Puck's fracture plane resistance $\bar{R}_{\perp\perp}^{A}$. In [*Puc96*] $\bar{R}_{\perp\perp}^{A}$ is used as a sixth, model-required 'strength' entity, see *Fig.6-6*.
If IFF occurs in a parallel-to-fibre plane of the UD lamina, the components of the failure stress vector are the normal Mohr stress σ_n and the two Mohr shear stresses τ_{nt} and τ_{n1}. The shear stress τ_{tl} and the normal stress σ_t will have no influence and is to be proven. τ_{n1} belongs to IFF 3 and therefore is not of interest in the following investigations.
The transformation of the SFC IFF2 in lamina stresses into a Mohr stresses one works via the addition theorems in *Table7-1.* In the equations the bar over is dropped.

<u>*LL*</u>***:***

- *(1) The Linear Mohr-Coulomb model can be employed to obtain a sufficiently good relationship for the determination of the friction value μ in the compressive stress point $\sigma_2 = -\bar{R}_{\perp}^{c}$.*
- *(2) Establishing the relationship it is assumed that the tangent of the FMC-curve has the same value as that of the straight Linear Mohr envelope curve $\tau_{nt}(\sigma_n)$ in the touch point with Mohr's circle, see respective figure*
- *(3) σ_1 is not relevant. The shear stress τ_{23} can be assumed zero because it would anyway vanish after a principal stress transformation. No reduction of generality is caused*
- *As can be concluded from Table-7-1: The stress σ_t has no influence! It is not representative such as Mohr supposes. Failure responsible are τ_{nt} and σ_n, only. But mind: For the differentiation σ_t cannot be simply set zero but must be considered due to its relation to σ_n,*
- *Above derivation further proves that, if really desired, the fracture plane angle Θ_{fp}^{c} of an UD-material could be determined from the FMC-based SFC formulated in structural stresses*
- *Viewing Fig.7-6 the cohesive strength $\bar{R}_{\perp\perp}^{\tau}$ still belongs to the transition zone of the normal fracture mode domain IFF1 and therefore not alone to the shear fracture mode domain IFF2.*

Table 7-1: Derivation of the Mohr stresses-transformed FMC-based strength failure conditions

$$Eff^{\perp\tau} \equiv F^{IFF2} = [a_{\perp\perp}\cdot I_2 + b_{\perp\perp}\cdot\sqrt{I_4}] \,/\, \bar{R}_{\perp}^{c} = 1, \quad a_{\perp\perp} = b_{\perp\perp} - 1 \text{ after inserting } \bar{R}_{\perp}{}^{c}$$

$$= [a_{\perp\perp}\cdot(\sigma_2+\sigma_3) + b_{\perp\perp}\cdot\sqrt{(\sigma_2-\sigma_3)^2+4\tau_{23}{}^2}] \,/\, \bar{R}_{\perp}^{c} = 1$$

$$= [a_{\perp\perp}\cdot(\sigma_2{}^{p}+\sigma_3{}^{p}) + b_{\perp\perp}\cdot\sqrt{(\sigma_2{}^{p}-\sigma_3{}^{p})^2+0^2}] \,/\, \bar{R}_{\perp}^{c} = 1 \;\leftarrow \text{ 2 structural stresses}$$

$$= [a_{\perp\perp}\cdot(\sigma_n+\sigma_t) + b_{\perp\perp}\cdot\sqrt{(\sigma_n-\sigma_t)^2+4\tau_{nt}{}^2}] \,/\, \bar{R}_{\perp}^{c} = 1 \quad \leftarrow \text{ 3 Mohr stresses.}$$

* Derivation of the IFF2 slope equation in Mohr stresses: $\sigma_\lambda = 0$

$$\frac{dF}{d\sigma_n}\cdot\bar{R}_{\perp}^{c} = a_{\perp\perp} + b_{\perp\perp}(\sigma_n-\sigma_t)/\sqrt{(\sigma_n-\sigma_t)^2+4\tau_{nt}{}^2}, \quad \frac{dF}{d\tau_{nt}}\cdot\bar{R}_{\perp}^{c} = 4\cdot b_{\perp\perp}\tau_{nt}/\sqrt{(\sigma_n-\sigma_t)^2+4\tau_{nt}{}^2}$$

$$\frac{d\tau_{nt}}{d\sigma_n} = -\frac{dF}{d\sigma_n}/\frac{dF}{d\tau_{nt}} = -\left[\frac{b_{\perp\perp}\cdot(\sigma_n-\sigma_t) + a_{\perp\perp}\cdot\sqrt{(\sigma_n-\sigma_t)^2+4\tau_{nt}{}^2}}{4\cdot b_{\perp\perp}\cdot\tau_{nt}}\right], \text{ impl. differentiation}$$

* Transformed structural stresses and addition theorems used: $\tau_{23} = 0$

$$\sigma_n = c^2\cdot\sigma_2 + s^2\cdot\sigma_3, \;\; \sigma_t = s^2\cdot\sigma_2 + c^2\cdot\sigma_3, \;\; \tau_{nt} = -s\cdot c\cdot\sigma_2 + s\cdot c\cdot\sigma_3;$$

$$s^2+c^2 = 1, \;\; S^2+C^2 = 1, \;\; C = c^2-s^2 = 2c^2-1, \;\; S = 2sc, \;\; c^2 = (C+1)\cdot 0.5, \;\; s^2 = (1-C)\cdot 0.5$$

$$\sigma_n+\sigma_t = \sigma_2+\sigma_3, \;\; \sigma_n-\sigma_t = C\cdot(\sigma_2-\sigma_3), \;\; \tau_{nt} = -s\cdot c\cdot(\sigma_2-\sigma_3) = -0.5\cdot S\cdot(\sigma_2-\sigma_3)$$

* Derivation of transformation relations for equalizing the angle in the touch point

$$\frac{d\tau_{nt}}{d\Theta_{fp}} = \frac{d(-s\cdot c\cdot\sigma_2 + s\cdot c\cdot\sigma_3)}{d\Theta_{fp}} = (s^2-c^2)\cdot(\sigma_2-\sigma_3), \quad \frac{d\sigma_n}{d\Theta_{fp}} = -2\cdot s\cdot c\cdot(\sigma_2-\sigma_3)$$

$$\frac{d\tau_{nt}}{d\sigma_n} = \frac{(s^2-c^2)\cdot(\sigma_2-\sigma_3)}{-2\cdot s\cdot c\cdot(\sigma_2-\sigma_3)} = \frac{C}{S}, \text{ valid if } \textit{uni}\text{- and if } \textit{bi}\text{- } \textit{axial} \text{ (like isotropic)}$$

In the touch point the curve must have the same slope:

$$\frac{d\tau_{nt}}{d\sigma_n} = \frac{C}{S} \;\leftrightarrow\; \frac{d\tau_{nt}}{d\sigma_n} = -\left[\frac{b_{\perp\perp}\cdot(\sigma_n-\sigma_t) + (b_{\perp\perp}-1)\cdot\sqrt{(\sigma_n-\sigma_t)^2+4\tau_{nt}{}^2}}{4\cdot b_{\perp\perp}\cdot\tau_{nt}}\right]$$

After inserting $\sigma_n-\sigma_t = C\cdot(\sigma_2-\sigma_3) = \mathrm{C}\cdot\eta$ vanishes σ_t

$$\frac{C}{S} = -\left[\frac{b_{\perp\perp}\cdot(C\cdot\eta) + a_{\perp\perp}\cdot\sqrt{(C\cdot\eta)^2+4\cdot(-0.5\cdot S\cdot\eta)^2}}{4\cdot b_{\perp\perp}\cdot(-0.5\cdot S\cdot\eta)}\right]$$

Dividing by S and η delivers the fracture angle measure C that defines $b_{\perp\perp} = a_{\perp\perp}+1$

$$C = -\left[\frac{b_{\perp\perp}\cdot C + a_{\perp\perp}\cdot\sqrt{C^2+4\cdot(-0.5\cdot\sqrt{(1-C^2)})^2}}{4\cdot b_{\perp\perp}\cdot(-0.5)}\right] \Rightarrow \mathrm{C} = C_{\mathrm{fp}}{}^{c} = \frac{-a_{\perp\perp}}{a_{\perp\perp}+1}.$$

* Mohr, linear fracture condition: $\tau_{nt} = \mathrm{R}^{\tau} - \mu_{\perp\perp}\cdot\sigma_n$ *or* $F = \dfrac{\tau_{nt}}{\mathrm{R}^{\tau}-\mu_{\perp\perp}\cdot\sigma_n} = 1$

$$\frac{d\tau_{nt}}{d\sigma_n} = -\frac{dF}{d\sigma_n}/\frac{dF}{d\tau_{nt}} = -\frac{\tau_{nt}\cdot\mu}{(\mathrm{R}^{\tau}-\mu\cdot\sigma_n)^2}/\frac{1}{\mathrm{R}^{\tau}-\mu\cdot\sigma_n} = -\frac{\tau_{nt}\cdot\mu}{(\mathrm{R}^{\tau}-\mu\cdot\sigma_n)} = -\mu_{\perp\perp} = \frac{C_{fp}{}^{c}}{S_{fp}{}^{c}}$$

* Relations between all friction-linked parameters including $a_{\perp\perp}$ as friction parameter

$$\mu_{\perp\perp} = \frac{a_{\perp\perp}}{1+a_{\perp\perp}} = -\tan\rho = \frac{-C_{\mathrm{fp}}{}^{c}}{S_{\mathrm{fp}}{}^{c}} \text{ for small angles } \mu_{\perp\perp} \cong -C_{fp}{}^{c}, \text{ further } \tan\phi \equiv \tan\rho$$

$$b_{\perp\perp} \cong \frac{1}{1-\mu_{\perp\perp}}, \; a_{\perp\perp} \cong \frac{\mu_{\perp\perp}}{1-\mu_{\perp\perp}} \text{ and if an angle is measured } C_{fp}{}^{c} = \cos\left(\frac{2\cdot\Theta_{fp}^{c}{}^{\circ}}{180^{\circ}}\cdot\pi\right).$$

$\Rightarrow$ $C_{fp}^{c} = -0.174$, $\Theta_{fp}{}^{\circ} = 51^{\circ}$, $a_{\perp\perp} = 0.26$, $\mu_{\perp\perp} = 0.18 \cong -C_{fp}^{c}$, $c_1 = 48.3$, $c_2 = 10.5$.

For general practice regarding the material: $\rightarrow$ $\mu_{\perp\parallel} \approx \mu_{\perp\perp}$, *see Annex* 2.

Thanks at this specific site to Professor A. Puck:
The author initiated in 1992 that colleague Puck used the mathematical transformation of structural into Mohr stresses (see Table 4-1) and was in exchange later grateful to him for his support and discussions considering the transformation of the structural stresses-formulated FMC-based SFCs by using addition theorems.

7.4 Determination of Mohr shear curve, touch point coordinates and guess of cohesive strength

Touch point coordinates $\tau_{nt}{}^{c}$, $\sigma_n{}^{c}$: see *Fig.7-8*

From transformation equations: $c = \cos(\Theta_{fp}^{c}) = \cos(\Theta_{fp}^{c\,\circ} \cdot \pi / 180^{\circ})$

$\sigma_n = c^2 \cdot \sigma_2, \quad \tau_{nt} = -s \cdot c \cdot \sigma_2$ and $\Theta_{fp}^{c\,\circ} = 51., \; \bar{R}_{\perp}^{c} = 104$ MPa

$\sigma_n{}^{c} = \cos(\Theta_{fp}^{c})^2 \cdot (-\bar{R}_{\perp}^{c}) = -41.3$ MPa, $\quad \tau_{nt}{}^{c} = -\sin(\Theta_{fp}^{c}) \cdot \cos(\Theta_{fp}^{c}) \cdot (-\bar{R}_{\perp}^{c}) = 50.9$ MPa

$\sigma_n{}^{c} = 0.5 \cdot (C+1) \cdot (-\bar{R}_{\perp}^{c}) = -41.3$ MPa, $\quad \tau_{nt}{}^{c} = -0.5 \cdot \sqrt{1-C} \cdot (-\bar{R}_{\perp}^{c}) = 50.9$ MPa

(for info $\sigma_t{}^{c} = -62.7$ MPa)

From Mohr circle geometry:

$\tan\rho = (0.5 \cdot \bar{R}_{\perp}{}^{c} - |\sigma_n{}^{c}|) / \tau_{nt}{}^{c}$ and $\tan\rho = \tau_{nt}{}^{c} / (\bar{R}_{\perp}{}^{c} - |\sigma_n{}^{c}|) = |\sigma_n{}^{c}| / \tau_{nt}{}^{c}$

$\rightarrow \tau_{nt}{}^{c} := \sqrt{|\sigma_n{}^{c}| \cdot (\bar{R}_{\perp}{}^{c} - |\sigma_n{}^{c}|)} = \left((0.5 \cdot \bar{R}_{\perp}{}^{c} - |\sigma_n{}^{c}|) / \tan\rho\right)^2$

$\rightarrow |\sigma_n{}^{c}| = (\bar{R}_{\perp}{}^{c} + \bar{R}_{\perp}{}^{c} \cdot \tan\rho^2) - \bar{R}_{\perp}{}^{c} \cdot \tan\rho \cdot \sqrt{1+\tan\rho^2} \; / (2 + 2 \cdot \tan\rho^2)$

Mohr shear curve $\tau_{nt}(\sigma_n)$: *based on IFF2, only, is an extrapolation from compressive strength*
In the case of brittle materials the Mohr-Coulomb curve is the result of two commonly acting failure modes. Now, neglecting IFF1 (the normal fracture part) and considering just the shear fracture IFF2 leads to the curve in *Fig.7-8* according to the relations

$$Eff^{\perp\tau} \equiv F^{IFF2} = [a_{\perp\perp} \cdot (I_2) \; + \; b_{\perp\perp} \cdot \sqrt{I_4}] \; / \bar{R}_{\perp}^{c} = 1 \text{ with } a_{\perp\perp} = b_{\perp\perp} - 1 \text{ after inserting } \bar{R}_{\perp}{}^{c}$$

$$= [a_{\perp\perp} \cdot (\sigma_n + \sigma_t) \; + \; b_{\perp\perp} \cdot \sqrt{(\sigma_n - \sigma_t)^2 + 4\tau_{nt}{}^2}] \; / \bar{R}_{\perp}^{c} = 1$$

$I_2 = \sigma_n + \sigma_t = \sigma_2 + \sigma_3$, $\sigma_n - \sigma_t = C \cdot (\sigma_2 - \sigma_3) = C \cdot \eta$, $\tau_{nt} = -0.5 \cdot \sqrt{1-C} \cdot \eta$

In the compression strength point $(\sigma_2 = -\bar{R}_{\perp}^{c}, \; \sigma_3 = 0)$, $\eta = -\bar{R}_{\perp}^{c}$ is obtained $C \rightarrow C^c$,

$$a_{\perp\perp} \cdot (2\sigma_n + C^c \cdot \eta) \; + \; b_{\perp\perp} \cdot \sqrt{(C^c \cdot \eta)^2 + 4\tau_{nt}{}^2}] \; / \bar{R}_{\perp}^{c} = 1 \quad \Rightarrow \quad \tau_{nt}(\sigma_n, \; C^c).$$

For a better orientation the four Mohr half-circles are included in Fig.7-8. Both the shear curves Linear Mohr-Coulomb and the FMC-based equation above – due to the definition of the friction value – are linear and equal, because $C = C^c(\mu_{\perp\perp})$ is constant along σ_2.
The touch point and the cohesive shear strength are depicted in the figure.

Cohesive strength $\bar{R}_{\perp\perp}^{\tau}$: *extrapolation from compressive strength point*

* From the Linear Mohr approach: $\bar{R}_{\perp\perp}^{\tau} = \tau_{nt}{}^{c} + \mu \cdot \sigma_n{}^{c} \quad \Rightarrow \bar{R}_{\perp\perp}^{\tau} = 42$ MPa.
* From the IFF2 equation : $\tau_{nt}(\sigma_n, \; C^c)$: $\bar{R}_{\perp\perp}^{\tau} = \tau_{nt}(\sigma_n = 0) = 42$ MPa.
* General note on prediction of $\bar{R}_{\perp\perp}^{\tau}$ and of A. Puck's $\bar{R}_{\perp\perp}^{A}$:

For the cohesive strength, denoted $\bar{R}_{\perp\perp}^{A}$ by Puck, he gave the formula $R_{\perp\perp}{}^{A} = R_{\perp}{}^{c} / (2+2 \cdot p_{\perp\perp}{}^{c})$ with $0.25 < p_{\perp\perp}{}^{c} > 0.30$ for CFRP. Inserting above set of strength properties $R_{\perp}{}^{c} = 104$ MPa, $R_{\perp}{}^{t} = 35$ MPa into Puck's formula $R_{\perp\perp}{}^{A}$ becomes 41 MPa.

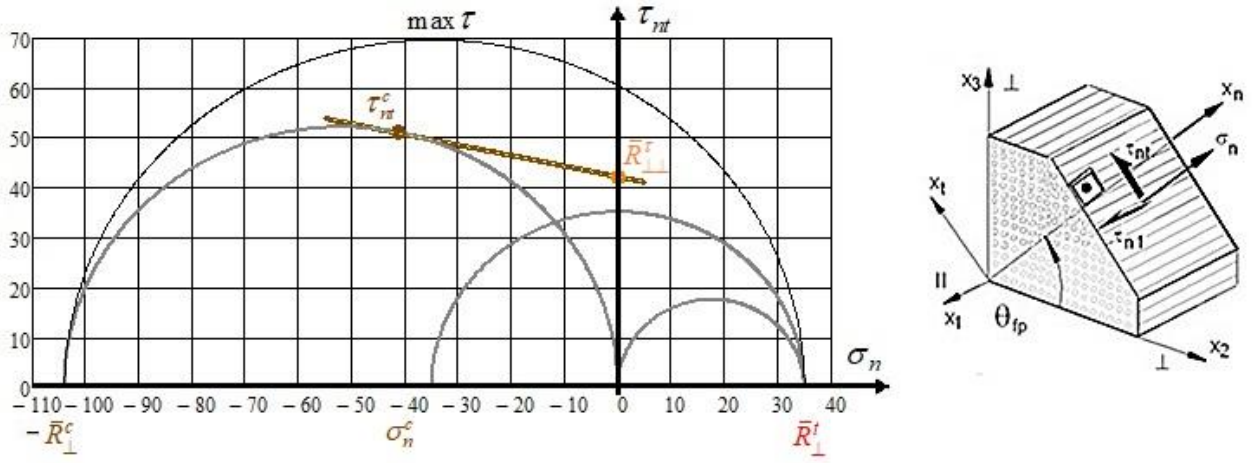

Fig. 7-8: Mohr shear curves τnt (σn) with its special end points and the four Mohr half-circles.
$\bar{R}^t_\perp = 35\text{MPa},\ \bar{R}^c_\perp = 104\ \text{MPa},\ \Theta^{c\,\circ}_{fp} = 51°,\ \bar{R}^\tau_{\perp\perp} = 42\ \text{MPa},\ \sigma_n{}^c = -41.3\ \text{MPa},\ \tau_{nt}{}^c = 50.9\ \text{MPa}$

7.5 Measurement of fracture angle $\Theta_{fp}{}^c$ and determination of friction values $\mu_{\perp\perp}, \mu_{\perp\parallel}$

Uni-axial compression test:

The fracture angle $\Theta_{fp}{}^c$ can be estimated via a uni-axial compression test, see *Fig. 7-9*, using

$$C^c_{fp} = \cos\left(\frac{2\cdot\Theta^{c\,\circ}_{fp}}{180°}\cdot\pi\right):\ \mu = -\tan\rho = -C^c_{fp} / S^c_{fp} = -C^c_{fp} / \sqrt{1-C^{c\,2}_{fp}} \cong -\ C^c_{fp}.$$

Bi-axial compression test:

Running a bi-axial compression test is effortful. In mechanical engineering the classical tension-compression/torsion test rig is used, see test points in *Fig. 7-9* and as well 2D- as 3D-tests are performed *(in civil engineering multi-axial tests are mandatory for an accurate design of concrete structures*). The evaluation of the measured failure curves is given in *Fig. 7-10*, formulas are shown. Friction test values are so-called physical properties where usually the estimation of an average value is sufficient for analysis but not for design verification in general because the upper or the lower bound of a physical property may define a limit state (i.e. Young's modulus considering natural frequencies). The friction properties are differently measured and evaluated:

- Simply, from two fracture stress points on the respective pure mode curve IFF2 ($\sigma^{fr}_2, \sigma^{fr}_3$) with ($-\bar{R}^c_\perp, 0$) for IFF3 ($\sigma^{fr}_2, \tau^{fr}_{21}$) with ($\bar{R}^c_{\perp\parallel}, 0$), where $\mu_{\perp\parallel} = (\bar{R}_{\perp\parallel} - \tau^{fr}_{21}) / \sigma^{fr}_2$. Adjustment may be required
- More sophisticated, by a fitting optimisation process of the course of test data of each pure mode
- If an adequate test rig for IFF2 is not available by an approximate procedure (*see Annex 2*).

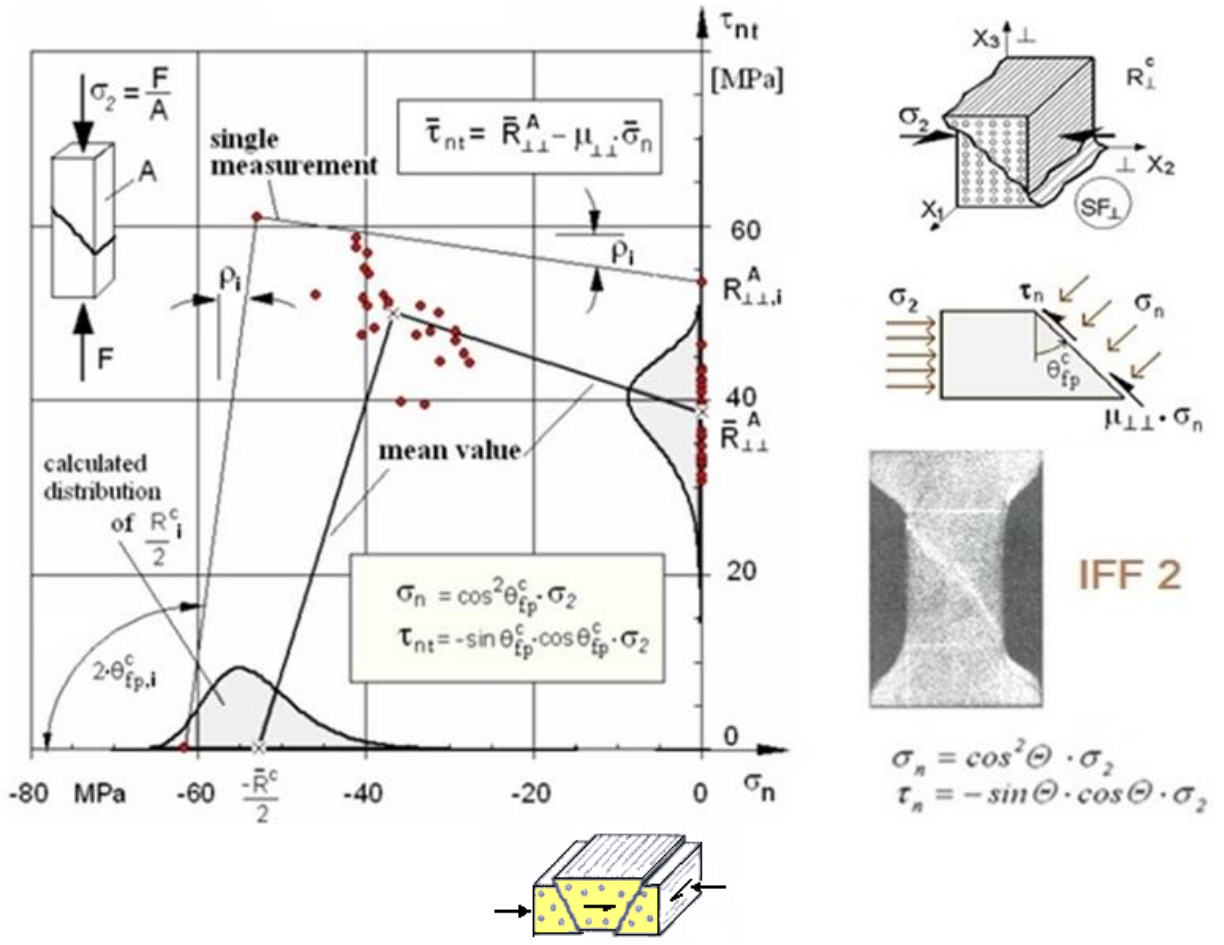

Fig.7-9: Measurement of friction values employing the traditional uni-axial tension-compression-torsion test rig and the associated tube test specimen. Here, the loading direction was taken for the definition of Θ_{fp}^{c}. R_{LL}^{A} is Linear Mohr-Coulomb-derived. Figure from a joint research project on Puck's theory [*Cun97*]

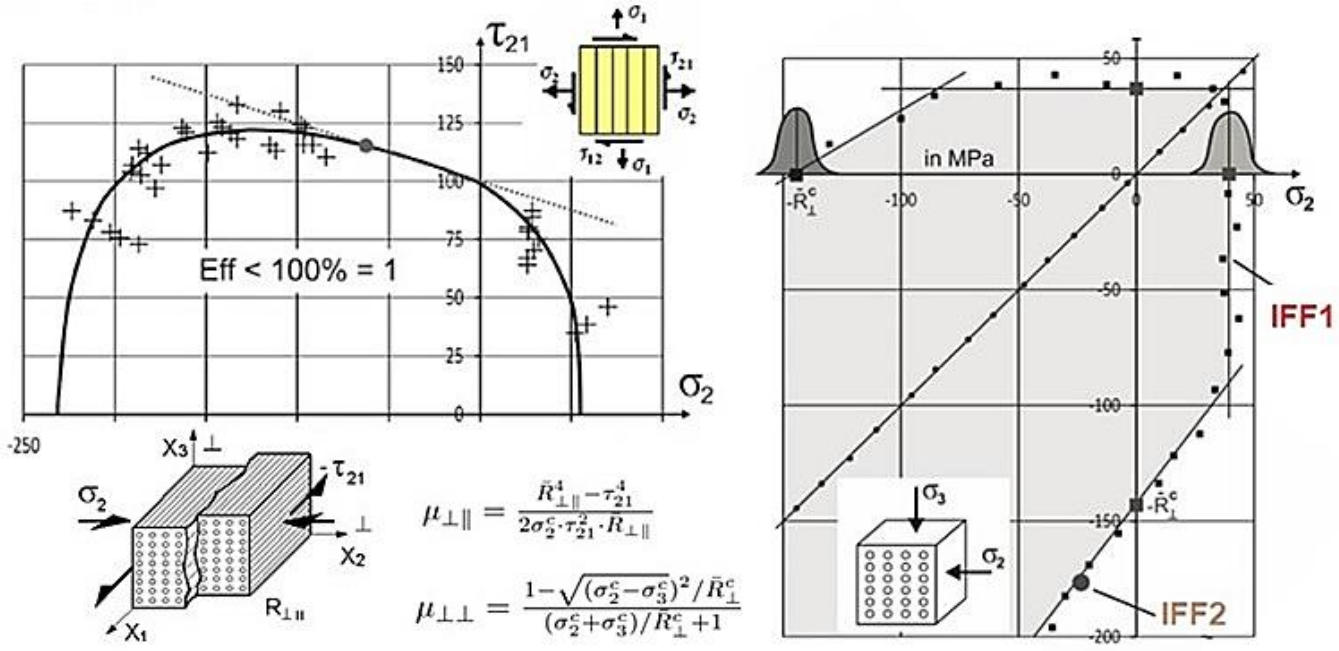

Fig.7-10: Estimation of the friction values $\mu_{\perp\perp}$, $\mu_{\perp\parallel}$ from a course of fracture test data

Table 7-2: Relationships during derivation of $\tau_{nt}(\sigma_n)$, $\Theta_{fp}°$ from a measured fracture curve $\sigma_3(\sigma_2)$

$$Eff^{\perp\tau} = Eff^{SF} = [a_{\perp\perp}\cdot(\sigma_2{}^p+\sigma_3{}^p) + b_{\perp\perp}\cdot\sqrt{(\sigma_2{}^p-\sigma_3{}^p)^2+0^2}\,]\ /\ \bar{R}_\perp^c = 1$$

$$= [a_{\perp\perp}\cdot(\sigma_n+\sigma_t) + b_{\perp\perp}\cdot\sqrt{(\sigma_n-\sigma_t)^2+4\tau_{nt}{}^2}\,]\ /\ \bar{R}_\perp^c = 1$$

$$Eff^{\perp\sigma} = Eff^{NF} = (\sigma_2{}^p+\sigma_3{}^p) + \sqrt{(\sigma_2{}^p-\sigma_3{}^p)^2+0^2}\,]\ /\ 2\cdot\bar{R}_\perp^t = 1$$

$$= [(\sigma_n+\sigma_t) + \sqrt{(\sigma_n-\sigma_t)^2+4\tau_{nt}{}^2}\,]\ /\ 2\cdot\bar{R}_\perp^t = 1\,.$$

Known: $\sigma_2{}^p$, $\sigma_3{}^p$. Searched: σ_n, τ_{nt}, $\Theta_{fp}(C=\cos(2\cdot\Theta_{fp}°\cdot\pi/180°))$

Two quantities are known and three are to be determined

Use of addition theorems, $\sigma_\lambda = 0$, index ^{p} now dropped

$$\sigma_n-\sigma_t = c^2\cdot(\sigma_2-\sigma_3)-s^2\cdot(\sigma_2-\sigma_3) = C\cdot(\sigma_2-\sigma_3),\ \ S=\sqrt{1-C^2}$$

$$\sigma_t = \sigma_n - C\cdot(\sigma_2-\sigma_3),\ C = c^2-s^2 = 2c^2-1 = 1-2s^2,$$

$$\sigma_n+\sigma_t = \sigma_2+\sigma_3,\ \ \tau_{nt} = -0.5\cdot S\cdot(\sigma_2-\sigma_3) = -0.5\cdot\sqrt{1-C^2}\cdot(\sigma_2-\sigma_3)$$

Fracture (interaction) equation ≡ mathematical equation of the fracture body

$$Eff = [(Eff^{NF})^m + (Eff^{SF})^m]^{m^{-1}} \quad or \quad \text{computationally simpler}$$

$$(Eff^{NF})^m + (Eff^{SF})^m = 1 = 100\% \quad \text{total effort.}$$

Differentiation of structural stresses-linked Mohr stresses delivers

$$\frac{d\tau_{nt}}{d\sigma_n} = \frac{(s^2-c^2)\cdot(\sigma_2-\sigma_3)}{-2\cdot s\cdot c\cdot(\sigma_2-\sigma_3)} = \frac{C}{S},\ \ \text{valid } \textit{uni}\text{- and } \textit{bi}\text{-}\textit{axial} \text{ (like isotropic!)}$$

Missing equation from differentiation of the interaction equation, σ_t to insert before,

$$\{[(\sigma_n+\sigma_n-C\cdot(\sigma_2-\sigma_3)) + \sqrt{(\sigma_n-\sigma_n-C\cdot(\sigma_2-\sigma_3))^2+4\tau_{nt}{}^2}\,]\ /\ 2\cdot\bar{R}_\perp^t\}^m +$$

$$+\{[a_{\perp\perp}\cdot(\sigma_n+\sigma_n-C\cdot(\sigma_2-\sigma_3)) +$$

$$+ b_{\perp\perp}\cdot\sqrt{(\sigma_n-\sigma_n-C\cdot(\sigma_2-\sigma_3))^2+4\tau_{nt}{}^2}\,]\ /\ \bar{R}_\perp^c\}^m = 1.$$

$$d[(Eff^{NF})^m+(Eff^{SF})^m]/\,d\sigma_n =$$

$$m\cdot\{2\sigma_n - C\cdot(\sigma_2-\sigma_3) + \sqrt{(C\cdot(\sigma_2-\sigma_3))^2+4\tau_{nt}{}^2}\,]/2\bar{R}_\perp{}^t\}^{m-1}/\bar{R}_\perp{}^t +$$

$$+2a_{\perp\perp}\mathrm{m}\cdot\{a_{\perp\perp}(2\sigma_n - C\cdot(\sigma_2-\sigma_3)) + b_{\perp\perp}\sqrt{(C\cdot(\sigma_2-\sigma_3))^2+4\tau_{nt}{}^2}\,]\ /\ \bar{R}_\perp{}^c\}^{m-1}/\bar{R}_\perp{}^c,$$

$$[d(Eff^{NF})^m+(Eff^{SF})^m]/d\tau_{nt} =$$

$$\frac{2m\cdot\tau_{nt}\cdot\{2\sigma_n - C\cdot(\sigma_2-\sigma_3) + \sqrt{(C\cdot(\sigma_2-\sigma_3))^2+4\tau_{nt}{}^2}\,]/2\bar{R}_\perp{}^t\}^{m-1}}{\bar{R}_\perp{}^t\cdot\sqrt{(C\cdot(\sigma_2-\sigma_3))^2+4\tau_{nt}{}^2}} +$$

$$+4b_{\perp\perp}\mathrm{m}\cdot\{a_{\perp\perp}(2\sigma_n - C\cdot(\sigma_2-\sigma_3)) + b_{\perp\perp}\sqrt{(C\cdot(\sigma_2-\sigma_3))^2+4\tau_{nt}{}^2}\,]\ /\ \bar{R}_\perp{}^c\}^{m-1}/\bar{R}_\perp{}^c.$$

Equating the two equations and replacing Mohr stresses by structural stresses

via $\sigma_n = (C+1)\cdot0.5\cdot\sigma_2 + (1-C)\cdot0.5\cdot\sigma_3,\ \tau_{nt} = -0.5\cdot\sqrt{1-C^2}\cdot(\sigma_2-\sigma_3)$

yields an equation for the fracture angle measure C; m vanishes

$$\frac{C(\sigma_2,\sigma_3)}{\sqrt{1-C^2}} = -\left[\frac{m\cdot A}{\bar{R}_\perp{}^t} + \frac{2\cdot a_{\perp\perp}\cdot m\cdot B}{\bar{R}_\perp{}^c}\right]/\left[\frac{2\cdot m\cdot A}{\bar{R}_\perp{}^t\sqrt{(\cdot\sigma_2-\sigma_3)^2}} + \frac{4\cdot b_{\perp\perp}\cdot m\cdot B\cdot\tau_{nt}}{\bar{R}_\perp{}^c\sqrt{(\cdot\sigma_2-\sigma_3)^2}}\right]$$

$$A = \left[\frac{\sigma_2+\sigma_3+\sqrt{(\sigma_2-\sigma_3)^2}}{2\cdot\bar{R}_\perp^t}\right]^{m-1},\ \ B = \left[\frac{a_{\perp\perp}\cdot(\sigma_2+\sigma_3)+b_{\perp\perp}\cdot\sqrt{(\sigma_2-\sigma_3)^2}}{\bar{R}_\perp^c}\right]^{m-1}$$

and finally $\Theta_{fp}°$ and the Mohr stresses σ_n, τ_{nt}

$$C = \cos(2\cdot\Theta_{fp}),\ \Theta_{fp} = 0.5\cdot\arccos C\,,\ \Theta_{fp}° = \Theta_{fp}\cdot 180°/\pi,\ \ c^2 = (C+1)\cdot0.5$$

$$\sigma_n = (C+1)\cdot0.5\cdot\sigma_2 + (1-C)\cdot0.5\cdot\sigma_3,\ \ \tau_{nt} = -0.5\cdot\sqrt{1-C^2}\cdot(\sigma_2-\sigma_3).$$

7.6 Derivation of the real $\tau_{nt}(\sigma_n)$ and of course of Θ_{fp} from a measured fracture curve $\sigma_3(\sigma_2)$

In the previous chapters, for isotropic materials the author proved that a transformation from structural stresses to the desired formulations in Mohr stresses is possible. The same is analogously possible for a UD material, where the quasi-isotropic plane has to be investigated in order to determine the lateral cohesive strength.
In *Table 7.2* all relations necessary for the transformation of a measured fracture curve $\sigma_3(\sigma_2)$ into a Mohr-Coulomb curve $\tau_{nt}(\sigma_n)$ are listed. The formulas for the searched entities τ_{nt}, σ_n, $\Theta_{fp}°$ are presented. These entities are only accurate if the physically necessary correction of the design-practical 'simple' IFF2 (or $Eff^{\perp\tau} = Eff^{SF}$) is considered by the decay function f_d. In order to implement f_d one just has to replace $a_{\perp\perp}$ by $f_d \cdot a_{\perp\perp}$ and $b_{\perp\perp}$ by $f_d \cdot b_{\perp\perp}$.

Fig.7-11 presents the full range of MathCad-computed Mohr entities:

Upper diagram: Mohr stresses

- straight Linear Mohr Coulomb curve (*extrapolation*)
- IFF2-determined Mohr-Coulomb fracture curve (*IFF2 extrapolation is like Mohr*)
- course of the fracture plane angle $\Theta_{fp}°$ *(bold, decay function corrected)*
- IFF2-IFF1-interacted Mohr-Coulomb fracture curve *(bold, decay function corrected)*

Lower diagram: structural stresses

- course of the fracture plane angle $\Theta_{fp}°/2$
- IFF2-IFF1- interacted fracture curve (*thin, original IFF2*)
- IFF2-IFF1- interacted fracture curve *(bold, IFF2 decay function corrected, which better maps the course of measured fracture stress data).*

In order to find all relationships in one diagram the Mohr stresses are inserted as functions of the structural stresses and not of σ_n, which is the usual diagram form and was used for the isotropic materials before. The figure further includes the development of the fracture plane angle as function of the structural stress σ_2 and the various predicted values for the cohesive strength R^{τ}.
The numerical example stems from a measurement of the fracture plane angle $\Theta_{fp}°$ in [*Cun97*].

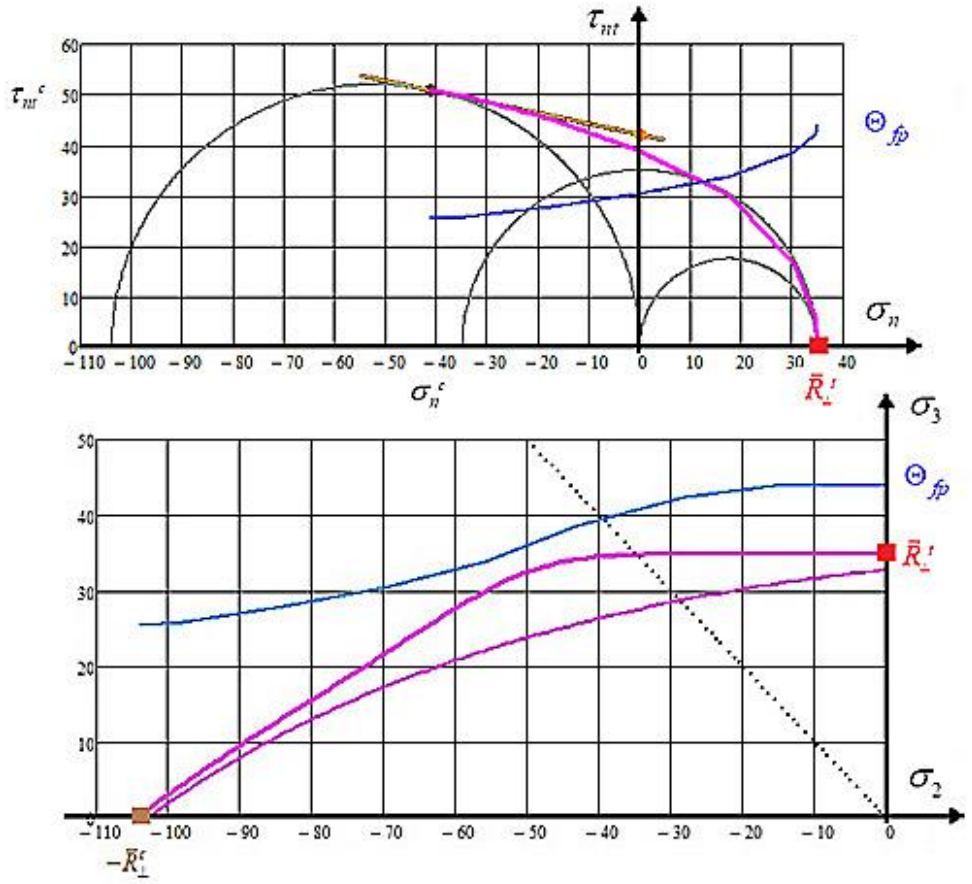

Fig.7-11: Joint display of the UD failure curve in Mohr stresses (above) with fracture angle increase $\Theta_{fp}°$ when approaching $\bar{R}_\perp^t$ and in structural stresses (below).

Linear: $\bar{R}_{\perp\perp}{}^{\tau} = 42$ MPa, $\Theta_{fp}^{c\,\circ} = 51°$, Improved by f_d: $\bar{R}_{\perp\perp}{}^{\tau} = 39$ MPa, $\Theta_{fp}{}^{\circ} = 61°$, σ_2 = -70 MPa, σ_3 = 22 MPa.

$\bar{R}_\perp^t = 35$ MPa, $\bar{R}_\perp^c = 104$ MPa, $\Theta_{fp}^{c\,\circ} = 51.0°$, $C^c = -0.206$, $\mu_{\perp\perp} = 0.211$, $\tau_{nt}^c = 50.9$ MPa, $\sigma_n^c = -41.3$ MPa

.

The interpretation of *Fig.7-11* leads to the following conclusions:

- ✓ *A SFC* in structural stresses can be transferred into a Mohr-Coulomb type
- ✓ The alteration of the fracture plane angle $\Theta_{fp}°$ can be determined, too
- ✓ The idea of the FMC that IFF1 and IFF2 commonly add its *Eff* portions lead to the result that the $\Theta_{fp}°$ is about 70° at the cohesive strength point $\bar{R}_{\perp\perp}^{\tau}$
- ✓ The simple IFF2 approach cannot offer a full accuracy of the realistically predicted Mohr-Coulomb curve. Just the *physically-based* decay function correction delivers the desired fidelity.

A thank you to Bernd Szelinski for his active and mental MathCad support.

Conclusions, Results

Primary intension of this investigation: *Generation of the Mohr-Coulomb failure curve*

1. Proof, that the structural stresses-formulated fracture curve σ_2 (σ_3) can be transferred into a Mohr-Coulomb one $\tau_{nt}(\sigma_n)$
2. Demonstration that a dependence of the shear fracture plane angle $\Theta_{fp}°$ with growing hydrostatic compressive stress is given, as far as SF is the primary failure mode. The angle decreases which looks like becoming more ductile. Failure occurs in that plane where the driving shear stress τ or equivalently where Eff^{SF} is maximum
3. The huge effort spent for the generation of $\Theta_{fp}°$ and the Mohr-Coulomb failure curve paid off for the isotropic and for the UD material as well. For the isotropic material the effort was even higher because $\Theta_{fp}°$ also alters with the meridian-marking Lode angle ϑ caused by the 120°-rotational symmetry which impacts $\tau_{nt}(\sigma_n)$
4. The determination of the cohesive strength $\bar{R}^{\tau}$, by considering the SF-mode only from touch point information ($\tau_{nt}^{c}, \sigma_n^{c}$), is just an *extrapolation,* because in the case of brittle materials $\bar{R}^{\tau}$ is usually located in the transition domain. Hence, a realistic cohesive strength can be not predicted by properties just belonging to the SF mode if the NF mode is activated, too. An interaction of the modes is mandatory.

   For Normal Concrete ($\bar{R}^{c} = 40MPa, \mu = 0.1??.$) the following predictions are obtained:

   - Linear Mohr-Coulomb, single mode SF: $\bar{R}^{\tau} = \tau_{nt}^{c} + \mu \cdot \sigma_n^{c} = \tau_{nt}^{c} + \mu \cdot \sigma_n^{c} = 17$ MPa
   - FMC-extrapolation, single mode SF, rot-symm: $\Theta^{CM} = \Theta^{c} = \text{constant} \rightarrow \bar{R}^{\tau} = 13.5$ MPa
   - FMC-extrapolation, single mode SF, 120°-model: $\bar{R}^{\tau} = 12.5$ MPa
   - FMC, interaction SF-NF, 120°-model, considering f_d: $\bar{R}^{\tau} = 11$ MPa .

Annexes:

- Output of the interesting failure angle relations bridging F^{SF} and F^{Mises}
- Successful evaluation of not very appropriate ARCAN test data to quantify $\mu_{\perp\perp}$
- Creation of a relatively simple novel model $IFF2^{porosity}$ for a porous UD material in the quasi-isotropic domain
- Visualization of the influence of 2D- and 3D-compression stress states on the strength capacity by the material stressing effort *Eff* and proving that all the failure stress states are located on the failure surface *Eff* = 100% (*the strength is not increased*)
- Determination of a Reserve Factor by application of a Safety Concept
- For mathematically homogeneous and non-homogeneous SFCs the difference of Failure Index |*F*| and material stressing effort *Eff* has been outlined. In this context the concept of 'proportional loading' and the concept idea of 'driving stress' were presented. This Annex invites for discussion regarding linear and non-linear stress analyses.

General regarding the presented FMC-based SFCs and the test input:

- A SFC has to map 3D stress states. It can be validated, principally, by 3D test data sets, only. If just 2D test data is available, then the 2D-reduced 3D-SFC is applied. This means that the necessary 3D mapping quality is not fully proven
- A test series along a tensile meridian (it delivers R^{t}, R^{cc}) or along a compressive meridian (delivers R^{c}, R^{tt}) alone is not sufficient. On both the meridians tests must be performed. For a general 3D-mapping multi-axial failure stress states (R^{tt}, R^{cc}) are required which generate two-fold failure modes. Then the significant inherent 120°-symmetry of brittle isotropic materials can be mapped

- Following Beltrami's statement, a successful demonstration of the advantageous use of the 'physics-based' invariants I_1 and J_2 for the very different materials Normal Concrete, Ultra-High-Performance-Concrete, PMMA [*Cun20b*] could be presented. For UD material the same happened
- The interaction formula well maps the course of test data in the mode transition zone. The mapping quality of $F^{SF} \equiv$ IFF2 is sufficient for design verification as it is conservative. For an accurate determination of the altering fracture plane angle $\Theta_{fp}°$ the SFC IFF2 had to made more 'physically correct' by the chosen exponential degradation function *f*
- Rounding-off, by employing an interaction equation in the transition zone of adjacent modal failure curves (2D) or of partial failure surfaces is leading to a pseudo-global failure curve or surface. In other words, again a 'single surface failure description' is achieved, however, without the well-known shortcomings of Global SFCs.
- When creating an SFC Eff^{mode} must become zero if the driving stress τ in the case of SF and σ^t in the case of NF becomes zero.

Some conclusions for isotropic material

- Shear fracture emerges orthogonally to that plane, where the maximum effort Eff^{SF} stresses the solid. Mechanically, this is as well given in the uniaxial compression case in the axial cross-section of the fracture body as in the bi-axial compression stress case.
- With the 'isotropic' invariant J_3 the bi-axial strength capacity of isotropic brittle materials is captured. This bi-axial strength capacity (σ_{fr}, σ_{fr}) is $\neq$ the uni-axial strength *R* in the compressive domain and in the tensile stress domain as well. For dense materials is valid $\sigma_{fr} > R$, and for porous materials $\sigma_{fr} < R$. J_3 can be employed in each case.
- Due to the Poisson effect, bi-axial compression leads to an axial tensile straining $\varepsilon_3 = -2\,\nu \cdot \sigma^{cc}/E$. This causes a closed 3D failure surface.

Conclusions for transversely-isotropic UD material, bi-axial**:**

- For UD materials the failure curve denting bi-axial strength capacity $R^t < R^{tt} = (\sigma_{fr}{}^t, \sigma_{fr}{}^t)$ could be captured by an additional part in IFF1, if required by the given special task
- Due to the Poisson effect, bi-axial compression leads to a tensile straining $\varepsilon_3 = \varepsilon_{\|}$ captured by a tensile stress of the axially placed fibers. This leads to an open 3D failure surface. And under hydrostatic pressure 'dense' UD materials fiber fracture due to $\varepsilon_{\|} \cdot E_{\|} = R_{\|}^t$ at about thousands of MPa.

- *LL:*
- *Flaw distribution effect: Activation of the critical fracture plane depends on the spatial distribution and orientation of the flaws*
- *The challenge is not the establishment of a SFC but the test data–based visualization of its associated fracture failure body and in this context the display of the failure curve in the principal stress plane as a bias cross-section of the body. In the case of brittle isotropic materials - heavy effort causes the depiction of the different meridian curves as the axial cross-sections of the failure body with inward and outward dents along the axis of the 120°-symmetric isotropic failure body*
- *The applicability of a SFC ends when the driving mode stress σ^t (Eff1) or τ (Eff2) becomes zero and the associate Eff becomes negative. Therefore, the traditional use to just apply the so-called 'Proportional Loading (stressing)' concept in order to derive Eff from F must be checked whether the condition above is fulfilled or not (see Annex 6)*
- *The use of the entity Eff excellently supports to understand a multi-axial strength capacity of a material (see Annex 5)*

- *'Touch point': It's coordinates (τ_{nt}^{c}, σ_{n}^{c}) in Mohr stresses correspond to the compressive strength point (R^{c}, 0) in structural stresses*
- *Friction quantities, which are determined in the touch point, of-course remain the same for the rotationally-symmetric model and for the 120°-rotationally-symmetric mode, $c_{2\Theta}^{SF} = c_{2}^{SF}$, μ, C^{c}*
- *Multi-axial compression works as plastifier*
- *An estimation of the cohesive strength value τ_{nt} ($\sigma_{n} = 0$) by using just $Eff^{SF} = 1$ is an extrapolation and leads to higher values dependent on the specific model applied*
- *Mind: Under multi-axial compression states the (material) strength is not increased but the risk of shear fracture failure is decreased, indicated by an $Eff^{SF} < 1$, see Annex 4*
- *Terms: It is too discriminate bi-axial fracture stress state and (uni-axial) strength, defined as strength in engineering. For practical reasons the term bi-axial strength (R^{tt} , R^{cc}) is used for marking the bi-axial fracture stress state.*

Thinking back at the various steps to finally successfully create
- after a very long time –
a transformation from the usual SFC formulation in structural stresses
to a formulation in Mohr stresses I would like to cite,
because I did so,

"Do first what is necessary, then the possible, and suddenly you create the impossible."
[Franz von Assisi]

Literature

[Boe87] Boehler J P : *Introduction to the invariant formulation of anisotropic constitutive equations*. 1987 In: Boehler J.P. (Ed.) *Applications of Tensor Functions in Solid Mechanics*. CISM Course no. 292. Springer-Verlag. In addition a personal note from J. Boehler on UD invariants which were later applied by the author in his FMC

[Cun97] Cuntze R, Deska R, Szelinski B, Jeltsch-Fricker R, Meckbach S, Huybrechts D, Kopp J, Kroll L, Gollwitzer S, and Rackwitz R: *Neue Bruchkriterien und Festigkeitsnachweise für unidirektionalen Faserkunststoffverbund unter mehrachsiger Beanspruchung –Modellbildung und Experimente –*.VDI-Fortschrittbericht, Reihe 5, Nr. 506 (1997), 250 pages. (*New fracture criteria (Puck's criteria) and Strength 'Proof of Design' for Uni-directional FRPs subjected to Multi-axial States of Stress –model development and experiments-*. In German) *

[Cun04] Cuntze R: *The Predictive Capability of Failure Mode Concept-based Strength Criteria for Multidirectional Laminates*. WWFE-I, Part B, Comp. Science and Technology 64 (2004), 487-516

[Cun05] Cuntze R.: *Is a costly Re-design really justified if slightly negative margins are encountered? Konstruktion*, März 2005, 77-82 and April 2005, 93-98 (reliability treatment of the problem)*

[Cun12] Cuntze R: *The predictive capability of Failure Mode Concept-based Strength Conditions for Laminates composed of UD Laminas under Static Tri-axial Stress States*. - Part A of the WWFE-II. Journal of Composite Materials 46 (2012), 2563-2594

[Cun12] HSB 02000-01 *Essential topics in the determination of a reliable reserve factor*. TIB Hannover, 20 pages

[Cun13] Cuntze R: *Comparison between Experimental and Theoretical Results using Cuntze"s „Failure Mode Concept" model for Composites under Triaxial Loadings* - Part B of the WWFE-II. Journal of Composite Materials, Vol.47 (2013), 893-924

[Cun14] Cuntze R: *The Fracture Failure Surface of Foams, derived on basis of the author's Failure Mode Concept*. PPT presentation, Carbon Composites e.V. (CCeV), meeting of the working group 'Engineering', July 11, 2014*

[Cun 14b] Cuntze R: *The WWFEs I and II for UD Materials – valuable attempts to validate failure theories on basis of more or less applicable test data*. In Conference Handbook SSMET 2014:= Europ. Conf. on Spacecraft Structures, Materials and Environmental Testing. Braunschweig, 1- 4 April 2014, 8 pages

[Cun15a] Cuntze R.: *Static & Fatigue Failure of UD-Ply-laminated Parts – a personal view and more*. ESI Group, Composites Expert Seminar, Uni-Stuttgart, January 27-28, keynote presentation*

[Cun15c] Cuntze R.: *Basis Document, Update ComPoLyX Manual chapter Cuntze and Relationship of Cuntze's UD friction parameters b with Mohr's friction coefficients.* CCeV website, May 4, 2015 *

[Cun16a] Cuntze R: *Fracture failure surface of the foam Rohacell 71G*. 3. NAFEMS Regionalkonferenz, 25.-27. April, 2016. Berechnung und Simulation, 35 slides*

[Cun16b] Cuntze R: *Introduction to the Workshop - from Design Dimensioning via Design Verification to Product Certification*. Experience Composites 16 (EC16), September 21 – 23, 2016, Augsburg. Extended Abstract in the Symposium Abstracts. 10 pages*

[Cun16c] Cuntze R: *Progress reached, in Static Design and Lifetime Estimation*? Mechanik-Kolloquium, TU-Darmstadt, December 21, 2016 (UD and isotropic materials, Extended Presentation, 150 slides)*

[Cun17] Cuntze R: *Fracture Failure Bodies of Porous Concrete Stone (isotropic foam-like), Normal Concrete, Ultra-High-Performance-Concrete and of the Lamella (sheet) - generated on basis of Cuntze's Failure-Mode-Concept (FMC).* NWC 2017, June 11-14 Stockholm. Extended Abstract, Symposium Handbook, 13 pages *

[Cun19a] Cuntze R: presentation in the author's working group CU AG "Engineering" on *3D-Festigkeitsbedingungen für spröde Werkstoffe isotrop, transversal–isotrope UD-Schicht und orthotropes Gewebe - ermittelt auf Basis des Failure-Mode-Concepts (FMC) von Cuntze*. June 25, 2019 Basel (English slides) *

[Cun19c] Cuntze R: *Technical terms for composite components in civil engineering and mechanical engineering*. Fachbegriffe mit Erklärung und Definition. In: *Fachbegriffe für Kompositbauteile – Technical terms for composite parts*. Springer Vieweg, Wiesbaden, 2019, 171 pages *

[Cun20a] Cuntze R: Einführungsvortrag des Autors als Leiter der AG „Bemessung und Nachweis“ zum CU-Thementag „*Richtlinien, bauaufsichtliche Zulassungen und Bauartgenehmigungen für die potentiellen Anwender Architekten, Tragwerksplaner und Bauherrn“*. Videokonferenz, 19. Nov. 2020. 40 (English and German) slides *

[Cun20b] Cuntze R: *Normal Yielding NY and Compression-induced Critical Stress Intensity Factor* K_{IIcr}^{c} *- Missing Links in an Isotropic ‘Closed’ Macro-Mechanics Building*. 30 pages *

[Cun21] Cuntze R: *Strength capacity of bi-axially compressed UD strands at turning points of rotor blade loops and of hangers of network arch bridges.* CU-AG “Engineering”, May 20. *

[Kup73] Kupfer H: *Das Verhalten des Betons unter mehrachsiger Kurzzeitbelastung unter besonderer Berücksichtigung der zweiachsigen Beanspruchung*. In Deutscher Ausschuss für Stahlbeton, Band 229, 1973

[Mathcad 15]: PTC mathematical program, used by the author

[Mur09] Murthy A R, Ch, Palani G S and Iyer N: *State-of-the-art review on fracture analysis of concrete structural components*. Sadhana Vol.34, Part 2, April 2004, 345-367

[Pet15] Petersen E, Cuntze R and Huehne C: *Experimental Determination of Material Parameters in Cuntze’s Failure-Mode-Concept-based UD Strength Failure Conditions.* Submitted to Composite Science and Technology 134, (2016), 12-25 *

[Puc02] Puck A and Schürmann H: *Failure Analysis of FRP Laminates by Means of Physically-based Phenomenological Models.* Composites Science and Technology 62 (2002), 1633-1662

[Rac87] Rackwitz R and Cuntze R: *System Reliability Aspects in Composite Structures*. Eng.' Opt. 11 (1987), 69-76

[Tsa71] Tsai S W and Wu E M: *A General Theory of Strength for An-isotropic Materials*. Journal Comp. Materials 5 (1971), 58-80

[VDI 06] VDI 2014: German Guideline, Sheet 3 “*Development of Fiber-Reinforced Plastic Components, Analysis*”. Beuth Verlag, 2006 (in German and English. Cuntze was convenor and contributor)

*https://www.carbon-connected.de/Group/CCeV.Fachinformationen/Dokumente/Documents/Index/10381
and loaded in Research Gate

ANNEX 1: Bridging Shear Fracture F^{SF} and Yield Failure F^{Mises} with view at failure 'planes'

The Failure-Mode-Concept is dedicated to brittle materials ($R^c/ R^t > 3$) whereas 'Mises' (Hencky-Mises-Huber, a Modal and Global SFC) describes the yield behavior of ductile materials ($R_{0.2}{}^t \approx R_{0.2}{}^c$).

Both the failure conditions shall be used to enlighten the difference between the failure function *F* of a SFC and an effort *Eff* of both the SFCs. The difference is essential in the elastic domain, where – caused by the design safety factor – most of the structural parts with its critical locations are to be strength-assessed.

Basis is the application of the so-called proportional loading, where all stress states alter proportionally. Difference comes up if *F* is not a so-called homogeneous function (see the respective Annex 6). The following table displays all the links:

* FMC-based Strength Failure Condition F^{SF} (non-homogeneous equation)

Porous: $\bar{R}^c > \cong 3\,\bar{R}^t$, rotational symmetry is assumed, $\Theta_\tau = 1$

$$F^{SF} = c_1^{SF} \cdot \frac{3J_2 \cdot \Theta_\tau}{\bar{R}^{c2}} + c_2^{SF} \cdot \frac{I_1}{\bar{R}^c} = 1 \qquad \text{..... Onset-of-Shear Fracture}$$

or in Eff after applying 'proportional loading'

$$c_1^{SF} \cdot \frac{3J_2 \cdot 1}{\bar{R}^{c2} \cdot Eff^2} + c_2^{SF} \cdot \frac{I_1}{\bar{R}^c \cdot Eff} = 1$$

$$Eff^{SF} = \frac{c_2^{SF} \cdot I_1 + \sqrt{(c_2^{SF} \cdot I_1)^2 + 12 \cdot c_1^{SF} \cdot J_2}}{2 \cdot \bar{R}^c} = 100\% \text{ ...Onset-o- Shear Fracture}$$

Inserting $(\bar{R}^c, 0)$ delivers $1 + c_2{}^{SF} = c_1{}^{SF} \cdot \Theta_\tau$; $c_2{}^{SF}$ is friction parameter

For a single failure mode like Onset-of-Shear Fracture F^{SF} or Onset-of-Yielding F^{Mises} equivalent stresses can be easily formulated

$$Eff^{SF} = \frac{c_2^{SF} \cdot I_1 + \sqrt{(c_2^{SF} \cdot I_1)^2 + 12 \cdot c_1^{SF} \cdot J_2 \cdot (1)}}{2 \cdot \bar{R}^c} = \sigma_{eq}^{SF} / \bar{R}^c$$

Transition to *Ductile*: (1) Failure angle $\Theta_{fp}° = 45°$, (2) $c_2{}^{SF} = 0$

$$F^{SF} = 1 \cdot \frac{3J_2 \cdot 1}{\bar{R}^{c2}} + 0 \cdot \frac{I_1}{\bar{R}^c} = \frac{3J_2}{\bar{R}^{c2}} = 1 \quad \rightarrow \quad \frac{\sqrt{3J_2}}{\bar{R}^c \cdot Eff} = 1$$

$$Eff^{SF} = \frac{0 + \sqrt{0 + 12 \cdot 1 \cdot 3J_2}}{2 \cdot \bar{R}^c} = \frac{\sqrt{3J_2}}{\bar{R}^c} = \sigma_{eq}^{SF} / \bar{R}^c, \quad C_{fp} = \cos\left(\frac{2 \cdot \Theta_{fp}°}{180°} \cdot \pi\right),$$

$\Rightarrow$ Bound of F^{SF}, $\mu = 0$: $c_2{}^{SF} = \frac{3\mu + 1}{-3\mu + 1} = 1$, $\mu \cong -C_{fp} = 0$, , $\Theta_{fp}° = 45°$

$\Rightarrow$ Ductile transfer , $c_2{}^{SF} = 0$: $c_2{}^{SF} = \frac{3\mu + 1}{-3\mu + 1} = 0$, $\mu \cong -C_{fp} = \frac{-1}{3}$, , $\Theta_{fp}° = 35.3°$.

* 'Mises' Yield Condition (homogeneous equation, $F = Eff$)

Ductile: $\bar{R}_{0.2}{}^t \cong \bar{R}_{0.2}{}^c = \bar{R}_{0.2}$ if very ductile

$$F^{Mises} = \frac{\sqrt{3J_2}}{\bar{R}_{0.2}} = 1 \qquad \rightarrow \quad \frac{\sqrt{3J_2}}{\bar{R}_{0.2} \cdot Eff} = 1$$

$$Eff^{Mises} = \frac{\sqrt{3J_2}}{\bar{R}_{0.2}} = \sigma_{eq}^{Mises} / \bar{R}_{0.2} \ .$$

For providing some more information on the differences of F^{SF}, F^{Mises} some features are presented:

Ductile: $I_1 < 0$, R_{02}^{c} $I_1 > 0$, R_{02}^{t}

In the case of very ductile materials - $R_{02}^{t} = R_{02}^{c}$ – the yield plane angle is caused by the shear stress τ_n on the sliding plane (*of course σ_n exists from equilibrium condition, too, but is not of influence; $\tau_{nt} = |\sigma_n| = \sigma_{ax}$).* The sliding angle is not dependent on the sign of I_1. It is derived as follows

Derivation of the slope equation in Mohr stresses, σ_λ, $\tau_{t\lambda}$, $\tau_{n\lambda} = 0$

$$F^{Mises} = \sqrt{\frac{3J_2}{\bar{R}^{c2}}} = \sqrt{\frac{3\cdot(\sigma_n-\sigma_t)^2+(\sigma_t-\sigma_\lambda)^2+(\sigma_\lambda-\sigma_n)^2+6\cdot(\tau_{nt}^{\,2}+\tau_{n1}^{\,2}+\tau_{t1}^{\,2})}{2\cdot\bar{R}^{c2}}} = 1$$

$$= \sqrt{\frac{3\cdot(\sigma_n-\sigma_t)^2+(\sigma_t-0)^2+(0-\sigma_n)^2+6\cdot(\tau_{nt}^{\,2}+0+0)}{2\cdot\bar{R}^{c2}}} = 1$$

$$\frac{d\tau_{nt}}{d\sigma_n} = -\frac{dF}{d\sigma_n} / \frac{dF}{d\tau_{nt}} \text{ (implicite differentiation)} = -\frac{2\cdot\sigma_n-\sigma_t}{6\cdot\tau_{nt}} .$$

Transformed structural stresses and addition theorems used:

$$\sigma_n - \sigma_t = C\cdot(\sigma_{II}),\ \tau_{nt} = -0.5\cdot S\cdot(\sigma_{II}),\ \sigma_n = 0.5\cdot(C+1)\cdot\sigma_{II}$$

Equal slope of curves in touch point: η is multi-axial and cut out

$$\frac{d\tau_{nt}}{d\sigma_n} = \frac{C}{S} = -\frac{2\cdot\sigma_n-\sigma_t}{6\cdot\tau_{nt}} = -\frac{\sigma_n+C\cdot(\sigma_{II})}{6\cdot(-0.5\cdot S\cdot\sigma_{II})}$$

$$\frac{C}{S} = -\frac{0.5\cdot(C+1)\cdot\sigma_{II}+C\cdot(\sigma_{II})}{6\cdot -0.5\cdot S\cdot(\sigma_{II})} \quad \Rightarrow\ C = \frac{1}{3}.$$

For additional information: The cohesive strength corresponding shear stress τ reads

$$\sqrt{\frac{3J_2}{\bar{R}_{02}^{\,2}}} = \sqrt{\frac{\sigma_{II}^{\,2}-\sigma_{II}\cdot\sigma_{III}+\sigma_{III}^{\,2}}{\bar{R}_{02}^{\,2}}} = \sqrt{\frac{\sigma_{II}^{\,2}-\sigma_{II}\cdot(-\sigma_{II})+(-\sigma_{II})^2}{\bar{R}_{02}^{\,2}}} = 1$$

$$\sqrt{\frac{\sigma_{II}^{\,2}-\sigma_{II}\cdot(-\sigma_{II})+(-\sigma_{II})^2}{\bar{R}_{02}^{\,2}}} = 1 \rightarrow \sigma_{II} = \bar{R}_{02}/\sqrt{3} = \tau.$$

Brittle: $-2\cdot R^{cc}$(TM) $< I_1 < -R^{c}$ (CM) < 0 mode domains $I_1 > 0 < R^{t}$ (TM) $< 2\cdot R^{tt}$ (CM)

Θ_{fp} of very brittle materials with R^{c} much larger than $3\cdot R^{t}$ is caused by

$(\tau_{nt}, \sigma_n^{\,c})$	$(\tau_{nt}, \sigma_n^{\,t})$
$> 45° < \Theta_{fp°} < 90°$, μ-dependent	$\Theta_{fp°} = 90°$ at critical plane

cohesive strength R^{τ} at $(\tau_{nt}, \sigma_n = 0)$ is NF-dominated → $R^{\tau} <= R^{t}$.

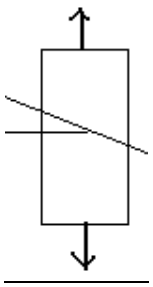

***LL**:*

(1) In the case of a mathematically homogeneous failure function Eff = F.

(2) *For shear was shown above, that F^{SF} can be transferred into the Mises yield function.*

ANNEX 2: Measurement of friction values $\mu_{\perp\parallel}$, $\mu_{\perp\perp}$ using the ARCAN test rig

Often, a tension-compression/torsion test rig is not in hand, but sometimes an ARCAN test rig may be available. This means, a compromise is to accept in order to estimate an approximate value at least. Nevertheless, employing an ARCAN test procedure causes a high effort for the preparation of the test specimen. About 30 mm thick plates must be fabricated to cut out the required test specimens, see [*Pet15*].

Both friction values are determined by bi-axial compression-shear tests employing the ARCAN test set-up. For $\mu_{\perp\parallel}$ IFF3 is to take and for $\mu_{\perp\perp}$ IFF1 with IFF2, because in the ARCAN test no pure bi-axial compression stress states can be generated, just compression combined with shear, composed of a tension IFF1 and a compression component IFF2. It is to note that IFF2 is the significant mode. The influence of the affected IFF1 mode can be considered by employing the interaction formula to resolve for the only unknown $\mu_{\perp\perp}$.

The ARCAN test specimen can be tested in a standard servo-hydraulic test machine to determine the material behavior under combined compression and shear stresses. The loads are introduced with disks mounted at a certain loading angle φ.

Fig.A2-1 depicts the test rig, the test specimens and the stress path with associated angle of the force where the measurements have been performed at.

Fig.A2-2 presents loading path plus results.

Good guess: Two points on the failure curve IFF3 are used to compute the friction parameter from average values of the strength point and a reasonable bi-axial failure stress state point (τ_{21}, σ_{2c}). For achieving a good guess the use of a straight line is sufficient, which represents a linear Mohr-Coulomb formulation.

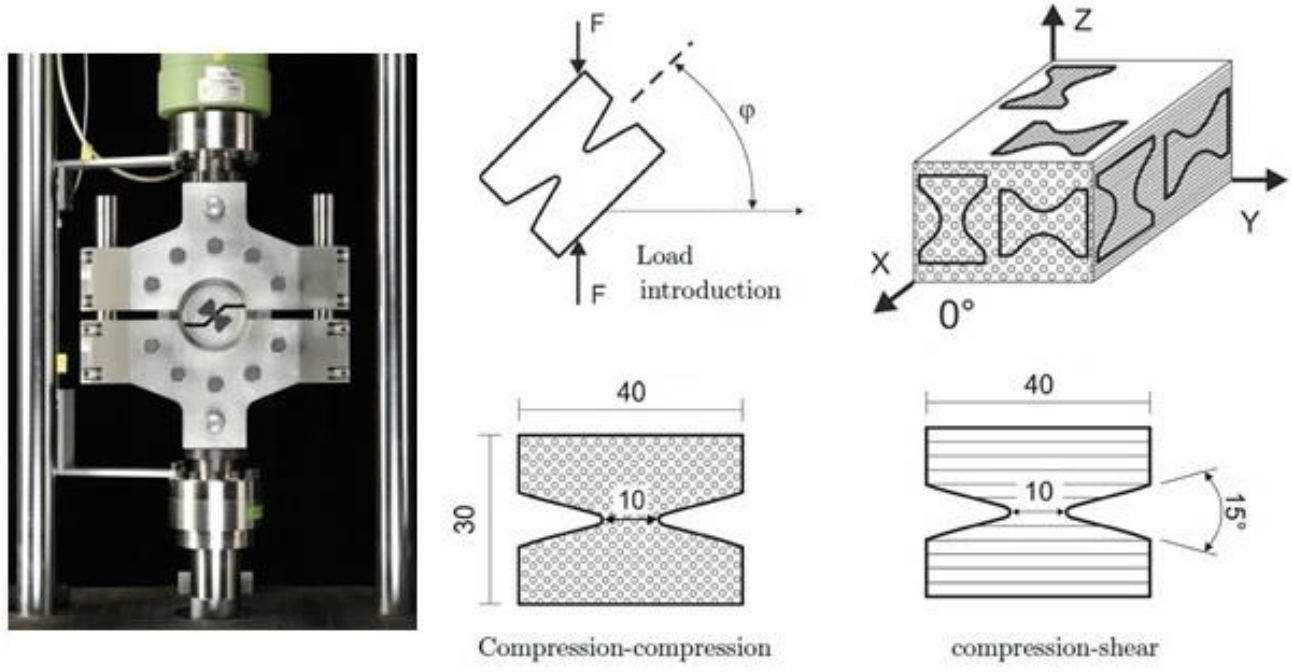

Fig.A2-1: ARCAN test rig with test specimens cut out of a thick UD panel

The test rig only allows running a $\mu_{\perp\perp}$-test in the transition zone, for the evaluation the interaction equation had to be employed, shown by the following procedure:

* Estimation of $\mu_{\perp\parallel}$: from $(0, \bar{R}_{\perp\parallel})$ + bi-axial compression-shear test $(\sigma^c_{2,fr}, \tau_{21,fr})$.

Test data: $\bar{R}_{\perp\parallel}$ = 202 MPa, m = 2.6; $\sigma^c_{2,fr}$ = 31 MPa , $\tau_{21,fr}$ = –145 MPa, τ_{23} = 0.

$$Eff^{\perp\parallel} = \{[\,2\mu_{\perp\parallel}\cdot(2\sigma_2\cdot\tau_{21}{}^2) + \sqrt{(2\mu_{\perp\parallel}\cdot(2\sigma_2\cdot\tau_{21}{}^2))^2 + 4\bar{R}_{\perp\parallel}{}^2\cdot\tau_{21}{}^4}\,]\,/\,2\bar{R}_{\perp\parallel}{}^3\,\}^{0.5}$$

$$\Rightarrow \quad \mu_{\perp\parallel} = 0.21$$

* Estimation of $\mu_{\perp\perp}$: from $(-\bar{R}^c_{\perp},0)$ + bi-axial compression-shear test $(\sigma^t_{2,fr},\sigma^c_{3,fr})$

Test data of the test in the transition zone of the two modes:

$\bar{R}^c_{\perp}$ = 202 MPa, $\bar{R}^t_{\perp}$ = 71 MPa, m = 2.6; $\sigma^t_{2,fr}$ = 31 MPa , $\sigma^c_{3,fr}$ = –145 MPa.

Application of the interaction formula:

$$Eff^{\perp\sigma} = [(\sigma_2+\sigma_3) + \sqrt{(\sigma_2-\sigma_3)^2+4\tau_{23}{}^2}\,]\,/\,2\bar{R}^t_{\perp}$$

$$Eff^{\perp\tau} = [(\frac{\mu_{\perp\perp}}{1-\mu_{\perp\perp}})\cdot(\sigma_2+\sigma_3) + \frac{1}{1-\mu_{\perp\perp}}\sqrt{(\sigma_2-\sigma_3)^2+4\tau_{23}{}^2}\,]\;/\,\bar{R}^c_{\perp}$$

Mathcad implicite calculation: *Vorgabe* $\mu_{\perp\perp}$:= 0.1 (estimation)

$$([(\sigma_2+\sigma_3) + \sqrt{(\sigma_2-\sigma_3)^2+0}\,]\,/\,2\bar{R}^t_{\perp}\;)^m + ([(\frac{\mu_{\perp\perp}}{1-\mu_{\perp\perp}})\cdot(\sigma_2+\sigma_3) + \frac{1}{1-\mu_{\perp\perp}}\sqrt{(\sigma_2-\sigma_3)^2+4\tau_{23}{}^2}\,]\;/\,\bar{R}^c_{\perp})^m = 1 = \; Eff = 100\% \;.$$

Search *Suchen* $(\mu_{\perp\perp})$ $\Rightarrow \mu_{\perp\perp} = 0.21$

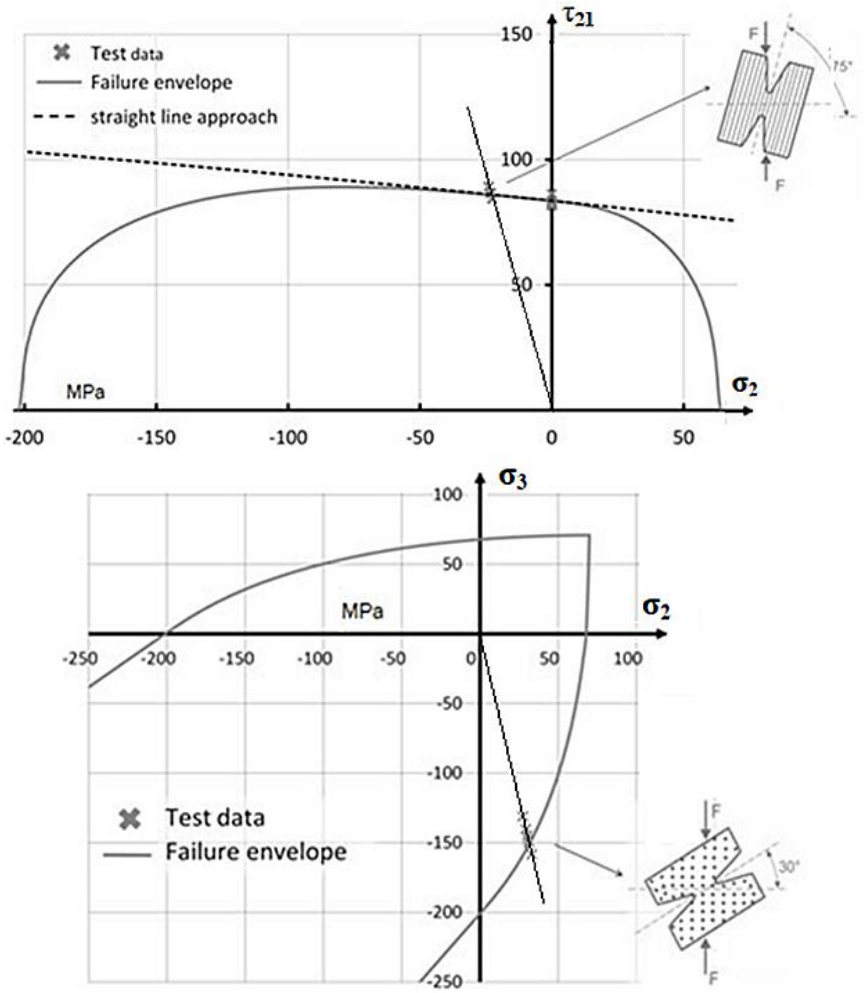

Fig.A2-2: ARCAN tests performed on distinct stress paths. UD prepreg material HexPly M21 / 34% / UD 194 g/m² / T700GC CFRP.

ANNEX 3: UD, Novel modelling of Porosity in the quasi-isotropic domain

The effect of friction is reduced by increasing porosity. In order to map this, the author proposes a simple failure function *F* that spans from dense to pretty porous materials. The following formulas for the transversely-isotropic UD material are the basis for the curves in *Fig.A3-1* below.

* Failure Function for a dense UD material

$$F^{SF} = [a_{\perp\perp} \cdot I_2 \; + \; b_{\perp\perp} \cdot \sqrt{I_4}\,] \; / \bar{R}_{\perp}^{c} = 1 \;\text{ with }\; a_{\perp\perp} = b_{\perp\perp} - 1 \;\text{ after inserting }\; \bar{R}_{\perp}^{\,c} = 104 \;\text{ MPa}$$

$$= [a_{\perp\perp} \cdot (\sigma_2 + \sigma_3) \; + \; b_{\perp\perp} \cdot \sqrt{(\sigma_2 - \sigma_3)^2 + 4\tau_{23}^{\,2}}\,] \; / \bar{R}_{\perp}^{c} = 1$$

$$= [a_{\perp\perp} \cdot (\sigma_2^{\,p} + \sigma_3^{\,p}) \; + \; b_{\perp\perp} \cdot \sqrt{(\sigma_2^{\,p} - \sigma_3^{\,p})^2 + 0^2}\,] \; / \bar{R}_{\perp}^{c} = 1 \;\leftarrow\; \text{2 structural stresses}$$

* Failure Function for a porous UD material (index por, *author's simple approach*)

$$F_{porosity}^{SF} = \sqrt{a_{\perp\perp po}^{\;2} \cdot I_2^{\,2} + \; b_{\perp\perp por}^{\;2} \cdot I_4} - \; a_{\perp\perp por} \cdot I_2 \;] \; / 2\bar{R}_{\perp}^{c} = 1 \,.$$

The two curve parameters are determined - as before performed - from insertion of the compressive strength point and from the bi-axial fracture stress point.

In the figure the parallel lines mark that a 'dense' UD material does not shear fracture. This is caused by the axial straining under a bi-axial compression stress state which is impeded by the constraining fibers.

When applying $a_{\perp\perp por} = 0$, then parallel lines can be obtained. The parallel lines represent density or zero porosity and exhibit the capability of the simple approach.

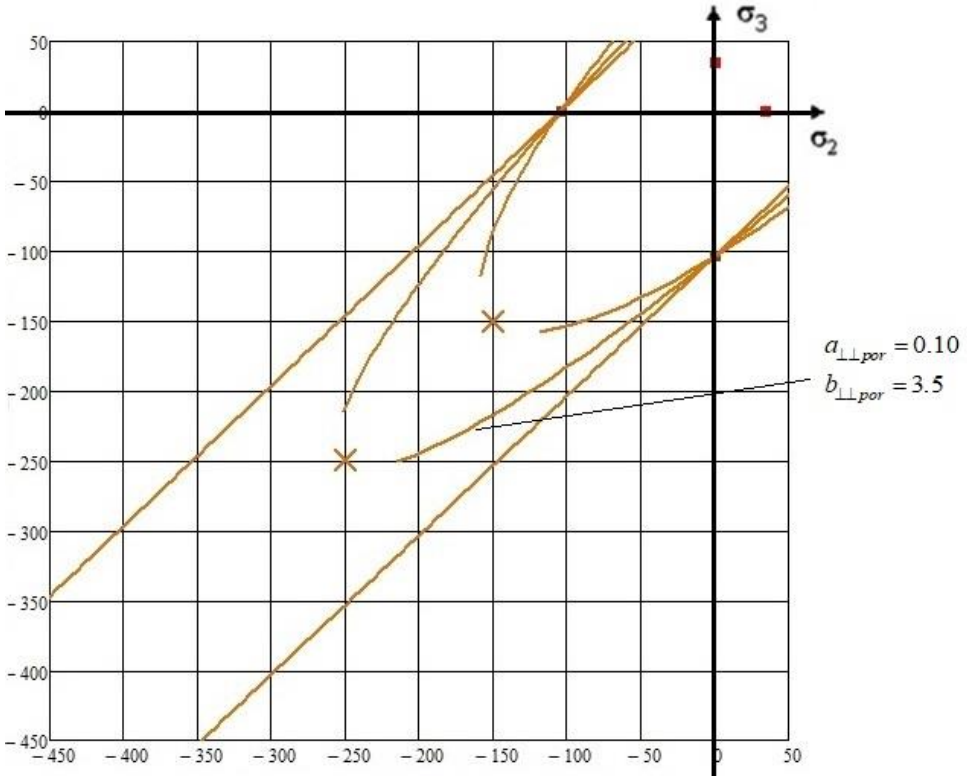

Fig. A3-1: Fracture failure curves of UD material regarding two different porosity grades. $a_{\perp\perp por}$ for 0, 0.10, 0.22 and $b_{\perp\perp por}$ for 4.0, 3.5, 2.9

Ideal dense materials possess no porosity.

A fully porous material may be defined by $R_{\perp}^{cc} \cong R_{\perp}^{c}$. This case can be modelled like foam materials in the quasi-isotropic domain [*Cun16a*].

ANNEX 4: Influence of 2D- and 3D-compression stress states on the strength capacity

On the surface of the fracture failure body the material stressing effort is 100%. Located on the surface are the uni-axial failure stress points, termed technical strengths, bi-axial 'strengths' and all other multi-axial failure stress points.
Keep in mind: 'Higher' muti-axial failure stresses have nothing to do with an increase of strength. In the case of multi-axial compression stress states of dense brittle materials the strength is not increased but the risk of shear fracture becomes smaller indicated by the smaller *Eff !*

1. Isotropic materials *(example concrete, UHPC test data, courtesy IfM Dresden)*

Test paths: tensile meridian $\sigma_I = \sigma_{II} > \sigma_{III}$ and compressive meridian $\sigma_I > \sigma_{II} = \sigma_{III}$. The test is performed by superimposing an axial stress σ_{ax} to a hydrostatic pressure p_{hyd}. σ_{III} is the mathematically lowest stress.

	Rotational Symmetry Stress States			Eff in %	120° Symmetry Stress States			Eff in %
	- p	- p	- p + σ_{ax}	100	- p	- p	- p + σ_{ax}	100
	σ_I	σ_{II}	σ_{III}		σ_I	σ_{II}	σ_{III}	
1D	0	0	- R^c	100	0	0	- R^c	100
2D	0	0.25 R^c	- R^c	72	0	0.25 R^c	- R^c	34
	0	- R^c	- R^c	60	0	- R^c	- R^c	35
3D	- 0.5 R^c	- 0.5 R^c	- R^c	16	- 0.5 R^c	- 0.5 R^c	- R^c	6
1D	UHPC test result [*Cun17*] in MPa				0	0	-160	100
3D	UHPC test result in MPa				-6	-6	-6 - 224	100

Conclusions:
(1) *Multiaxial compression lowers Eff. (2) 2D compression generates a tensile strain in axial direction, which is to be considered in design. (3) The physically accurate 120°-rotationally–symmetric model delivers a lower Eff-value for the stress states above.*

2. Transversely-isotropic UD materials *(example CFRP)*

Here, the difference between a proportionally-stressing derived *Eff* and a driving stress-derived *Eff* is intentionally outlined. The two concepts invite for discussion.

Stress States			Eff in %	Eff in %
	σ_2	σ_3		
1D	0	$-R_{\perp}^c$	100	100
2D	- 0.5 $R_{\perp}^c$	- $R_{\perp}^c$	24	45
	- $R_{\perp}^c$	- $R_{\perp}^c$	-52	0
			$a_{\perp\perp} = 0.26$, $b_{\perp\perp} = a_{\perp\perp} + 1$	as = 0.26, bs = 2.52
			proportional	driving stress

Conclusions:
(1) *Again, multiaxial compression lowers Eff. (2) In the case of 'dense' UD materials bi-axial compression causes no fracture failure, Eff < 0. (3) 2D compression generates a tensile stress because the fibers withstand axial straining. This stress from the constraint situation is usually easily captured by the fiber, on top of the loading stress* $\sigma_1 = \sigma_{\parallel}$.

The 'driving stress concept' leads to higher Effs. About its general value discussion is desired, ⊥ = s.

$$Eff2 := \frac{(\sigma 2 + \sigma 3)\cdot ass + \sqrt{(\sigma 2 - \sigma 3)^2}\cdot bss}{Rsc} \qquad Eff2 := \frac{bs\cdot\sqrt{0.25(\sigma 2 - \sigma 3)^2}}{Rsc - as\cdot(\sigma 2 + \sigma 3)}$$

ANNEX 5: Determination of a Reserve Factor applying Safety Concepts

A Safety Concept implements the necessary reliability into the structural component, to robustly endure uncertain design parameters (variables) [*Cun05*]. Different formats are available to capture the uncertainties of the design parameters and to implement the necessary reliability:

* Lumped Safety Factor Concept:

Concept, that deterministically accounts for design uncertainties in a lumped manner through enlarging the 'design limit loads' by multiplication with a design Factor of Safety FoS j. This provides an unknown not really deterministically quantifiable 'safety distance' between load and load resistance ('strength') represented by the required positive Margin of Safety ($MoS = RF$-1). *Note, please: A FoS is given, and it is not to calculate like the Margin of Safety*.

* Partial Safety Factor Concept:

Concept, that semi-probabilistically bridges the deterministic format and the more complicated probabilistic format. A probabilistic format can model each single design parameter's uncertainty into a stochastic uncertainty described by a probability density function. Accounting for uncertainties informs about the robustness of the design and considers the correlations of the design variables.

In the deterministic formats the worst case scenario is usually applied for loadings considering temperature, moisture, undetected damage. Further a load is to increase by a design FoS and the resistances are to decrease. For strength, statistical distributions are used. If the loading is also based on a statistical distribution, then one speaks about a semi-probabilistic format.

FoS capture uncertainties, small inaccuracies, and simplifications in analyses w.r.t. manufacturing process, tolerances, loadings, material properties (strength, elasticity, ..), geometry, strength failure conditions etc. FoS j or FoS γ (in civil engineering) do not capture missing accuracies in modeling, analysis, test data generation and test data evaluation! FoS are used to counteract the risk of a structural failure or to decrease the chance of failure by capturing the uncertainties of all the given variables outside the control of the designer. Presently, in mechanical engineering the loading is increased by one lumped FoS j and in civil engineering the procedure is improved by using several partial FoS γ for the uncertain stochastic design variables.

Engineers in mechanical and in civil engineering practically want to know "How much can one further increase the loading"? In this context, for the ultimate load case (DUL, ULS, GZT) it is to demonstrate in *strength design verification*:

Linear analysis is sufficient: $\sigma \sim$ load $\rightarrow RF \equiv f_{RF}$

material reserve factor $$f_{RFult} = \frac{\text{Strength Design Allowable}}{\text{Stress at } j_{ult} \cdot \text{Design Limit Load}} > 1,$$

Non-linear analysis required: σ not proportional to load

reserve factor (load-defined) $$RF_{ult} = \frac{\text{Predicted Failure Load at } Eff = 100\%}{j_{ult} \cdot \text{Design Limit Load}} > 1.$$

In order to use hidden load carrying reserves, structural analysis is to perform until material failure is reached in the critical location which is indicated for the exhausted material by $Eff = 100\%$.

In construction, the material reserve factor is defined, fully analogous to mechanical engineering and to aerospace by a formulation $f_{RF} = (f_{ck} / \gamma_c) / (\sigma \cdot \gamma_m)$ with f_{ck} the characteristic strength of concrete (index c) and the partial safety factors γ_c for loading and for material scatter γ_m.

Unfortunately still nowadays, instead of the term strength design allowable the not anymore allowed old term 'allowable stress' is used, despite of the fact: Allowable stress · j ≡ Strength design allowable R.

ANNEX 6: Failure Index |*F*| versus Material Stressing Effort *Eff*, example UD

The use of |F| alone is only possible if a 'global' SFC is applied. In the case of the physically better mapping 'modal' SFCs an interaction of the modes is faced and Effs are required to 'feed' the interaction equation.

In design, from cyclic loading comes the denotation 'Proportional Loading' for the increase of the stress state under a loading. As 'loading' in general is not proportional to 'stressing' the concept as it is applied in the elastic static cases should read 'proportional stressing'. Stressing is terminated if the driving shear stress or driving tensile stress becomes zero. Some differences shall be pointed out in the following discriminating the standard "Proportional Loading concept" from a "Failure stress-driven loading" concept. The latter is useful if the SFC does not become zero with the failure driving stress, see below.

Table A6-1: Derivation of Effs for the chosen failure function F, $^{p} = {}^{pr}$

Homogeneous mathematical function *F*

* Concept of proportional loading (stressing): index ^{p} for principal stresses

$$F^{IFF1} = [I_2 + \sqrt{I_4}] / 2\bar{R}_\perp^c = [(\sigma_2{}^p + \sigma_3{}^p) + \sqrt{(\sigma_2{}^p - \sigma_3{}^p)^2 + 0^2}] / 2\bar{R}_\perp^c$$

$$\rightarrow [(\sigma_2{}^p + \sigma_3{}^p) + \sqrt{(\sigma_2{}^p - \sigma_3{}^p)^2}] / (2\bar{R}_\perp^c \cdot Eff^{\perp\sigma}) = 1$$

$$Eff^{\perp\sigma} \equiv [(\sigma_2{}^p + \sigma_3{}^p) + \sqrt{(\sigma_2{}^p - \sigma_3{}^p)^2}] / 2\bar{R}_\perp^c$$

$$F^{IFF2} = [a_{\perp\perp} \cdot I_2 + b_{\perp\perp} \cdot \sqrt{I_4}] / \bar{R}_\perp^c = [a_{\perp\perp} \cdot (\sigma_2{}^p + \sigma_3{}^p) + b_{\perp\perp} \cdot \sqrt{(\sigma_2{}^p - \sigma_3{}^p)^2}] / \bar{R}_\perp^c$$

$$\rightarrow [a_{\perp\perp} \cdot (\sigma_2{}^p + \sigma_3{}^p) + b_{\perp\perp} \cdot \sqrt{(\sigma_2{}^p - \sigma_3{}^p)^2}] / (\bar{R}_\perp^c \cdot Eff^{\perp\tau})$$

$$Eff^{\perp\tau} \equiv a_{\perp\perp} \cdot (\sigma_2{}^p + \sigma_3{}^p) + b_{\perp\perp} \cdot \sqrt{(\sigma_2{}^p - \sigma_3{}^p)^2}] / \bar{R}_\perp^c \Rightarrow \text{ no difference } |F| \leftrightarrow Eff$$

$$F^{IFF3,\,2D} = \tau_{21} / (\bar{R}_{21} - \mu_{\perp\|} \cdot \sigma_2) \quad \text{simple 2D formulation}$$

$$\frac{\tau_{21}}{Eff^{IFF3,\,2D}} / (\bar{R}_{21} - \mu_{\perp\|} \cdot \frac{\sigma_2}{ff^{IFF3,\,2D}}) = 1 \rightarrow Eff^{IFF3,\,2D} = \frac{\tau_{21} + \mu_{\perp\|} \cdot \sigma_2}{\bar{R}_{21}} \quad \text{not permitted}$$

$\Rightarrow$ Eff does not become zero if the driving stress becomes zero

$$\frac{\tau_{21}}{Eff^{IFF3,\,2D}} / (\bar{R}_{21} - \mu_{\perp\|} \cdot \sigma_2) = 1 \quad \rightarrow \quad Eff^{IFF3,\,2D} = \frac{\tau_{21}}{\bar{R}_{21} - \mu_{\perp\|} \cdot \sigma_2} \quad \text{permitted}$$

* Concept of factorizing the driving stress: *invitation for discussion*

$$\rightarrow [\frac{(\sigma_2{}^p + \sigma_3{}^p)}{Eff^{\perp\sigma}} + \sqrt{(\sigma_2{}^p - \sigma_3{}^p)^2}] / 2\bar{R}_\perp^c = 1$$

$$Eff^{\perp\sigma} \equiv (\sigma_2{}^p + \sigma_3{}^p) / [2\bar{R}_\perp^c + \sqrt{(\sigma_2{}^p - \sigma_3{}^p)^2}],$$

$$\rightarrow [a_{\perp\perp} \cdot (\sigma_2{}^p + \sigma_3{}^p) + b_{\perp\perp} \cdot \frac{\sqrt{(0.5 \cdot \tau_I)^2}}{Eff^{\perp\tau}}] / \bar{R}_\perp^c = 1, \quad \sigma_2{}^p - \sigma_3{}^p = 0.5 \cdot \tau_I$$

$$Eff^{\perp\tau} \equiv b_{\perp\perp} \cdot \sqrt{(\sigma_2{}^p - \sigma_3{}^p)^2}] / [\bar{R}_\perp^c - a_{\perp\perp} \cdot (\sigma_2{}^p + \sigma_3{}^p)] \Rightarrow \text{ difference } |F| \leftrightarrow Eff$$

Non-homogeneous mathematical function *F* * *Concept of proportional loading*

$$F^{IFF2} = [a_{\perp\perp} \cdot I_2 + b_{\perp\perp} \cdot I_4 / \bar{R}_\perp^c] / \bar{R}_\perp^c$$

$$\rightarrow [a_{\perp\perp} \cdot (\sigma_2{}^p + \sigma_3{}^p) + b_{\perp\perp} \cdot (\sigma_2{}^p - \sigma_3{}^p)^2 / (\bar{R}_\perp^c \cdot Eff^{\perp\tau})] / (\bar{R}_\perp^c \cdot Eff^{\perp\tau}) = 1$$

$$Eff^{\perp\tau} \equiv a_{\perp\perp} \cdot (\sigma_2{}^p + \sigma_3{}^p) + b_{\perp\perp} \cdot \sqrt{(\sigma_2{}^p - \sigma_3{}^p)^2}] / \bar{R}_\perp^c, \text{ difference } |F| \leftrightarrow Eff.$$

.